1-1-2015

In Vivo Genome Editing: Proof of Concept in Neonatal and Adult Mouse Liver

Rajiv Sharma
University of Pennsylvania, rajs@mail.med.upenn.edu

In Vivo Genome Editing: Proof of Concept in Neonatal and Adult Mouse Liver

Abstract
Adeno-associated viral (AAV) vectors show great potential for therapeutic gene delivery for monogenic diseases, including hemophilia. Major limitations of this approach are the inability to persist in dividing cells and the restrictive packaging capacity of AAV. Gene targeting, the ability to make site-directed changes to the genome, has been a powerful tool for genetic discovery. Until recently, the low efficiency of targeting has rendered it unlikely to be of therapeutic value for most genetic diseases. Zinc finger nucleases (ZFNs) are engineered proteins capable of site-directed DNA cleavage, known to increase the efficiency of gene targeting. Our lab has previously demonstrated in vivo gene targeting of the liver using AAV to deliver ZFNs and therapeutic donor in neonatal mice, where the rapid proliferation of hepatocytes may promote genome editing through homology directed repair (HDR). It was unknown whether the success of this approach could be replicated in adult mice (with predominantly quiescent hepatocytes, unlikely to be amenable to HDR). We hypothesized that in the absence of HDR, the non-homologous end-joining (NHEJ) pathway may promote gene targeting in adult mice. Indeed, homology independent vector integration was sufficient to drive robust expression of clotting factor IX, deficient in hemophilia B, and correct the disease phenotype in mice treated as adults. This approach was adapted to create a general platform for liver-directed protein replacement therapy. Using ZFNs targeting the mouse albumin locus, we achieved long-term therapeutic expression of human factors VIII and IX in mouse models of hemophilia A and B as well as four different therapeutic enzymes deficient in lysosomal storage disorders. To test our hypothesis that in vivo genome editing relies on different DNA repair mechanisms in neonatal and adult mice, we applied multiple techniques including a novel reporter construct, southern blot, comparisons of donors with and without arms of homology, and a mouse model of NHEJ deficiency. These data indicate HDR is the primary mechanism of genome editing in neonatal mouse livers, and dispensable for therapeutically relevant levels of genome editing in adult mice. These results have implications in designing safer and more efficacious genome editing therapies.

Degree Type
Dissertation

Degree Name
Doctor of Philosophy (PhD)

Graduate Group
Cell & Molecular Biology

First Advisor
Katherine A. High

Keywords
Gene Therapy, Genome Editing, Genome Engineering, Hemophilia

IN VIVO GENOME EDITING: PROOF OF CONCEPT IN NEONATAL AND ADULT MOUSE LIVER

Rajiv Sharma

A DISSERTATION

in

Cell and Molecular Biology

Presented to the Faculties of the University of Pennsylvania

in Partial Fulfillment of the Requirements for the

Degree of Doctor of Philosophy

2015

Supervisor of Dissertation

_____

Katherine A. High, M.D.

Professor, Department of Pediatrics

Graduate Group Chairperson

_____

Daniel S. Kessler, Ph.D.

Associate Professor, Department of Cell and Developmental Biology

Cell and Molecular Biology Graduate Group Chair

Dissertation Committee

Frederic D. Bushman, Ph.D.

Carl H. June, M.D.

Matthew D. Weitzman, Ph.D.

Roger A. Greenberg, M.D., Ph.D.

IN VIVO GENOME EDITING: PROOF OF CONCEPT IN

NEONATAL AND ADULT MOUSE LIVER

ACKNOWLEDGMENTS

I would like to thank my thesis mentor, Dr. Katherine High, for accepting me as a graduate student in her lab, and for fostering an open and collaborative community that has played a large part in my training in the last five years. I will continue to hold her work ethic and openness to having her opinion changed by data as traits to aspire to in my scientific career. In addition, I would like to thank Xavier Anguela, with whom I worked closely on these projects. Xavi has taught me perhaps the most important scientific lesson of all, which is never to expect a new technique or experiment to support your hypothesis. Xavi is one of the most careful scientists I know, and has been like an older brother to me through all of the frustrations and small victories over the years. I would also like to thank our collaborators at Sangamo Biosciences, especially Yannick Doyon, Michael Holmes, Phillip Gregory, Thomas Wechsler, and Sunnie Wong, for ZFN design and construction, Cel-I and PCR-based genotyping, and for conducting experiments for lysosomal storage diseases.

I owe all of the members of the lab for not only teaching me techniques, but also providing a fun and supporting work atmosphere. Research can be filled with periods of disappointing results, and I can't imagine going through them without being around happy and helpful colleagues. In particular I would like to thank: John Finn for teaching me many of the basics of molecular biology and giving me career advice along the way. Hojun Li for setting the bar extremely high as a graduate student, and teaching me to be almost pathologically skeptical of my own data. Paul Gadue, for mentoring me and giving invaluable technical and professional advice, and more generally for being one of the most knowledgeable scientists I know who places great emphasis on the practicality of an approach. Virginia Haurigot and Federico Mingozzi, for allowing me to interrupt your

experiments to ask endless questions when I first rotated in the lab. My thesis committee and especially Frederic Bushman, who has always been willing to grab a pencil and discuss complicated data. George Buchlis, for being so lovable that everyone would show up when he organized a lab social event. Daniel Hui, Robert Davidson, Yifeng Chen, Mustafa Yazicioglu, Alex Tai, and Giulia Pavani, and everyone in the Center for Cellular and Molecular Therapeutics, for being friends. I would also like to thank the Gene Therapy and Vaccines program, and specifically the chairperson David Weiner, for supporting a great learning environment for students.

Finally, I would like to thank my family and friends that have helped me become the scientist I am. My family has supported me mostly through love and encouragement, with the exception of my grandfather (Pata) who also literally taught me science.

ABSTRACT

IN VIVO GENOME EDITING: PROOF OF CONCEPT IN

NEONATAL AND ADULT MOUSE LIVER

Rajiv Sharma

Katherine A. High

Adeno-associated viral (AAV) vectors show great potential for therapeutic gene delivery for monogenic diseases, including hemophilia. Major limitations of this approach are the inability to persist in dividing cells and the restrictive packaging capacity of AAV. Gene targeting, the ability to make site-directed changes to the genome, has been a powerful tool for genetic discovery. Until recently, the low efficiency of targeting has rendered it unlikely to be of therapeutic value for most genetic diseases. Zinc finger nucleases (ZFNs) are engineered proteins capable of site-directed DNA cleavage, known to increase the efficiency of gene targeting. Our lab has previously demonstrated *in vivo* gene targeting of the liver using AAV to deliver ZFNs and therapeutic donor in neonatal mice, where the rapid proliferation of hepatocytes may promote genome editing through homology directed repair (HDR). It was unknown whether the success of this approach could be replicated in adult mice (with predominantly quiescent hepatocytes, unlikely to be amenable to HDR). We hypothesized that in the absence of HDR, the non-homologous end-joining (NHEJ) pathway may promote gene targeting in adult mice. Indeed, homology independent vector integration was sufficient to drive robust expression of clotting factor IX, deficient in hemophilia B, and correct the disease phenotype in mice treated as adults. This approach was adapted to create a general platform for liver-directed protein replacement therapy. Using ZFNs targeting the mouse

albumin locus, we achieved long-term therapeutic expression of human factors VIII and IX in mouse models of hemophilia A and B as well as four different therapeutic enzymes deficient in lysosomal storage disorders. To test our hypothesis that *in vivo* genome editing relies on different DNA repair mechanisms in neonatal and adult mice, we applied multiple techniques including a novel reporter construct, southern blot, comparisons of donors with and without arms of homology, and a mouse model of NHEJ deficiency. These data indicate HDR is the primary mechanism of genome editing in neonatal mouse livers, and dispensable for therapeutically relevant levels of genome editing in adult mice. These results have implications in designing safer and more efficacious genome editing therapies.

TABLE OF CONTENTS

List of Figures

CHAPTER 1: INTRODUCTION

Gene Therapy

Gene therapy, the transfer genetic material to correct or ameliorate disease, has made major progress in the last few decades. The modern concept of using viral vectors to transfer genes was first proposed in 1972 (Aposhian, Qasba, Osterman, & Waddell, 1972), and since then the investment in resources as well as advances in our understanding of biological principles have culminated in promising clinical trials results. Among the first candidates for the development of these novel therapies were monogenic diseases that cause immunodeficiencies, inherited blindness, and hemophilia.

Retroviral Vectors

Early studies demonstrating the use of retroviruses as a gene transfer agent were published in the early 1980s (Shimotohno & Temin, 1981; Tabin, Hoffmann, Goff, & Weinberg, 1982; Wei, Gibson, Spear, & Scolnick, 1981). These tools improved rapidly, due in large part to the retroviral virology of the prior decade, with the development of non-infectious vector systems and stable packaging lines (Mann, Mulligan, & Baltimore, 1983; Markowitz, Goff, & Bank, 1988; Miller & Buttimore, 1986). These vectors emerged as a highly capable method of transduction of many different cell lines and primary cell types *in vitro*.

Gene therapy for SCID-X1

The severe combined immunodeficiency characteristic of X-linked SCID disease is caused by a deficiency in the “common gamma” cytokine receptor (IL2RG) and is in many ways an ideal target for gene therapy. The devastating disease results in a

complete lack of T and NK cell subsets within the immune system (Noguchi et al., 1993). Due to the lack of T cell "help," deficient B cell antibody production renders patients susceptible to many opportunistic infections. Allogeneic bone marrow transplant, the only known cure, is not possible in all circumstances. The etiology of SCID-X1 is well characterized, and, based on data from animal models and in human cells, introduction of a wild-type IL2RG gene to a patient's own hematopoietic stem cells (HSCs) would be expected to restore functional signaling through IL-2, 4, 7, 9, 15, and 21 receptors (which all form complexes with the gamma chain) and rescue the disease phenotype. The successfully transduced cells are endowed with a competitive advantage over those that harbor the defective gene, and are able to expand by several orders of magnitude to reconstitute the immune system with functional B, T, and NK cells.

The first trials were conducted with gamma retroviral vectors to deliver the IL2RG gene, and corrected HSCs were successful in reconstituting the immune systems of most patients (Cavazzana-Calvo et al., 2000; Howe et al., 2008). Unfortunately, the treatment was also associated with leukemia in 25% of the 20 subjects treated. The proposed mechanism of this adverse event was the integration of the vector used to deliver IL2RG in the vicinity of oncogenes, causing upregulation (Howe et al., 2008); reviewed in (Bushman, 2014). This hypothesis was supported by studies demonstrating integration of the retroviral provirus within the first intron of the LMO-2 gene, and upregulation of expression of LMO-2, previously shown to be upregulated in T cell leukemias (Rabbitts et al., 1999). Although four of these five patients' leukemias were treatable, it became clear that insertional oncogenesis would be the most important safety concern for gene therapies that modify the genome. Going forward, developments

in vector technology such as the inclusion of insulator sequences and replacing retroviral vectors with HIV-based lentiviral vectors (which are thought to have integration preferences less compatible with transformation) have been incorporated to treat other immunodeficiencies and thalassemia. These design changes appear to lessen, but not completely remove, the risk of uncontrolled proliferation due to insertional mutagenesis. These results in patients make the strongest empirical case for the development of methods to increase the specificity of DNA targeting in diseases that require an integrated copy of the corrective gene.

AAV Vectors

As opposed to retroviral vectors, adeno-associated viral vectors (AAV) are primarily non-integrating, persisting mainly in the form of extrachromosomal “episomes” outside of the genome. AAV was originally discovered as a contaminant in adenoviral cell cultures, and researchers have since discovered hundreds of natural variants differing primarily in capsid structure. Various serotypes (namely AAV2 and AAV8) have emerged as a highly efficient means to deliver genetic material to multiple tissues. The virus contains three capsid proteins (VP1, VP2, VP3) at a 5:5:50 ratio in a T=1 icosahedral structure, which encapsulate a single stranded genome of roughly 4.7kb. The only *cis* requirements for packaging are the inverted terminal repeat (ITR) sequences on each end of the viral genome, meaning the viral genes can be substituted with other sequences to create a viral vector. Recombinant vector can be produced in cell culture by triple transfection of: (i) helper plasmid (as a dependovirus, AAV requires elements from other viruses such as adenovirus), (ii) wild type AAV genes encoding Rep and Cap, and (iii) the vector genome flanked by ITRs. Upon reaching the nucleus of

target cells, vectors uncoat, releasing their vector genome, which will persist predominantly in the form of concatamers joined together end to end (Duan, Yue, & Engelhardt, 2003; Yang et al., 1999).

Due to the AAV genome's low rate of integration and inability to actively segregate with centromeres upon cell division, expression is lost dramatically upon cell division. Cells that undergo even small numbers of divisions exhibit a considerable reduction in AAV expression. As a result, standard AAV approaches are poorly suited to treat immune deficiencies or other diseases in which cells need to divide substantially after treatment. However, gene delivery with AAV is ideal for targeting organs such as liver, muscle, or brain, which do not typically divide and are not amenable to *ex vivo* manipulation, and for diseases in which the target cells do not typically divide.

Hemophilia

Hemophilia B, an inherited bleeding disorder caused by mutations in the Factor 9 (F9) gene results in deficiency of the Factor IX (F.IX) enzyme within the clotting cascade. Hemophilic patients harboring mutations in F9 have been treated with blood transfusions or protein replacement therapy in which hF.IX protein is intravenously injected 2-3 times per week. The cost of this prophylactic treatment with recombinant clotting factor can exceed $250,000 per year for the life of the patient (Nathwani et al., 2014). Many patients in developing countries cannot afford this treatment, and as a result are faced with a shorter life expectancy. Even when receiving this therapeutic regimen, patients remain at high risk for uncontrolled bleeds during intervals between protein therapy infusions. Therefore, hemophilia is an excellent candidate for gene therapy, in which

stable production of the wild-type F9 gene could potentially cure a patient for life. One of the major limitations to gene therapy has been the low efficiency of stable gene expression leading to *therapeutic* levels of protein production *in vivo*. However, hemophilia B is a particularly good candidate for gene therapy development as achieving even 1% of normal hF.IX activity can greatly mitigate disease, and above 5% is considered a mild phenotype, with far fewer bleeding risks in normal circumstances.

Most AAV serotypes, including the best characterized AAV2 and AAV8, are particularly efficient in transducing liver, which, as a large and well-vascularized organ, is proficient at secretion of multiple proteins present in the blood. In preclinical models targeting quiescent adult livers, the predominantly non-integrating AAV vector supports long-term expression of F.IX in murine, canine, and non-human primate models, persisting for over 10 years. Clinical trials have shown great potential for AAV based therapies in the treatment of hemophilia, demonstrating over 3 years of stable hF.IX expression following a single infusion of AAV8 vector (Nathwani et al., 2014; 2011). It is unknown whether stable AAV-mediated expression can be achieved in the clinic when treating proliferating tissues, where a strategy based on chromosomal integration would be ideal.

Genome Editing

Site-specific targeting of the genome has been used to disrupt as well as introduce DNA into genes in mouse embryonic stem cells for nearly three decades. By introducing DNA containing the intended payload flanked by sequences identical to the target site (arms of homology), a small fraction of cells will incorporate the desired

changes into their genome (Thomas & Capecchi, 1987). Various strategies used to overcome the low efficiency by selecting for targeted clones made it possible to expand and characterize the edited cells. These methods fostered the development of purposefully designed knock-out and knock-in mice, and have become a pillar in modern biology. Site-specific correction of a mutated gene is in many ways the holy grail of gene therapy. The corrected gene would be indistinguishable from a wild-type (non-diseased) allele, and the resulting gene product would retain all of its natural regulatory mechanisms. Unfortunately, the low absolute efficiency of the process meant it was unlikely to find therapeutic application for most diseases.

Maria Jasin and colleagues noted that the targeting efficiency can be increased by several orders of magnitude by creating a DNA break at the intended target site (Rouet, Smih, & Jasin, 1994a). Following a DNA double strand break, the cell can utilize one of two major pathways of repair: non-homologous end joining (NHEJ), and homology directed repair (HDR). NHEJ is more active in mammalian cells, and as the name implies does not require a homologous template, instead resolving the break by ligating the free ends. The other pathway, HDR, is known to be upregulated during the S and G2 phases of the cell cycle, when the sister chromatid is available as a template, and is capable of both error free repair and gene targeting if a homologous donor is provided as the repair template. (These mechanisms will be discussed in greater detail in chapter 4). Historically, gene targeting has been used synonymously with one of the two major DNA double strand break repair pathways: homology directed repair. The other, non-homologous end-joining, is typically associated with mutagenic disruption of

genes due to the fact that small (< 5) insertions and deletions of nucleotides are often observed at sites of repetitive DNA cleavage.

Zinc Finger Nucleases

Zinc finger nucleases (ZFNs) are chimeric proteins that contain two linked modules: a DNA binding domain and a DNA cleavage domain. These tools were originally developed by Chandrasegaran and colleagues (Bibikova et al., 2001), and were shown to be effective in stimulating homologous recombination in human cell lines (Carroll, 2011; Porteus, Cathomen, Weitzman, & Baltimore, 2003) as well as primary cells (Urnov et al., 2005). The DNA binding domain consists of multiple Cys_2His_2 zinc-finger motifs often found in eukaryotic transcription factors, which each typically recognize a 3bp DNA sequence (**Figure 1.1**). The DNA cleavage domain comes from the bacterial FokI restriction enzyme, which must dimerize to create a double strand break. Two ZFNs can bind neighboring DNA regions to bring the weakly interacting FokI domains in close proximity (and thus a high local concentration) to achieve efficient cleavage. Compared to the majority of bacterial restriction enzymes used in molecular biology, which generally have a 4-8bp target, ZFNs are capable of much longer recognition sequences to the point where they are likely to be unique in the large mammalian genome. Assuming bases are distributed randomly, an 18bp address would occur once in $6.8x10^{10}$ bp, compared to $3.5x10^9$ bp in the human genome (Q. Liu, Segal, Ghiara, Barbas, III, 1997). A pair of ZFNs, each with 4 ZF modules, can be generated to target almost any existing gene.

Figure 1.1
ZFN Schematic

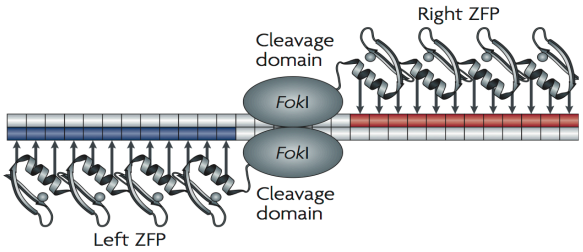

AAV and Gene Targeting

AAV vectors can promote up to 1000-fold greater levels of genome editing relative to plasmid DNA or other delivery vectors. This phenomenon appears to be only partially explained simply by a high rate of transduction of many cell types. Multiple attributes of the AAV vector may explain these incompletely understood observations. A major difference between plasmids and AAV vector genomes is that standard AAV genomes are single stranded, except for the ITRs on each end which form hairpins and small stretches of double stranded DNA. Studies indicate that the unusual DNA conformation is recognized as DNA damage (Hendrie, Hirata, & Russell, 2003; Hirata & Russell, 2000), and suggests recruitment of proteins involved in HDR could increase the likelihood of a cell using AAV as the template for repair.

In Vivo Genome Editing Using Zinc Finger Nucleases

Combining the tools for highly efficient gene delivery to the liver (AAV) and the ability to generate site-directed DNA breaks (ZFNs), our lab demonstrated successful genome editing *in vivo* in a mouse model of hemophilia B. The mouse model, designated h*F9*mut, contained an truncated human F9 mini-gene under the control of a liver specific enhancer and promoter. The strategy for in vivo genome editing involved co-delivery of two AAV8 vectors: (i) Expressing a ZFN pair which targets intron 1 of the integrated hF9mut cassette, and (ii) Donor containing a corrective therapeutic transgene, flanked by arms of homology to the ZFN target site. By treating mice with these vectors at day 1-2 of life (as neonates), we observed secretion of human F.IX in the plasma of these mice

only when they were treated with both vectors, and only in mice that harbored the hF9mut cassette (Li et al., 2011). Importantly, the process was efficient enough to produce plasma hF.IX concentrations of over 200 ng/mL (4% of normal) and phenotypically correct hemophilic mice, restoring their ability to form blood clots in a well-characterized *in vitro* assay (aPTT). These findings established that therapeutic benefit could be achieved through targeted genome editing even without a selective advantage for the gene-targeted cells.

Hypotheses and Rationale for Dissertation Studies

At the time these dissertation studies began, we were encouraged by the success of in vivo genome editing in neonatal mice. At the same time, we began generating data that suggested HDR was not the sole mechanism responsible for the observed donor integration, as our donor design allowed for both vector integration and HDR events to support expression of a functional hF.IX protein. We hypothesized that in the absence of substantial cell proliferation, where HDR is not thought to be active, the NHEJ pathway would promote site directed genome editing in adult mice. The goals of the experiments presented in this dissertation were: a) To determine whether homology independent mechanisms could permit therapeutic gene addition, which may be necessary in quiescent adult livers, and b) To investigate the mechanisms of *in vivo* genome editing.

CHAPTER 2: ROBUST ZFN-MEDIATED GENOME EDITING IN ADULT HEMOPHILIC MICE

This chapter was adapted from (Anguela et al., 2013)

Summary

Monogenic diseases, including hemophilia, represent ideal targets for genome editing approaches aimed at correcting a defective gene. Here we report that systemic adeno-associated viral vector (AAV) delivery of zinc finger nucleases (ZFNs) and corrective donor template to the predominantly quiescent livers of adult mice enables production of high levels of human Factor IX (hF.IX) in a murine model of hemophilia B. Further, we show that off-target cleavage can be substantially reduced while maintaining robust editing by using obligate heterodimeric ZFNs, engineered to minimize unwanted cleavage due to homodimerization of the ZFNs. These results broaden the therapeutic potential of AAV/ZFN mediated genome editing in the liver and could expand this strategy to other non-replicating cell types.

Introduction

We previously reported successful *in vivo* gene targeting in a neonatal mouse model of hemophilia B (HB). Specifically, we demonstrated that systemic co-delivery of AAV vectors, encoding a ZFN pair targeting the human *F9* gene (AAV-ZFN) and a gene targeting vector with arms of homology flanking a corrective cDNA cassette (AAV-Donor), resulted in the correction of a defective h*F9* gene engineered into the mouse genome (referred to as h*F9*mut locus) in the livers of neonatal HB mice. Importantly, we obtained stable levels of hF.IX expression sufficient to normalize clotting times (Li et al., 2011).

However, the neonatal model differs from the anticipated clinical setting (Nathwani et al., 2011) in the degree of hepatocyte proliferation. While neonatal mouse livers undergo multiple rounds of cell division during development, the rate of turnover in adult hepatocytes is very low (Magami et al., 2002). In the quiescent or G0 phase of the cell cycle, DNA double strand breaks (DSBs) such as those created by ZFNs are expected to be repaired mainly by non-homologous end joining (NHEJ), one of two major repair pathways (Branzei & Foiani, 2008; Moynahan & Jasin, 2010). Despite NHEJ being the predominant repair choice in mammalian cells, few approaches have exploited this mechanism. Genome editing has traditionally been considered synonymous with the other repair pathway, homology directed repair (HDR), which is mainly active in the S/G2 phases of the cell cycle. We therefore investigated whether ZFN-driven gene targeting could be generalized to adult animals where the impact of a largely quiescent liver could be assayed.

Materials and Methods

Animal experiments

Animal experiments were approved by the Institutional Animal Care and Use Committee at the Children's Hospital of Philadelphia. Previously described heterozygous male h*F9*mut transgenic mice (Li et al., 2011) or wild type littermate controls, 8 to 10 weeks of age, were used. h*F9*mut/HB male mice were obtained by crossing male homozygote h*F9*mut mice with previously described HB females (Li et al., 2011). Partial hepatectomies were performed as previously described (Mitchell & Willenbring, 2008). AAV vector was diluted to 200 µl with PBS + 0.001% Pluronics before tail-vein injection. Plasma for human factor IX ELISA was obtained by retro-orbital bleeding into heparinized capillary tubes. Plasma for aPTT was obtained by tail bleeding, 9:1 into 3.8% sodium citrate. Tissue for nucleic acid analysis was immediately frozen on dry ice after necropsy.

ZFN reagents and targeting vectors

ZFNs targeting the h*F9*mut locus and F9 targeting vectors have been previously described (Li et al., 2011), as well as the ELD:KKR mutations to the FokI domain to construct the obligate heterodimeric ZFNs (Doyon et al., 2011). Experiments shown in Figure 2.2 used the wild-type FokI domain with the exception of Figure 2.2D in which the obligate heterodimeric ZFNs were used. AAV serotype 8 vectors were produced and titered as previously described (Ayuso et al., 2009)' (Wright & Zelenaia, 2011).

Factor IX levels and activity

Human factor IX ELISA kit (Affinity Biologicals; Ancaster, ON, Canada) was used to quantify plasma hF.IX. All readings below the last value of the standard curve (15 ng/ml) were arbitrarily given the value of 15 ng/ml except where otherwise indicated. The activated partial thromboplastin time (aPTT) assay was performed by mixing sample plasma 1:1:1 with pooled hemophilia B human plasma (George King Biomedical, Inc.; Overland Park, KS, USA) and aPTT reagent (Trinity Biotech; Bray, Wicklow, Ireland), followed by a 180s incubation period at 37°C. Coagulation was initiated after the addition of 25 mM calcium chloride. Time to clot formation was measured using a STart 4 coagulation instrument (Diagnostica Stago; Parsippany, NJ, USA).

PCR-based genotyping

Primers binding to a sequence upstream of exon 1 unique to the h*F9*mut mini-gene and within a sequence unique to the donor were used to amplify targeting events from genomic DNA. Genomic DNA from mouse liver was isolated using the MasterPure complete DNA purification kit (Epicentre Biotechnologies; Madison, WI, USA). To detect the targeting of the donor cassette via NHEJ or HDR, gDNA was amplified using the P1 (5'ACGGTATCGATAAGCTTGATATCGAATTCTAG3') and P5 (5'GCCCTTCTGGAACTGGACGAACC3') primers binding respectively to a sequence upstream of exon 1 unique to the h*F9*mut mini-gene and within a sequence unique to the donor found in exon 8 of hF9. The PCR reactions were performed using Phusion High-fidelity DNA polymerase (New England BioLabs; Ipswich, MA, USA) in conjunction with GC Buffer and 3% dimethylsulphoxide for 25 cycles (10" denaturation at 98°C, followed by 1'50" of extension at 65°C). The PCR products were then purified with G50 columns, resolved by 5% PAGE and autoradiographed.

Clustered integration site analysis (CLIS)

The mapping of *in vivo* ZFN cleavage sites was performed as previously described[4], using sequencing data from our previous study (Li et al., 2011). For a CLIS to be scored required two integrations within 500bp in all six ZFN treated mice. This analysis revealed nine potential ZFN off-target sites of which four were confirmed by Cel-I assays in adult mice treated with AAV8-ZFN (on target activity observed at >40%).

Surveyor nuclease (Cel-I) assay

Assay was performed as described previously (Doyon et al., 2011; Li et al., 2011). Genomic DNA from mouse liver was isolated using the MasterPure complete DNA purification kit (Epicentre Biotechnologies) and the assay was performed as described previously (Doyon et al., 2011; Li et al., 2011). Loci were amplified for 30 cycles (60 °C annealing and 30" elongation at 68 °C). The following primers were used for Chr.1 (5' GCAGAGAGTTCA GGTCGCCTAGCC 3' and 5' TGAACCAGTCCATCAGCAGGTGAC 3'), Chr.2 (5' TCACCC TGCCTTGTTCCTCTGGA 3' and 5' ACCGAAAGCTCAGGCGGGTA 3'), Chr.6 (5' TGGGAGCGTCATCGTGGGTC 3' and 5' CCGGCAAAGCAAAGAGGTTCGC 3'), Chr.13 (5' TGACAAGGGACGCATCACCCGA 3' and 5' AGGGGCAGTGAAGAGACTCATGTGG 3'), and the h*F9*mut locus (5' CTAGTAGCTGACAGTACC 3' and 5' GAAGAACAGAAGCCTAATTA TG 3').

Liver function tests

Quantification of plasma alanine aminotransferase (ALT) was performed using an ALT colorimetric assay (Teco Diagnostics; Anaheim, CA, USA).

IHC analysis

IHC staining was performed using Ki-67 antibody (abcam ab16667) to stain formalin-fixed, paraffin embedded tissue. Ki67 antibody (Abcam ab16667; Cambridge, UK) was used to stain formalin-fixed, paraffin–embedded tissue. Parraffin was cleared with xylene and slides were rehydrated through descending concentrations of ethanol. Slides were then treated with 3% H2O2/methanol for 30min. Sides were pretreated in a pressure cooker (Biocare medical; Concord, CA, USA) in Antigen Unmasking solution (Vector Labs H3300; Burlingame, CA, USA). Slides were rinsed in 0.1M Tris Buffer then blocked with 2% fetal bovine serum for 15 min. Slides were additionally blocked for endogenous biotin using the avidin biotin blocking kit (Vector Labs SP2001). Slides were then incubated with Ki67 antibody at a 1:400 dilution for 1hr at room temperature. Slides were again rinsed then incubated with biotinylated anti-rabbit IgG 1:200 dilution (Vector Labs) for 30min at room temperature. After rinsing, slides were then incubated with the avidin biotin complex (Vector Labs) for 30 min at room temperature. Slides were then rinsed and incubated with DAB (DAKO Cytomation; Carpinteria, CA, USA) for 10 min. at room temperature. Slides were then rinsed and counterstained with Hematoxylin (Fisher Scientific) for approximately 30 seconds, then rinsed, dehydrated through a series of ascending concentrations of ethanol and xylene, then coverslipped. Stained slides were scanned at 20x magnification using an Aperio ScanScope OS slide scanner. Aperio's Image Analysis Toolkit was used to score a minimum of 90,000 nuclei (Nuclear v9 algorithm) to quantify the percentage of Ki-67+ nuclei.

RT-PCR

Tissues were homogenized in Qiazol and cellular RNA was isolated with miRNeasy Mini kits (Qiagen; Valencia, CA, USA), treated with DNaseI (Life Technologies; Carlsbad, CA, USA) and 1μg reverse-transcribed using the High Capacity RNA-to-cDNA Kit (Life Technologies). PCR was performed using AccuPrime Pfx SuperMix (Life Technologies). The following pairs of primers were used: hF9Fw (5' CCTCATCACCATCTGCCTTT 3'), which anneals to exon 1 within the h*F9*mut genomic locus, and hF9Rv (5' GGGCAGCAGTTACAATCCAT 3'), that anneals to exon 7 in the AAV Donor; Gapdh1 (5' CTCTCAATGACAACTTTGTCAAG 3') and Gapdh2 (5' TCCTTGGAGGCCATGTAGGC 3'). The following cycling conditions were used: 95°C for 10 min, followed by 35 cycles of 95°C for 30", 60°C for 60" and 68°C for 60".

qRT-PCR

qPCR was performed using Ambion's High Capacity RNA-to-cDNA and Fast SYBR Green Master Mix (Applied Biosystems; Foster City, CA, USA) according to manufacturers instructions. The following primers were used: mFATP2-Fw (5' CAACATTCGTGCCAAGTCTC 3'), mFATP2-Rv (5' GACACGGCATCCTTTTTCAG 3'), mFATP2-Mut-Rv (5' TACCTCTTTGGCCGATTCAG 3'). Cycling conditions were: 95°C for 2', followed by 40 cycles of 95°C for 15 s, 60°C for 30".

Statistics

Graphpad Prism was used to perform all the statistical tests. If data passed the D'Agostino & Pearson normality test, then a two-sided t-test was used. Otherwise, the nonparametric Mann-Whitney test (two-tailed) was used. In all tests, $p<0.05$ was considered significant.

Results

Eight week-old h*F9*mut mice (harboring the ZFN target site) were treated with $1x10^{11}$ vg of AAV-ZFN, expressing the h*F9* specific ZFN pair and $5x10^{11}$ vg of AAV-Donor, containing arms of homology flanking the corrective partial cDNA cassette (**Figure 2.1**). Treated animals exhibited long term expression (>60 weeks) of hF.IX averaging 23% of normal (1146±100 ng/mL) at week 60 (**Figure 2.2A**). In contrast, plasma hF.IX levels in mice co-injected with a luciferase expressing AAV-Mock vector and AAV-Donor or mice injected with AAV-ZFN alone were below the limit of detection (15 ng/mL) (**Figure 2.2A**). Treatment of h*F9*mut/HB mice with AAV-ZFN and AAV-Donor produced similarly high hF.IX expression levels (**Figure 2.2B**) and reduced clotting times to those of WT mice (**Figure 2.2C**). Mice aged 7-8 months at initial injection exhibited lower but nonetheless therapeutic levels of hF.IX (**Figure 2.3**). hF.IX expression was derived predominantly from stably integrated, on-target gene correction based on two independent observations. First, following 2/3 partial hepatectomy (PHx), known to induce hepatocyte proliferation and subsequent loss of episomal AAV genomes(Song et al., 2004), plasma hF.IX levels were not reduced (**Figure 2.2D**). Second, treatment of wild-type littermates lacking the h*F9*mut locus (and therefore the ZFN target site) supported just ~50 ng/mL hF.IX (**Figure 2.2E**). As predicted by the use of a liver-specific promoter to drive ZFN expression and the hepatotropism of the AAV8 serotype, hF9 mRNA was exclusively detected in the liver and only when both the ZFN and Donor vectors were administered (**Figure 2.4)**. Proliferation levels in adult mouse liver were confirmed to be low by Ki-67 staining shortly after treatment (**Figure 2.5**). Non-quantitative PCR-based molecular analyses 5 months post injection revealed gene

insertion in the liver through both homology-directed and homology independent processes precisely at the ZFN-specified locus, each of which is predicted to result in hF.IX expression (**Figure 2.2F and Figure 2.6**). We next sought to determine the impact of arms of homology on genome editing. We measured hF.IX levels resulting from treatment of h*F9*mut mice with ZFN and donors containing no substantial homology to the target site, establishing that homology arms are not required for clinically meaningful levels of correction (**Figure 2.7)**. Together these data demonstrate that nuclease-driven gene targeting in the quiescent livers of adult mice via IV administration of AAV vectors results in substantial levels of hF.IX, sufficient to correct the phenotypic defect in hemophilia B mice.

For therapeutic application the risk of ZFN cleavage at off target sites should be minimized. To assay off-target activity we first identified potential cleavage sites using a genome-wide clustered integration site (CLIS) analysis (Gabriel et al., 2011) of 454 deep sequencing data from our previous *in vivo* ZFN study (Li et al., 2011). To identify integration sites attributed to ZFN activity, we compared integration sites in ZFN- versus Mock-treated animals, excluded those common to both groups of mice, which generated a list of nine potential off-target sites in the ZFN-treated mice. Next, using the Cel-I assay (Perez et al., 2008) we confirmed four of these sites as *bona fide* targets of ZFN cleavage in livers of mice treated with AAV-ZFN at week 4 post treatment (**Figure 2.8A**). Since all four cleavage sites mapped to a ZFN target sequence resulting from the homodimerization of one of the two ZFNs we constructed an AAV-ZFN vector employing an obligate heterodimeric FokI architecture containing the ELD:KKR mutations in the dimerization interface between the two ZFNs to reduce cleavage (Doyon et al., 2011).

On target activity was similar for the WT and ELD:KKR ZFNs as measured by the levels of hF.IX expression (**Figure 2.8B**) and cleavage at the h*F9*mut locus at week 4 post treatment (**Figure 2.8C**). In h*F9*mut mice treated with the obligate heterodimeric AAV-ZFN$^{ELD:KKR}$ vector, the levels of off-target cleavage/repair were significantly reduced (relative to AAV-ZFN^{WT} controls) at all sites analyzed (**Figure 2.8A**). Consistent with this reduction in off-target cleavage, the low background levels of hF.IX expression observed in AAV-ZFN^{WT} treated mice that lack the h*F9*mut locus, potentially arising from an integration event on chr2 (**Figure 2.9**), were reduced to below our limit of detection by the ELD:KKR variants (**Figure 2.8D**). Thus, while the use of WT ZFNs appears to be well tolerated, producing stable hF.IX expression over 60 weeks without change in circulating liver enzymes (**Figure 2.2A, Figure 2.10**), these data support the use of the obligate heterodimeric ZFNs which provide an increase in specificity without reducing hF.IX expression.

Discussion

In summary, these data provide the first demonstration of robust *in vivo* genome editing in the context of the predominantly quiescent hepatocytes of adult animals, resulting in complete amelioration of the extended clotting times in HB mice. We observe an approximately 5-fold increase in hF.IX expression compared with our previous study in mice treated as neonates, which could be due to the loss of AAV vector genomes during neonatal liver development and/or differential promoter activity in each group. Alternatively, the difference could reflect increased genome editing activity in adult mice. Importantly, we demonstrate substantial levels of genome editing in the absence of homology arms, which may further expand the utility of this approach by: a) allowing correction of cells unlikely to be amenable to HDR, b) increasing the effective packaging capacity of donor vectors by obviating the need for homology arms, and c) permitting efficient targeting without the need to design donors which incorporate patient specific polymorphisms. Lastly, by using obligate heterodimer FokI nuclease domains we show a marked enhancement in the specificity of ZFN action *in vivo*. Future directions include determining whether the levels of hF.IX observed in this model can be achieved by targeting endogenous loci, which may differ in chromatin status and promoter activity. The findings presented in this study serve to demonstrate the feasibility of genome editing in adult, non-cycling tissues as a potential approach to the treatment of a wide range of monogenic disease

Figure 2.1

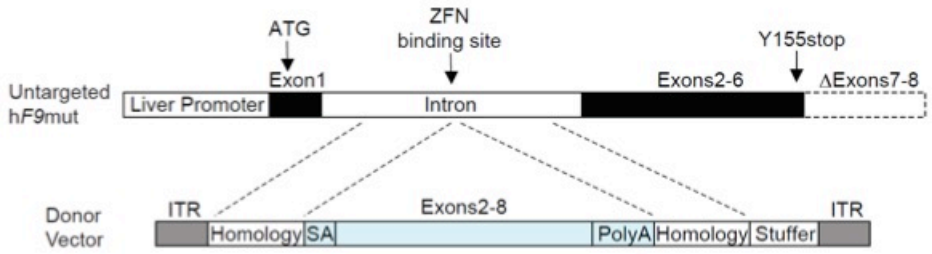

Figure 2.1 Schematic of h*F9*mut mouse model and targeting strategy.

Mouse contains the depicted knock in construct (top) at the Rosa26 locus. The ApoE enhancer/Human alpha-1-antitrypsin promoter drives expression of a truncated human factor 9, devoid of catalytic exons 7-8. Untreated h*F9*mut mice exhibit no detectable hF.IX protein in plasma above the limit of detection (<15ng/mL). Donor vector (bottom) contains a splice acceptor (SA) followed by corrective wild-type exons 2-8 and poly A, flanked by arms of homology to the ZFN target site within intron 1. ZFN mediated targeting of the donor to h*F9*mut intron 1 results in splicing with Exon 1 to produce a wild type transcript.

Figure 2.2

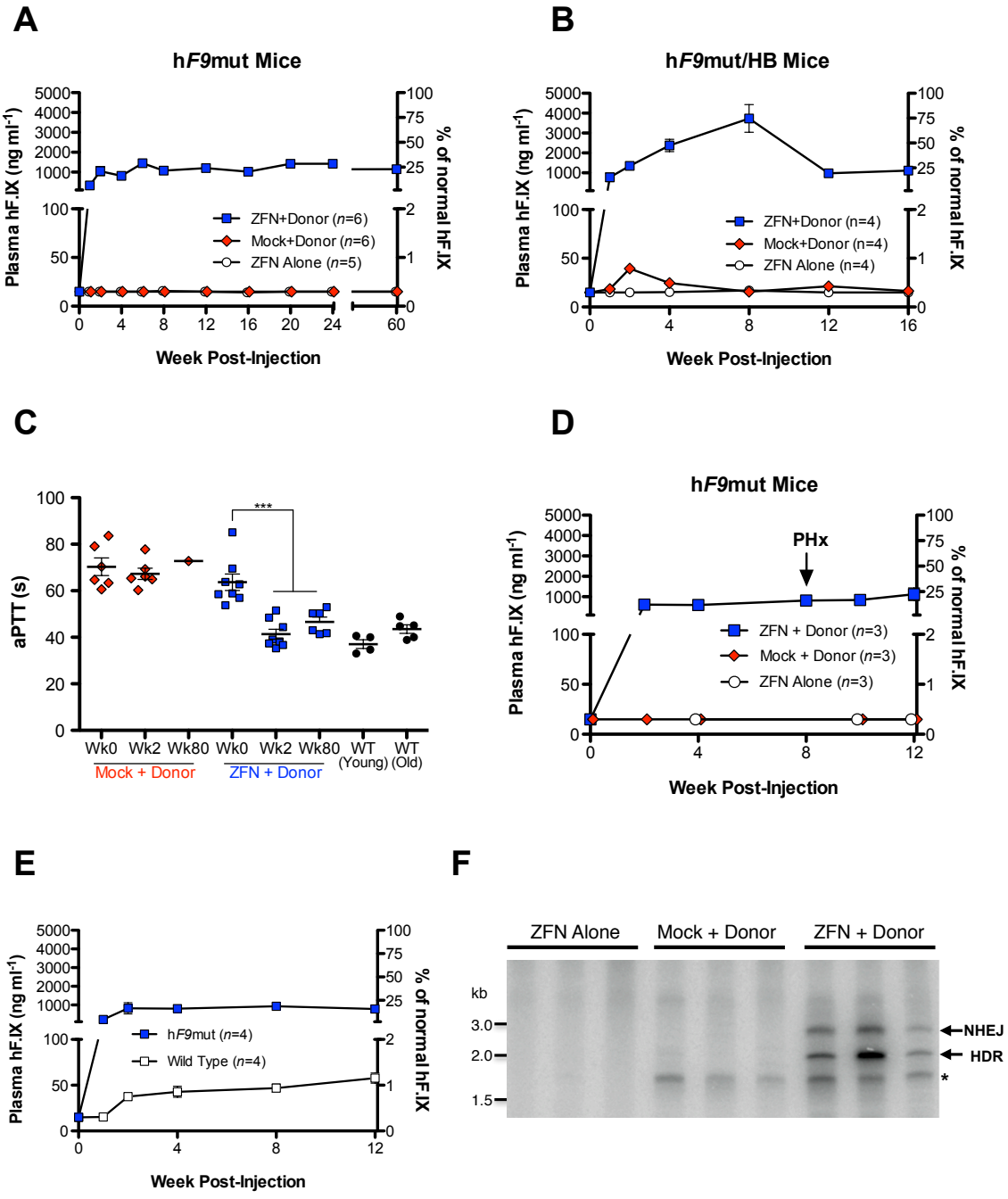

Figure 2.2 *In vivo* gene correction in adult mice results in stable circulating hF.IX levels and correction of clotting times in hemophilic animals.

(**A-B**) Levels of hF.IX in plasma of h*F9*mut (A) and h*F9*mut/HB (B) mice following i.v. injection at week 8 of life with 1 x 10^{11} v.g. AAV8-ZFN alone, 1 x 10^{11} v.g. AAV8-Mock and 5 x 10^{11} v.g. AAV8-Donor, or 1 x 10^{11} v.g. AAV8-ZFN and 5 x 10^{11} v.g. AAV8-Donor. The previously described (Li et al., 2011) h*F9*mut mouse model of human Factor IX deficiency contains a liver specific promoter-driven human coagulation f9 cDNA devoid of necessary catalytic exons 7-8 knocked into the Rosa26 locus. (**C**) Measurement of clot formation by activated partial thromboplastin time (aPTT) prior to, two weeks, and 80 weeks after AAV administration. The aPTT of wild-type mice is shown for comparison. A two-tailed Mann-Whitney test was used to compare two groups. n.s., non-significant. (**D**) Levels of hF.IX in treated mice remain stable following 2/3 Partial Hepatectomy (PHx). (**E**) hFIX expression is over 10-fold greater following AAV8-ZFN and AAV8-Donor treatment in h*F9*mut mice harboring the ZFN target site (h*F9*mut) compared with littermate controls that do not (wild type). (**F**) PCR analysis showing successful gene targeting by both HDR and NHEJ 5 months after i.v. co-injection of ZFN and Donor vectors. PCR products were resolved by 5% PAGE and autoradiographed. See Supplementary Figure 2 for maps. Mice treated with ZFN alone or with Mock and Donor showed no evidence of targeting. Identity of the PCR products was confirmed by sequencing. * Lower band appears in all donor treated samples, which is an artifact apparently generated by the reverse primer and the AAV-ITR resulting in amplification from non-integrated AAV genomes. hF.IX plasma levels were assayed by ELISA and represent repeated measurements, obtained by serial bleeding, on the same group of animals over the time of the study. *n*=number of mice in each cohort. Error bars denote s.e.m. Plasma hF.IX data are representative of at least two independent experiments.

Figure 2.3

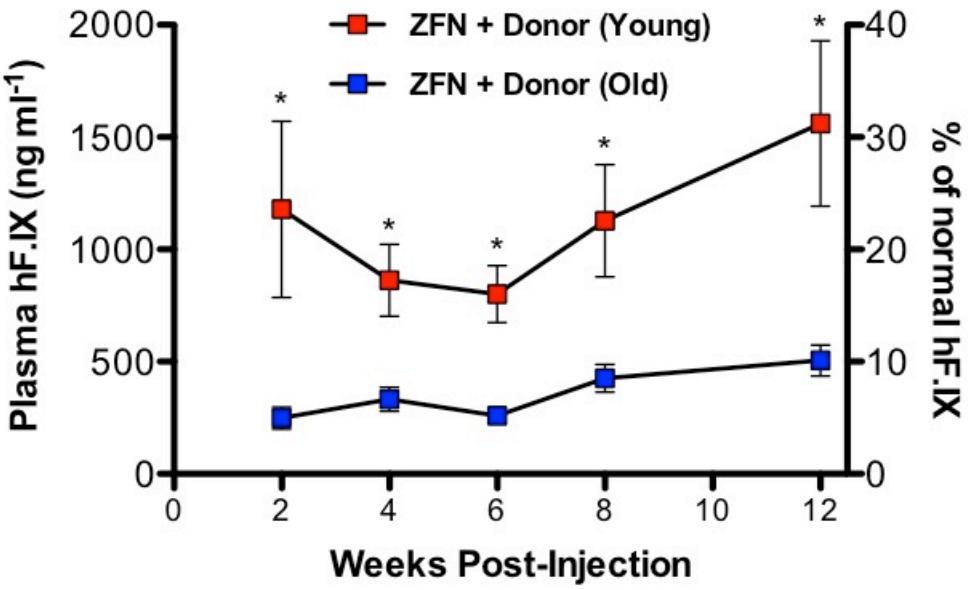

Figure 2.3 *In vivo* genome editing reduced in older mice.

Levels of hF.IX in plasma of h*F9*mut mice following i.v. injection at either week 8 or week 30 of life with 1 x 10^{11} v.g. AAV8-ZFN and 5 x 10^{11} v.g. AAV8-Donor. A two-tailed Mann-Whitney test was used to compare two groups. * $p<0.05$

Figure 2.4

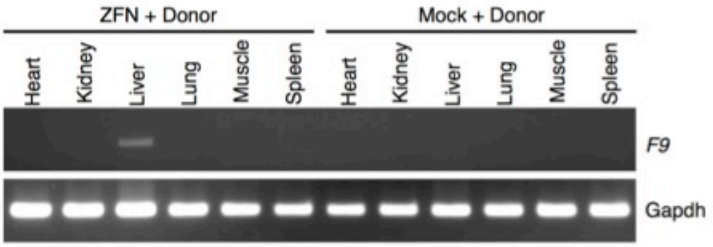

Figure 2.4 Liver-specific hF9 mRNA expression following ZFN-mediated gene targeting.

Total RNA was isolated from tissues, reverse-transcribed and analyzed by PCR. F9 forward primer anneals to Exon 1 within the h*F9*mut genomic locus while F9 reverse primer lands in Exon 8 in the AAV Donor. A unique band corresponding to site-specific genome editing and rescue of wild type factor IX transcript was detected only in livers of mice treated with ZFN and Donor vectors.

Figure 2.5

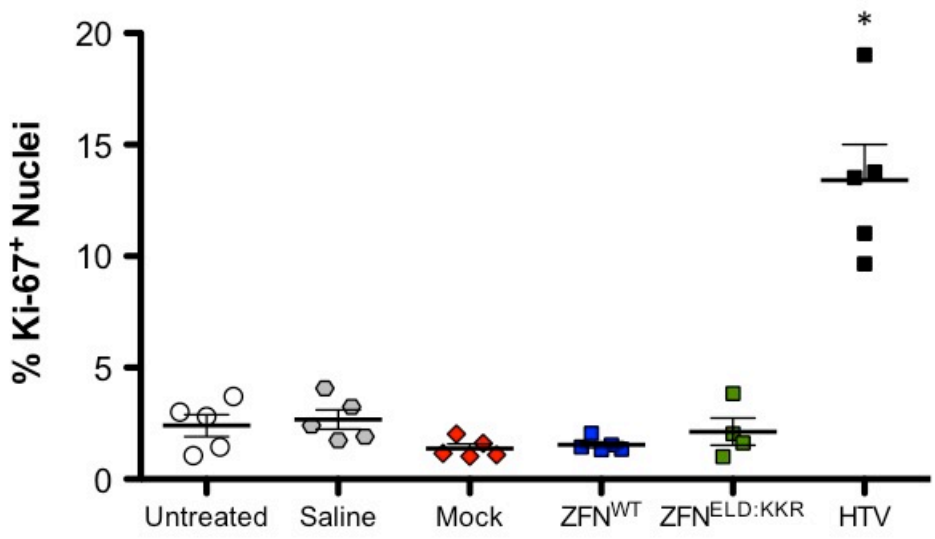

Figure 2.5 Minimal levels of liver cell proliferation in adult mice.

Two days after administration of either saline or $1e^{11}$ vg of AAV-Mock (Luciferase), $1e^{11}$ vg of AAV-ZFN^{WT} or $1e^{11}$ vg of AAV-$ZFN^{ELD:KKR}$, animals were sacrificed and immunostaining for the proliferation marker Ki67 was used to identify replicating liver cells. As a comparison, percentage of $Ki67^{+}$ nuclei in uninjected and hydrodynamically-injected mice is shown. * $p<0.05$ vs. Untreated.

Figure 2.6

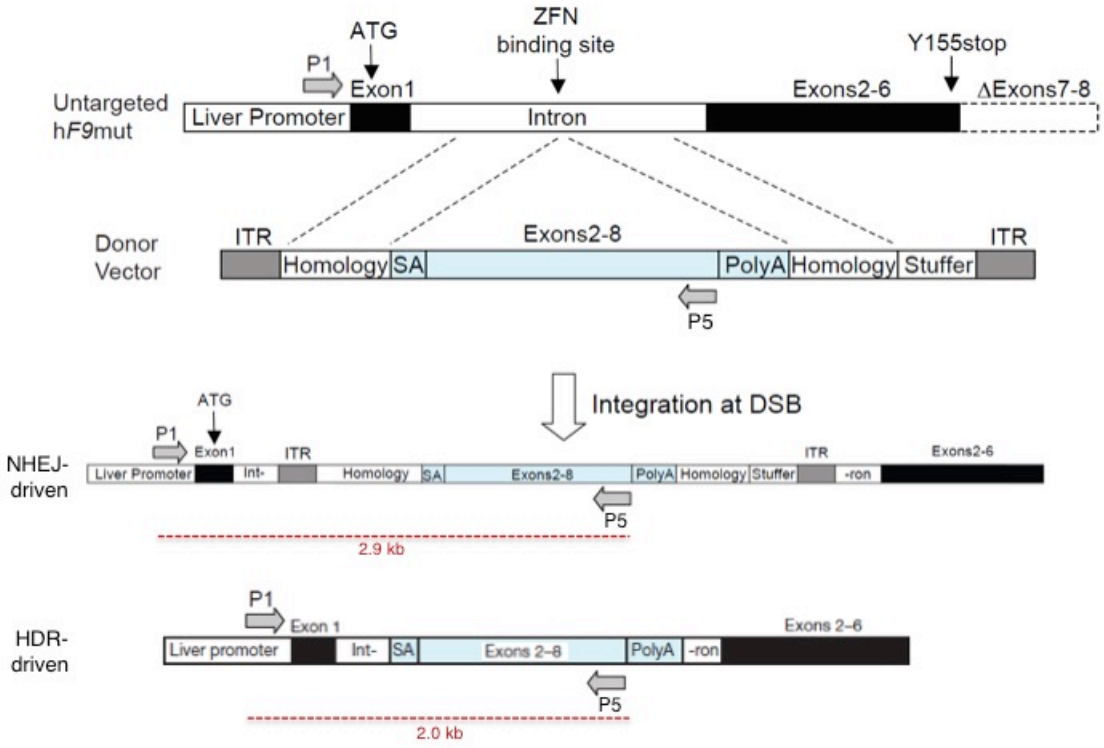

Figure 2.6 Targeted integration of the corrective h*F9* partial cDNA cassette.

Genotyping using primers P1 and P5 allow the detection of integration events occurring via homology-directed repair or end-capture of the AAV donor genome at the ZFN cleavage site.

Figure 2.7

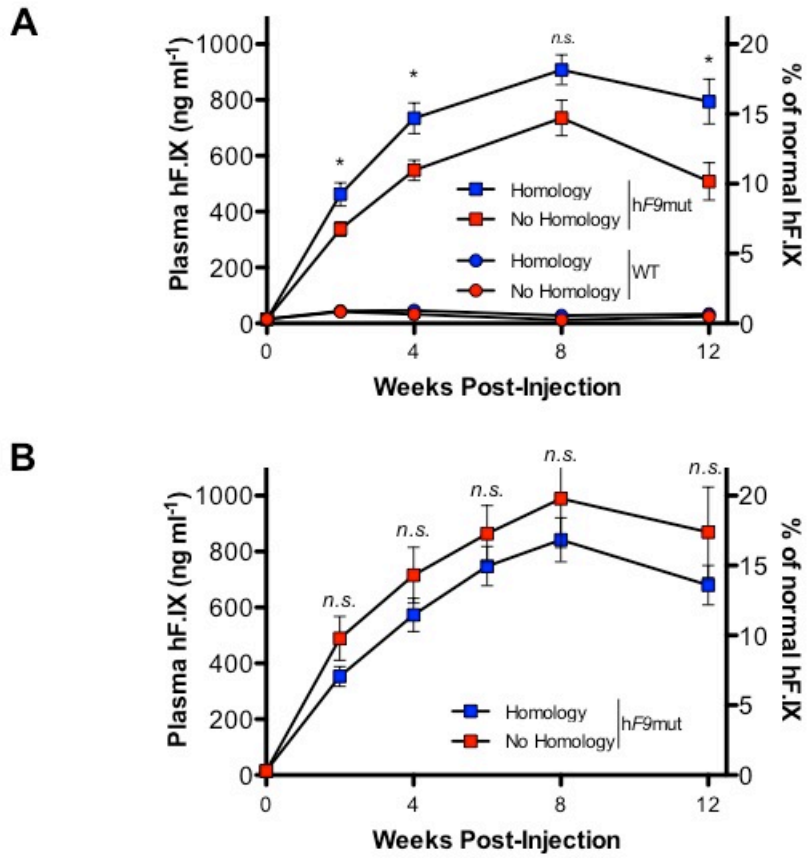

Figure 2.7 Homology arms in the donor vector are not required to achieve robust levels of genome editing.

(A) Levels of hF.IX in plasma of h*F9*mut and wild type mice following i.v. injection at week 8 of life with 1 x 10^{11} v.g of AAV8-ZFN and 5 x 10^{11} v.g. of either AAV8-Donor containing arms of homology to the ZFN target site (human F9 intron 1) or AAV8-Donor containing arms without substantial homology†. (B) Levels of hF.IX in plasma of h*F9*mut mice following i.v. injection at week 8 of life with 1 x 10^{11} v.g of AAV8-ZFN and 5 x 10^{11} v.g. of either AAV8-Donor containing arms of homology to the ZFN target site or AAV8-Donor with "irrelevant" arms‡ with homology to mouse albumin intron 1. The F9 coding

sequence (identical in all 3 donor vectors) was modified and synthesized by GeneArt, optimizing codon usage, G/C content, secondary structures, alternative open reading frames, and cryptic splice sites. † Derived from canine F9 intron 1: Left arm, <5% homology; right arm, <70% homology. ‡ Both arms have less than 5% homology to the ZFN target locus.

Figure 2.8

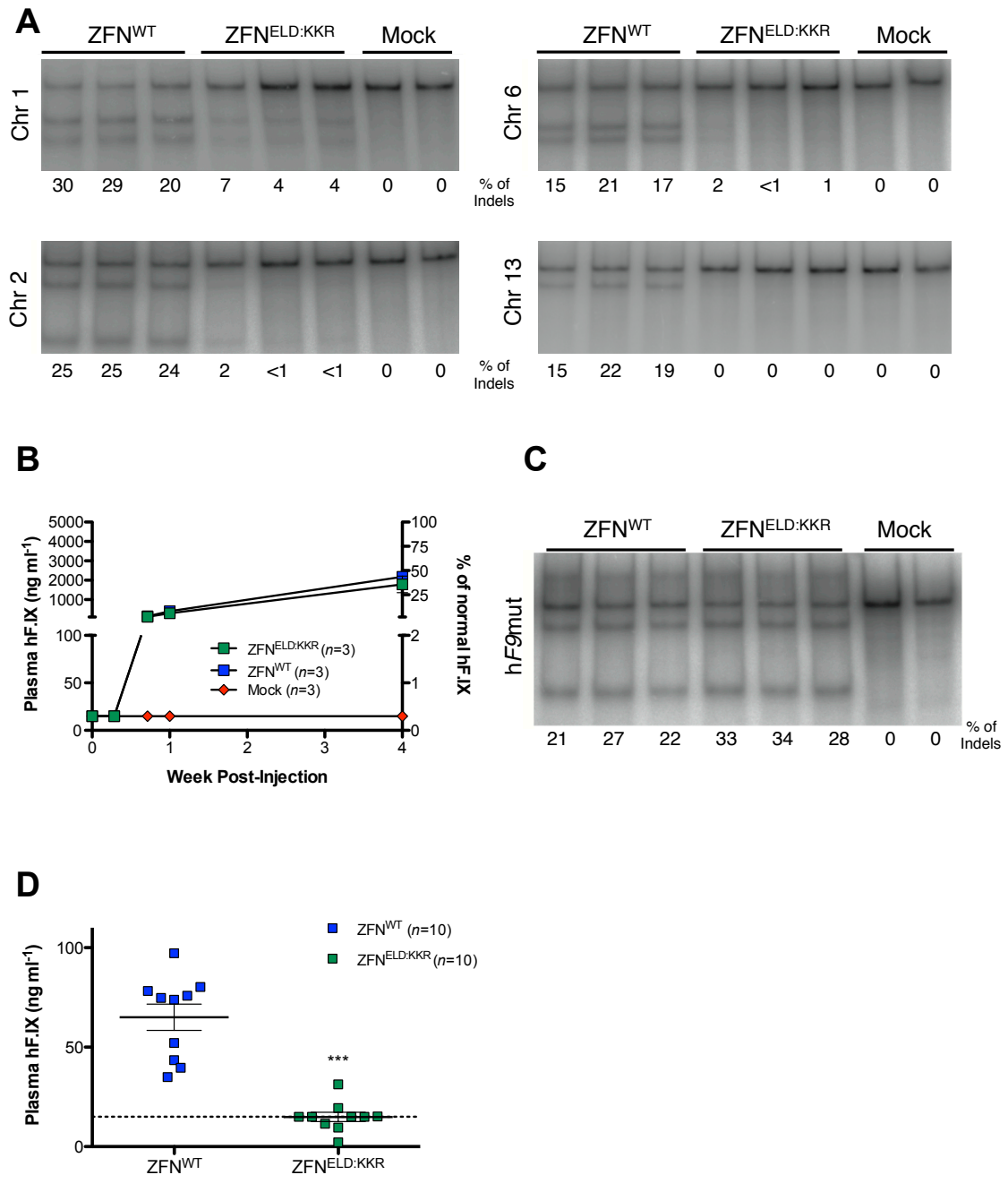
A
ZFN^WT
ZFN^ELD:KKR
Mock
Chr 1
30 29 20 7 4 4 0 0
% of Indels
Chr 6
15 21 17 2 <1 1 0 0
Chr 2
25 25 24 2 <1 <1 0 0
Chr 13
15 22 19 0 0 0 0 0
B
Plasma hF.IX (ng ml-1)
% of normal hF.IX
ZFN^ELD:KKR (n=3)
ZFN^WT (n=3)
Mock (n=3)
Week Post-Injection
C
hF9mut
21 27 22 33 34 28 0 0
D
ZFN^WT (n=10)
ZFN^ELD:KKR (n=10)
***

Figure 2.8 Obligate heterodimer ZFNs reduce off-target cleavage *in vivo* while preserving equivalent levels of hF.IX secretion.

(**A**) Cel-I cleavage at the 4 validated off targets identified by clustered integration site analysis 4 weeks after treatment with 5 x 10^{11} v.g. AAV8-Donor and either 1 x 10^{11} v.g. AAV8-ZFN^{WT}, 1 x 10^{11} v.g. AAV8-ZFN$^{ELD:KKR}$ or 1 x 10^{11} v.g AAV8-Mock. (**B**) Plasma hF.IX levels following treatment. (**C**) On-target cleavage measured by Cel-I assay 4 weeks after AAV injection. (**D**) hF.IX expression in wild type mice lacking ZFN target site 5 weeks after injection of 5 x 10^{11} v.g. AAV8-Donor and either 1 x 10^{11} v.g. AAV8-ZFN^{WT} or 1 x 10^{11} v.g. AAV8-ZFN$^{ELD:KKR}$. hF.IX plasma levels were assayed by ELISA. Two-tailed t-test was used. *** $p<0.0001$ compared with ZFN^{WT}. *n*=number of mice in each cohort. Error bars denote s.e.m. Frequency of ZFN-induced insertions and deletions is indicated as '% of Indels' below each lane. Each lane represents an individual mouse. Plasma hF.IX data are representative of at least two independent experiments.

Figure 2.9

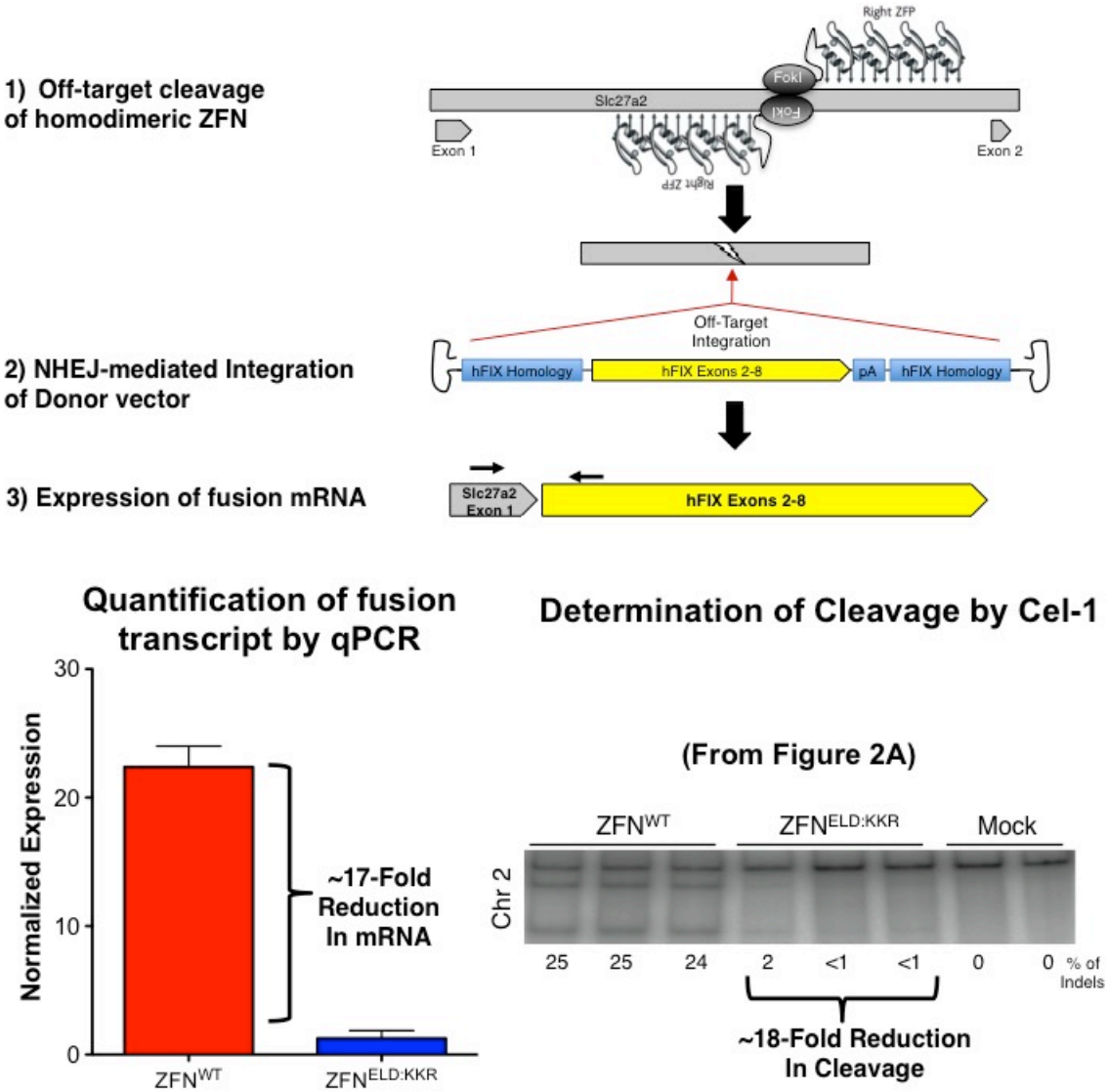

Figure 2.9 Putative mechanism of hF.IX expression in WT mice.

Detectable hF.IX in wild type mice may result from donor integration into one of the predominant off-target cleavage sites in mouse chromosome 2. The integration site is located in the first intron of a gene encoding FATP-2 (Fatty acid transport protein 2), which is expressed in liver and is predicted to splice in frame with the donor cDNA. Exon

1 of FATP-2, a transmembrane protein, could provide a signal peptide upon splicing with the hF9 Exon 2-8 donor, supporting some secretion of the fusion protein. We quantified this “fusion transcript” in mice treated with the wild type ZFN at a frequency ~17x higher than in mice treated with identical doses of the obligate heterodimer. These data are consistent with results shown in Figure 2.8A (chr2 panel).

Figure 2.10

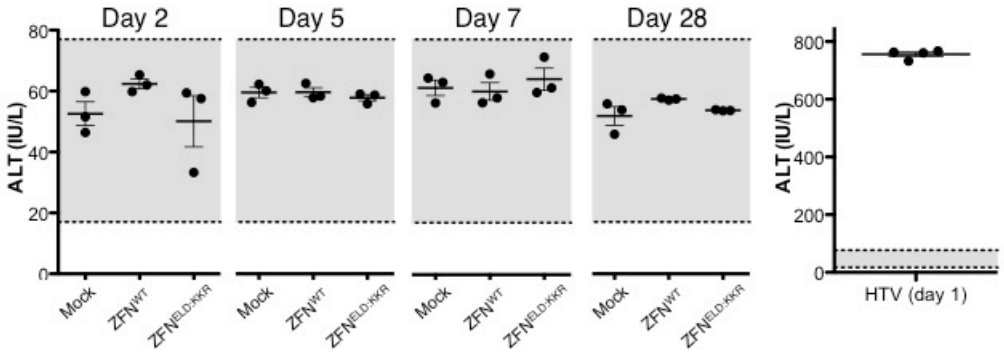

Figure 2.10 Comparison of alanine aminotransferase in mice treated with Mock, ZFN^{WT} and ZFN$^{ELD:KKR}$.

Plasma ALT values following treatment did not deviate from normal range (shaded area) in any of the groups. ALT levels 24 hours following hydrodynamic tail vein (HTV) injection are shown for comparison (right panel).

CHAPTER 3: IN VIVO GENOME EDITING OF THE MURINE ALBUMIN LOCUS AS A PLATFORM FOR PROTEIN REPLACEMENT THERAPY

This work is currently under review for publication.

Summary

Site specific editing of the genome is a promising approach to achieving long-term, stable therapeutic gene expression. This has been successfully applied in a variety of preclinical models, generally focused on targeting of the diseased locus itself; however, limited targeting efficiency or insufficient expression from the endogenous promoter may impede the translation of these approaches, particularly if the desired editing event does not confer a selective growth advantage. Here we report a general strategy for liver-directed protein replacement therapies that addresses these issues: Zinc Finger Nuclease (ZFN)-mediated site-specific integration of therapeutic transgenes within the albumin gene. Employing adeno-associated viral vector (AAV) delivery *in vivo*, we achieved long-term expression of human factors VIII and IX (hF.VIII and hF.IX) in mouse models of hemophilia A and B at therapeutic levels. Using the same targeting reagents in wild type mice, we expressed lysosomal enzymes that are deficient in Fabry and Gaucher diseases, as well as in Hurler and Hunter syndromes. The establishment of a universal nuclease-based platform for secreted protein production would represent a critical advance in the development of safe, permanent, and functional cures for diverse genetic and non-genetic diseases.

Introduction

Adeno-associated viral (AAV) vectors are showing great promise in clinical trials to deliver therapeutic genes for treatment of monogenic disorders (Bennett et al., 2012; Nathwani et al., 2014). For gene delivery to the liver, the standard approach is to deliver an expression cassette that persists primarily in the form of extra-chromosomal episomes. Episomal expression faces two major limitations: (1) dilution of expression in proliferating cells, and (2) restricted packaging capacity of the AAV vector. Site-specific integration of a corrective donor cassette allows therapeutic gene expression to persist through cell divisions, and increases the effective carrying capacity of the vector by obviating the need for enhancer/promoter elements within the corrective donor.

Genome editing has been successfully applied in a variety of preclinical models, both *ex vivo* and *in vivo* (Genovese et al., 2014; Li et al., 2011; Lombardo et al., 2007; Perez et al., 2008; Yin et al., 2014). Historically, the efficiency of gene specific editing in mammalian cells has been very low, limiting its therapeutic potential. The targeting process is known to be greatly enhanced (100-1000 fold) by the induction of a DNA double strand break at the target site (Porteus et al., 2003; Rouet, Smih, & Jasin, 1994b). The development of customized DNA cleaving enzymes, such as ZFNs, has made it possible to achieve far greater genome editing efficiencies. ZFNs function as dimers by coupling DNA binding motifs from transcription factors with the FokI endonuclease domain to generate double stand breaks at their target site.

A typical genome editing approach is to target the disease locus itself; however, the proportion of alleles targeted may not express sufficient levels of protein to alleviate

the disease phenotype. Alternatively, integration into a locus with high transcriptional activity (“safe harbor”) would address this limitation and provide a versatile platform to express various proteins, substituting the donor for each respective therapeutic transgene.

For our studies, the albumin locus was chosen as the genomic harbor due to its very high expression level and the tractability of liver for gene delivery and *in vivo* editing, relative to other tissues. In addition, the albumin gene structure is well suited for transgene targeting into intronic sequences as its first exon encodes a secretory peptide that is cleaved from the final protein product. By analogy to our previous work on hF9 (Anguela et al., 2013; Li et al., 2011), we reasoned that integration of a promoterless cassette bearing a splice acceptor and therapeutic transgene would support expression and secretion of many different proteins, as signal peptides are often functionally interchangeable (Gierasch, 1989; Tan, Ho, & Ding, 2002).

Materials and Methods

Animal experiments

AAV vector was diluted to 200 μl with PBS + 0.001% Pluronic F68 before tail-vein injection. Plasma for hF.IX ELISA was obtained by retro-orbital bleeding into heparinized capillary tubes. Plasma for aPTT was obtained by tail bleeding, 9:1 into 3.8% sodium citrate. Tissue for nucleic acid analysis was immediately frozen on dry ice after necropsy. Wild type C57BL6 mice were purchased from the Jackson Laboratory. Hemophilia B and Hemophilia A/CD4 null mice have been previously described (Anguela et al., 2013; Siner et al., 2013). Minimum sample sizes were determined by estimating mean values and standard deviations based on previous in vivo ZFN studies, using an alpha value of .05 and a power of .80. Randomization and blinding were not conducted.

ZFN reagents and targeting vectors

Heterodimeric ZFNs targeting the mAlb locus contain the ELD:KKR mutations to the FokI domain (Doyon et al., 2011). The promoter-less hF9 donor vector, containing a cDNA cassette with exons 2-8 of the hF9 gene, has been previously described (Anguela et al., 2013). All the hF8 donors carry a splice acceptor sequence derived from the hF9 gene followed by a B-domain-deleted F8 cDNA (devoid of the first 57 nucleotides encoding the signal peptide). hF8 Donor 1 contains the SQ amino acid sequence(Lind et al., 1995) and was codon optimized by DNA2.0. hF8 Donor 2 was codon optimized and contains a putative glycosylation sequence and a shorter polyA sequence as described (McIntosh et al., 2013) (summarized in Figure 3.5A). hF9 and hF8 donors do not contain

arms of homology to the target site. The donors used in Figure 3 carry a hF9 splice acceptor sequence followed by the cDNA encoding for α-galactosidase A, acid β-glucosidase, α-L-iduronidase and iduronate-2-sulfatase, respectively. These donors contain arms of homology of approximately 600bp to the mouse albumin target site. AAV8 vectors were produced and titered as previously described (Ayuso et al., 2009; Wright & Zelenaia, 2011). Sequences of mAlb-targeted ZFNs are provided in Figure 3.10.

Factor IX antigen and activity

Human factor IX ELISA kit (Affinity Biologicals) was used to quantify plasma hF.IX. All readings below the last value of the standard curve (15 ng/ml) were arbitrarily given the value of 15 ng/ml. hF.IX activity levels in citrated mouse plasma were determined using chromogenic assay (Aniara, A221802).

hF.VIII activity and aPTT assay

Coagulant activity of hF.VIII in citrated mouse plasma was determined by Coatest SP4 F.VIII (Chromogenix). The aPTT assay was performed by mixing sample plasma 1:1:1 with pooled hemophilia B (Figure 3.1F) or Hemophilia A (Figure 3.7B) human plasma (George King Biomedical, Inc) and aPTT reagent (Trinity Biotech), followed by a 180s incubation period at 37°C. Coagulation was initiated after the addition of 25 mM calcium chloride. Time to clot formation was measured using a STart 4 coagulation instrument (Diagnostica Stago).

Western blot analysis of liver homogenates

Western blot detection from liver homogenates was carried out thirty days after treatment. Highly abundant proteins (albumin and IgG) were depleted from liver homogenates in RIPA buffer. Primary antibodies: IDUA (MAB4119, R&D Systems, 1:1000), IDS (MAB2449, R&D Systems, 1:500), GLA (12078-R001, Sino Biological, 1:1000), GBA (sc-100544, Santa Cruz, 1:500). Secondary antibodies were from Santa Cruz (Mouse, sc-2005; Rabbit, sc-2004).

Surveyor nuclease (Cel-I) assay

Genomic DNA from mouse liver was isolated using the MasterPure complete DNA purification kit (Epicentre Biotechnologies) and the assay was performed as described previously (Doyon et al., 2011; Li et al., 2011). Loci were amplified for 30 cycles (60 °C annealing and 30" elongation at 68 °C). The following primers were used to detect DNA cleavage at the albumin locus: (5' CCT GCT CGA CCA TGC TAT ACT 3' and 5' CAG GCC TTT GAA ATG TTG TT 3').

RT-PCR and quantitative PCR

Reverse transcription followed by qPCR was performed using Ambion's High Capacity RNA-to-cDNA and Fast SYBR Green Master Mix (Applied Biosystems) according to manufacturers' instructions. The following primers were used: mAlb Fw1 (5' tgggtaacctttctcctcctc 3') with mAlb Rv (5' gggaaaaggcaatcaggact 3') and mAlb Fw2 (5' gtctccggctctgctttttc 3') with hF9 Rv (5' caggattttgttggcgtttt 3'). Cycling conditions were: 95 °C for 2 min, followed by 40 cycles of 95 °C for 15 s, 60 °C for 30 s. The delta-delta-Ct method (2-ΔΔCt) described by Livak (Livak & Schmittgen, 2001) was used to relatively quantitate the expression of the transcripts of interest.

In vitro AAV transduction of primary human hepatocytes

48-well cell culture dishes (Lifetech, CM1048) were either purchased pre-coated, or plates (VWR, 3548) were coated with a mixture of 250 μl BD Matrigel (BD Biosciences) in 10 ml hepatocytes basal medium (HBM from Lonza, CC-3199) (150 μl per well). Plates were incubated for 1 hour at 37°. Thawing/plating media was prepared by combining 18 ml InVitroGRO CP medium (BioreclamationIVT) and 400 μl Torpedo antibiotic mix (Celsis In Vitro Technologies). Once the plates were prepared, the female plateable human hepatocytes, (lot# AKB cat# F00995-P) were transferred from the liquid nitrogen vapor phase directly into the 37° water bath. The vial was stirred gently until the cells were completely thawed. The cells were transferred directly into a 50 ml conical tube containing 5 ml of pre-warmed thawing/plating medium. To transfer cells completely, the vial was washed with 1 ml of thawing/plating medium. The cells were resuspended by gently swirling the tube. A small aliquot (20 μl) was removed to perform a cell count and to determine cell viability using trypan blue solution, 1:5 (Cellgro, 25-900-C1). The cells were then centrifuged at 75 x g for 5 minutes. The supernatant was decanted completely and the cells were resuspended at $1x10^6$ cells/ml. The matrigel mixture was aspirated from the wells and cells were seeded at $2x10^5$ cells/well in a 48 well dish. Cells were then incubated in 37°C/5% CO2 incubator. At the time of transduction, cells were switched to maintenance medium HCM (HBM from Lonza, CC-3199 and HCM SingleQuots, CC-4182). AAV6 particles were diluted in HCM medium and added to cells at indicated MOI. Transfection of mALB ZFN mRNA was carried with Lipofectamine RNAiMAX (Lifetech). After 24h the medium was replaced by fresh HCM

medium, which was done daily to ensure maximal health of the primary hepatocyte cultures. For experiments where hF.IX detection by ELISA was required, the medium sometimes was not exchanged for several days to accumulate hF.IX in the supernatants.

Indel detection using next-generation sequencing

Loci were PCR amplified from genomic DNA, and the levels of modification determined by paired-end deep sequencing on an Illumina MiSeq. Paired sequences were merged via SeqPrep (John St. John, https://github.com/jstjohn/SeqPrep, unpublished). Merged FASTQ reads were filtered on the following criteria: quality score >= 15 at all positions; the 5' and 3' terminal 23bp must match the expected amplicon exactly; the read must not map to a different locus in the target genome as determined by Bowtie2 with default settings (Langmead and Salzberg, Nat Methods. 2012 Mar 4; 9(4): 357–359); deletions must be <70% of the amplicon size or <70bp long. Filtered sequences are then aligned to the expected sequence using the Needleman-Wunsch algorithm with penalties set to prioritize single insertions or deletions. Contiguous gaps in either the target or query alignment were counted as indels. PCR primers for mouse Albumin locus (adapter regions are bracketed):

mALB-MQ-I1-Fwd3

5' [ACACGACGCTCTTCCGATCT] NNNN GTT TGA ATG CAC AGA TAT AAA CAC 3'

mALB-MQ-I1-Back3

5' [GACGTGTGCTCTTCCGATCT] NNNN GTA ATA TGC TGC TTT TTG TTC TTC 3'

For the analysis of off target activity, genomic DNA was isolated from mouse liver 30 days after transduction with mALB ZFNS and GBA donor (Figure 3.8D, animal 22) or from control mouse injected with formulation buffer. ZFN activity was determined by deep sequencing at either on-target (mouse Albumin) or off-target (Rank 1-40 off-target sites as predicted by SELEX profile of mALB ZFNs) sites for both the PBS control and the ZFN + Donor treated animal. Loci were PCR amplified from genomic DNA, and the levels of modification determined by paired-end deep sequencing on an Illumina MiSeq, as described above. To control for sequence-specific MiSeq and PCR-induced indels, control samples were compared to treated samples. Control sample alignments were visually inspected to ensure no treated sample PCR contamination was present. All indels encountered in an alignment were considered when binning the read into an indel type if more than one was present. Indel types shared between control and treated samples were excluded from further analysis. After removal of indel types, the statistical test described in Pattanayak et al. (Nature Methods 2011) was applied to the number of sequences scored as indels and the total number of sequences for both the ZFN treated sample and the cognate control (Pattanayak, Ramirez, Joung, & Liu, 2011). Loci with p-values < 0.05 (adjusted for multiple comparisons with a Bonferroni correction) were considered significant.

Statistics

Graphpad Prism was used to perform all statistical tests. For comparisons with groups in which values were unmeasurable (below limit of detection), a two-sided Fisher's exact test was used. If data passed the D'Agostino & Pearson normality test, a

two-sided t-test was used. Otherwise, the nonparametric Mann-Whitney test (two-tailed) was used. In all tests, $p<0.05$ was considered significant.

Results

As an initial test of the feasibility of the strategy outlined in **Figure 3.1A**, we transduced human primary hepatocytes with an AAV6 vector containing the human factor 9 (hF9) donor sequence together with transfection of mRNA encoding a ZFN pair targeting a site within the first intron of human albumin. Hepatocytes treated with donor and ZFNs exhibited measurable hF.IX in the culture supernatant (**Figure 3.2**).

We next sought to demonstrate this approach *in vivo* in the mouse. To accomplish this, we first engineered a ZFN pair targeting an analogous site in mouse albumin (mAlb) intron 1 and confirmed its activity *in vitro* in murine hepatoma cells (**Figure 3.3A**). Next, we assessed activity *in vivo* via tail vein injection of eight-week-old, C57BL/6 mice with $1x10^{11}$ vg of an AAV8 vector encoding the ZFN pair (AAV8-ZFN) followed by Cel-I assay of the target albumin locus from liver genomic DNA, seven days post vector administration. We observed cleavage at frequencies ranging from 12% to 17% (**Figure 3.1B**), indicative of small insertions and deletions (indels) characteristic of break repair by non-homologous end-joining (NHEJ). This result demonstrated that these ZFNs can efficiently cleave their endogenous target in the livers of adult mice and established their suitability for studies of the albumin locus for therapeutic transgene expression.

Hemophilia B represents an ideal disease for a liver-directed genome editing strategy as modest levels of hF.IX activity (>1% of normal) can greatly ameliorate the disease phenotype. To determine whether ZFN-mediated insertion of a hF9 therapeutic donor could yield stable hF.IX expression, we treated wild type mice with $1x10^{11}$ vg of

AAV8-ZFN and $5x10^{11}$ vg of AAV8-hF9-Donor, where the donor construct encoded a promoterless hF9 cassette containing exons 2-8 of the hF9 gene flanked by a splicing acceptor signal and a poly A sequence (Anguela et al., 2013; Li et al., 2011). Consistent with ZFN-driven targeted integration, mice receiving the hF9 donor and the mAlb-targeted ZFNs exhibited high circulating human hF.IX levels (>3000 ng/mL; **Figure 3.1C**). Our protocol was well tolerated, and follow up studies revealed stable hF.IX expression levels (>1 year; **Figure 3.3B**) as well as no significant alterations in levels of serum alanine aminotransferase (**Figure 3.3C**) or plasma albumin (data not shown). Although substantial levels of h.FIX were obtained, the hybrid mAlb-hF9 mRNA represented a small fraction (0.5%) of total wild type mAlb transcript, as determined by RT-qPCR analysis on liver-extracted RNA samples. This indicates only a small fraction of hepatocytes need to be modified in order to achieve high levels of hF.IX in the blood (**Figure 3.3D**). We also demonstrated that hF.IX levels could be adjusted by varying the dose of AAV. At a fixed 1:5 ratio of ZFN to donor, transgene expression was proportional to the AAV dose within a range of over 2 orders of magnitude, yielding ~ 100 to 15000 ng/mL of hF.IX two weeks post treatment (**Figure 3.1D**).

Our strategy relies on splicing between albumin exon 1 and the integrated donor and is predicted to create a hybrid mRNA, resulting in the substitution of a novel tripeptide for the two amino terminal residues of the hF.IX pro-peptide. However, once processed, the resulting mature polypeptide should be identical to wild type hF.IX (**Figure 3.4A**). To test whether these substitutions affected enzyme function, we assessed clotting activity in hemophilia B mice. We observed a correction of the hemophilic phenotype in mice treated with AAV8-ZFN and AAV8-hF9-Donor as

measured by activated partial thromboplastin time (aPTT) (**Figure 3.1E, F**). Using a chromogenic activity assay, we then confirmed that the F.IX enzymatic activity in plasma correlated with the antigen levels with a 1:1 ratio (**Figure 3.4B**), indicating that the activity of the mature protein is not compromised. Collectively, these data show that long-term corrective levels of hF.IX can be achieved following a single treatment with ZFN and therapeutic donor vectors.

One of the main advantages of our targeting strategy is that it allows production of any secretable protein without the need to change the ZFN reagent for each specific disease. In order to test the generality of the approach, we pursued a similar strategy for therapeutic expression of hF.VIII in a mouse model of hemophilia A (HA/CD4null). The use of hemophilia A mice in a CD4null background allowed us to measure circulating human hF.VIII without interference from neither endogenous mouse F.VIII nor the development of inhibitors against the human exogenous protein. As the length of the coding sequence for this gene (7kb) substantially exceeds the packaging capacity of AAV (~4.7kb) an important aspect of these studies involved reducing the donor size to a length approaching this threshold. Accordingly, our donor encoded a truncated hF.VIII variant that has also been engineered for reduced size and more efficient expression(McIntosh et al., 2013). The resulting donor is summarized in **Figure 3.5** ("hF8 Donor 2"). To increase integration activity further, we also delivered ZFNs individually using separate vectors (rather than a single vector encoding a dual expression cassette), since in a preliminary study this yielded a >3-fold increase in ZFN potency *in vivo* at equivalent vector doses (**Figure 3.6**). Combining these improvements to ZFN and Donor design, injection of $5x10^{10}$ vg of each individual AAV8-mAlb-ZFN and

$1x10^{11}$ vg of AAV8-hF8-Donor 2 resulted in hF.VIII activity levels of 37 ± 5.5% of normal (**Figure 3.7A**). Of note, the wild type F.VIII protein does not contain a propeptide whereas the predicted hybrid mAlb-FVIII fusion will contain the murine albumin propeptide at the N-terminus. In order to demonstrate full functionality of the mature hF.VIII protein *in vivo*, we performed an aPTT assay in mice treated with AAV8-hF8-Donor 2 and either AAV8-ZFN or AAV8-Mock vectors. Importantly, the observed hF.VIII levels were able to correct the aPTT in treated hemophilia A animals (**Figure 3.7B**), demonstrating that *in vivo* genome editing targeting the albumin locus is able to restore hemostasis in mouse models of both hemophilia A and B.

Liver-directed gene transfer is attractive for the treatment of lysosomal storage diseases due to the liver's ability to secrete large amounts of protein into the blood and the ability of many lysosomal enzymes to be taken up by cells in the periphery ("cross correction (Fratantoni, Hall, & Neufeld, 1968)." It is anticipated that treatment of these progressive diseases as early as possible will provide the greatest therapeutic benefits. However, long term expression following conventional, predominantly non-integrating, AAV administration in young patients may be compromised due to episomal dilution as hepatocytes divide (L. Wang, Wang, Bell, McMenamin, & Wilson, 2012). Integration of a donor into the albumin locus could potentially address this limitation. We treated adult wild-type mice with AAV8-ZFN and four donors encoding either human α-Galactosidase A, ß-Glucosidase, Iduronate-2 Sulfatase, or α-L-Iduronidase i.e. the genes which are deficient in patients with Fabry, Gaucher, Hunter, and Hurler's disease/syndromes, respectively. Wild type mice were treated with $1x10^{11}$ vg of AAV8-ZFN and $1x10^{11}$ or $5x10^{11}$ vg of AAV8-Donor for each transgene as indicated (**Figure 3.8A-D**). Four weeks

following administration, all four lysosomal enzymes were detectable by Western blot in liver lysates of treated mice. Overall, these data provide a proof of principle demonstrating the versatility of albumin as a targeting platform for various transgenes in multiple species.

Finally, in order to measure ZFN off-target activity *in vivo* we performed deep sequencing analysis on genomic DNA from animals treated with vehicle only or AAV8-ZFN and the GBA Donor (**Figure 3.8D**, animal 22). We quantified rates of insertions and deletions (indels) in the top 40 off-target sites predicted by SELEX analysis of mAlb-ZFN binding both as homodimers and heterodimers. The on-target activity of the ZFN pair was 31.4% whereas only 11 out of 40 potential off-target sites exhibited measurable cleavage activity between 0.12 – 1.92% (**Figure 3.9**). This results in an on-target to off-target ratio between 16:1 and 262:1. Of the 11 off-target sites, 8 were mapped to introns of annotated genes while the other 3 sites were found in intergenic regions. While these results illustrate the high specificity of the mAlb ZFN pair used in this study, it is important to note that the safety evaluation of the final optimized reagents for clinical trials should not be reduced to the absolute specificity of cleavage. As seen in clinical trials, patterns of integration are difficult to predict from non-human genomes, and safety concerns are highly dependent on the exact nature of the target locus and transgene that is inserted. These reagents have only been optimized to a certain degree and clinical application of ZFNs will undoubtedly benefit from further refinement to achieve the highest possible safety profile.

Discussion

Recent clinical trials using AAV-mediated gene transfer have highlighted the tremendous potential of gene therapy (Bennett et al., 2012; Nathwani et al., 2011). However, an unanswered question is whether episome-derived liver expression will be sustained in a setting of substantial liver proliferation, as in pediatric patients (the liver quadruples in size during the first 4-5 years of development (Stocker, Dehner, & Husain, 2012)) or those with liver disease (e.g. hepatitis and/or cirrhosis). For these cohorts, site-specific integration of the transgene to avoid AAV dilution and loss of expression could be especially beneficial. We have previously shown that *in vivo* genome editing can be applied successfully with therapeutic benefit in an engineered Rosa26 locus (Anguela et al., 2013; Li et al., 2011). Here, we demonstrate this is not a phenomenon limited to a uniquely recombinogenic region, with insertion of a variety of transgenes into the endogenous albumin locus of wild-type C57Bl/6 mice.

In the specific context of in vivo gene targeting, where corrected cells may not be able to be positively selected, targeting of a limited number of cells may not result in optimal amounts of secreted protein to correct a disease phenotype. In addition, targeted integration of a therapeutic transgene may not be a viable solution for some diseased loci due to mutations in the regulatory elements that control gene expression (e.g. hemophilia B Brandenburg). The results presented here support the notion that a ZFN pair targeting a highly expressed locus such as mouse albumin may be used to overcome these limitations, representing an attractive platform for expression of multiple therapeutic genes.

Recently, it has been reported that AAV mediated targeting of the albumin locus with no nuclease may be sufficient to correct disease (Barzel et al., 2014). We have not observed measurable hF.IX protein in mice that did not receive a nuclease, however these differences may be attributable to differences in our systems. The first is that our donors do not contain the full hF.IX open reading frame, but rather exons 2-8 preceded by a splice acceptor, rendering it extremely unlikely to produce mature protein as a result of basal promoter activity from the AAV inverted terminal repeats or cryptic promoter sequences in the targeting construct. In addition, the length of homology arms and precise region of albumin targeted in the two studies were different. Nonetheless, based on our results as well as the genome editing literature, we would predict that adding a nuclease to this strategy would substantially improve the efficiency. This is an important consideration as it is well known that mouse liver transduction with AAV is particularly efficient compared to large animals (~50-100x greater at equivalent vg/kg doses). An unanswered question is whether genome editing, in the absence of the nuclease, would be efficient enough to elicit robust levels of protein production in large animal models that have been shown to better predict human therapeutic doses. We believe it is reasonable to expect that adding a nuclease would allow us to use considerably lower AAV doses while retaining similar levels of expression to those seen by Barzel and colleagues. With regard to safety, the critical question will be whether a high dose of donor vector alone, which presumably relies on spontaneous DNA damage to initiate targeting, is preferred over a potentially lower dose of donor and nuclease. In addition, strategies based on non homologous end joining will require a nuclease and are a promising approach for diseases such a hemophilia A, in which the transgene, even without flanking arms of homology, pushes the limits of AAV packaging.

Cleavage specificity of designer nucleases remains an area of active inquiry. It is clear that patterns of unintended cleavage depend on the specific enzyme employed, target tissue (and species of genome), and magnitude/duration of nuclease expression. Additionally, some of the challenges for successful clinical application of genome editing are related to the currently available technology for nuclease delivery. An optimal vector would permit short-lived nuclease expression in a large majority of target cells, mediating donor integration through DNA break-repair mechanisms while minimizing risk of off-target effects. In the proof of concept study presented here, we utilized adeno-associated viral vectors for nuclease and donor delivery to achieve efficient hepatocyte transduction. While AAV vectors are well fit for donor delivery they may not be ideal for nuclease expression. Nonetheless, characterization of a single, universal reagent as opposed to multiple enzymes represents a critical advance for maximizing the safety profile of gene editing technologies.

In summary, our results demonstrate phenotypic correction of mouse models of two disorders, hemophilia A and B, following the administration of AAV vectors encoding a donor construct and a ZFN pair targeting the albumin locus. This strategy can be extended to multiple indications beyond hemophilia, with the potential for use in diverse protein replacement therapies. *In vivo* experiments in large animal models are warranted to establish a basis for clinical translation of this technology to treat a range of monogenic diseases.

Figure 3.1

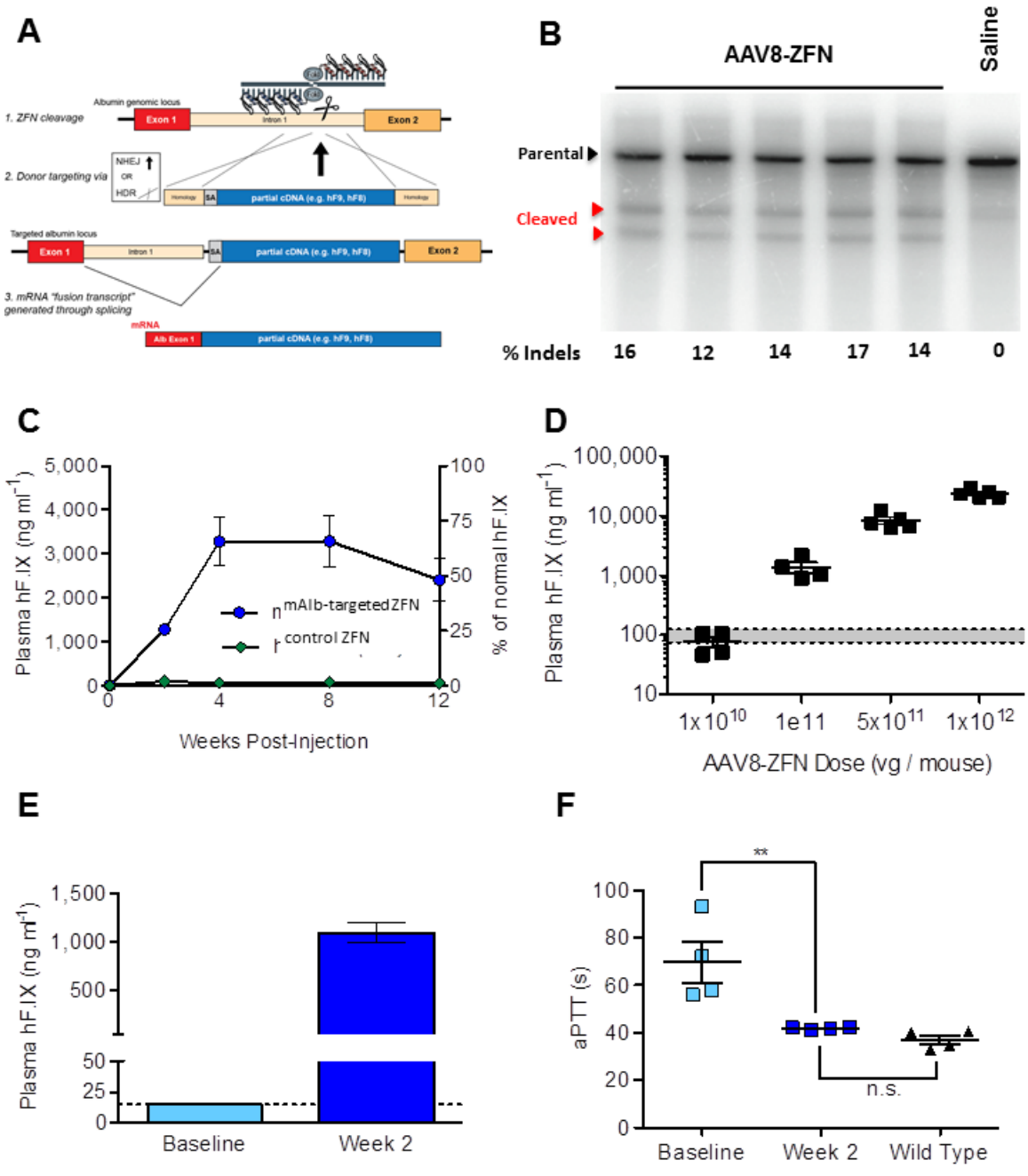

Figure 3.1 Hepatic gene targeting of the mouse albumin locus results in phenotypic correction of hemophilia B.

(**A**) Schematic illustrating albumin targeting strategy. (**B**) Cel-I nuclease assay from liver DNA measuring ZFN-induced indels within albumin intron 1. Lanes represent individual mice at day 7 post AAV8-mALB-ZFN treatment. (**C**) hF.IX in mouse plasma following treatment with AAV8-hF9-Donor and either AAV8-mALB-ZFN (●) or AAV8-hF9-ZFN (♦, with a target sequence not present in the mouse genome). n=3 mice per group (**D**) hF.IX levels at week 2 post-treatment are proportional to AAV dose (1:5 ZFN to Donor). Grey line: normal levels. Points represent individual mice. (**E**) hF.IX levels in hemophilia B mice two weeks after treatment with AAV8-mALB-ZFN and AAV8-hF9-Donor. n=4 mice per group. *p=0.029, Fisher's exact test (**F**) Clot formation in mice (panel E) measured by aPTT prior to and 2 weeks after treatment. The aPTTs of wild-type mice are shown for comparison. **P<0.01, 2-tailed Mann-Whitney test. *n.s.* = non-significant.

Figure 3.2

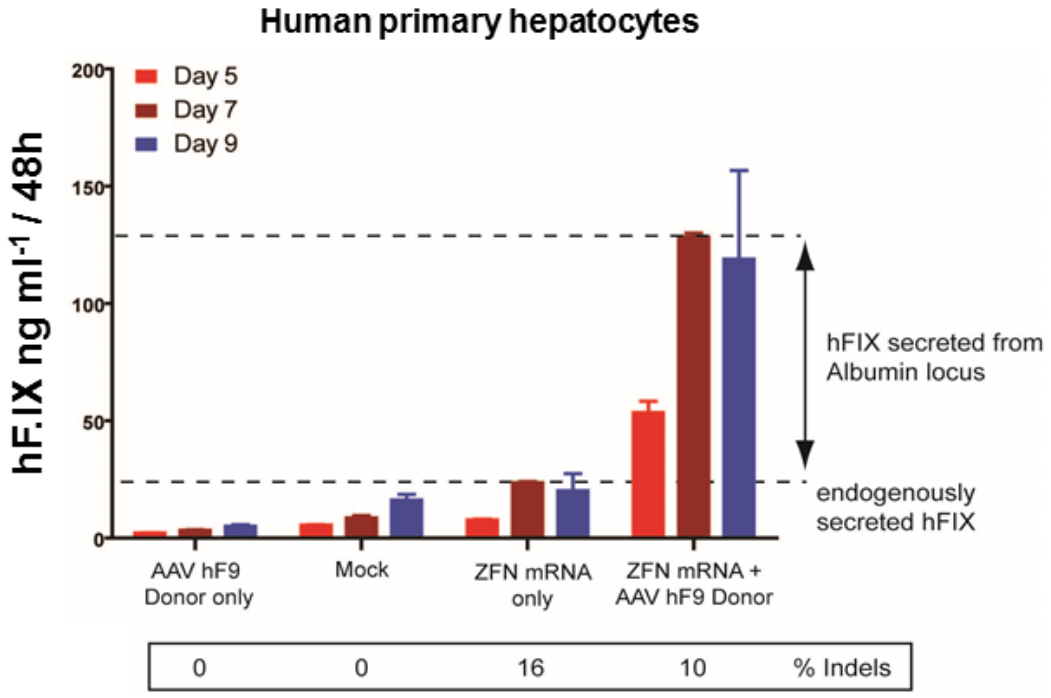

Figure 3.2 ZFN mediated targeting of the albumin locus in primary human hepatocytes.

Human primary hepatocytes were transduced in vitro with AAV6 hF9 donor (MOI $9x10^5$ vg/cell) and 24h later with 500ng of mRNA encoding albumin-targeted ZFNs. Bottom panel: % of albumin sequences with insertions and deletions (indels) as measured by MiSeq analysis. Supernatants taken at Day 5, 7 and 9 were analyzed for hF.IX levels by ELISA. Error bars = s.e.m. Data are representative of at least 2 independent experiments.

Figure 3.3

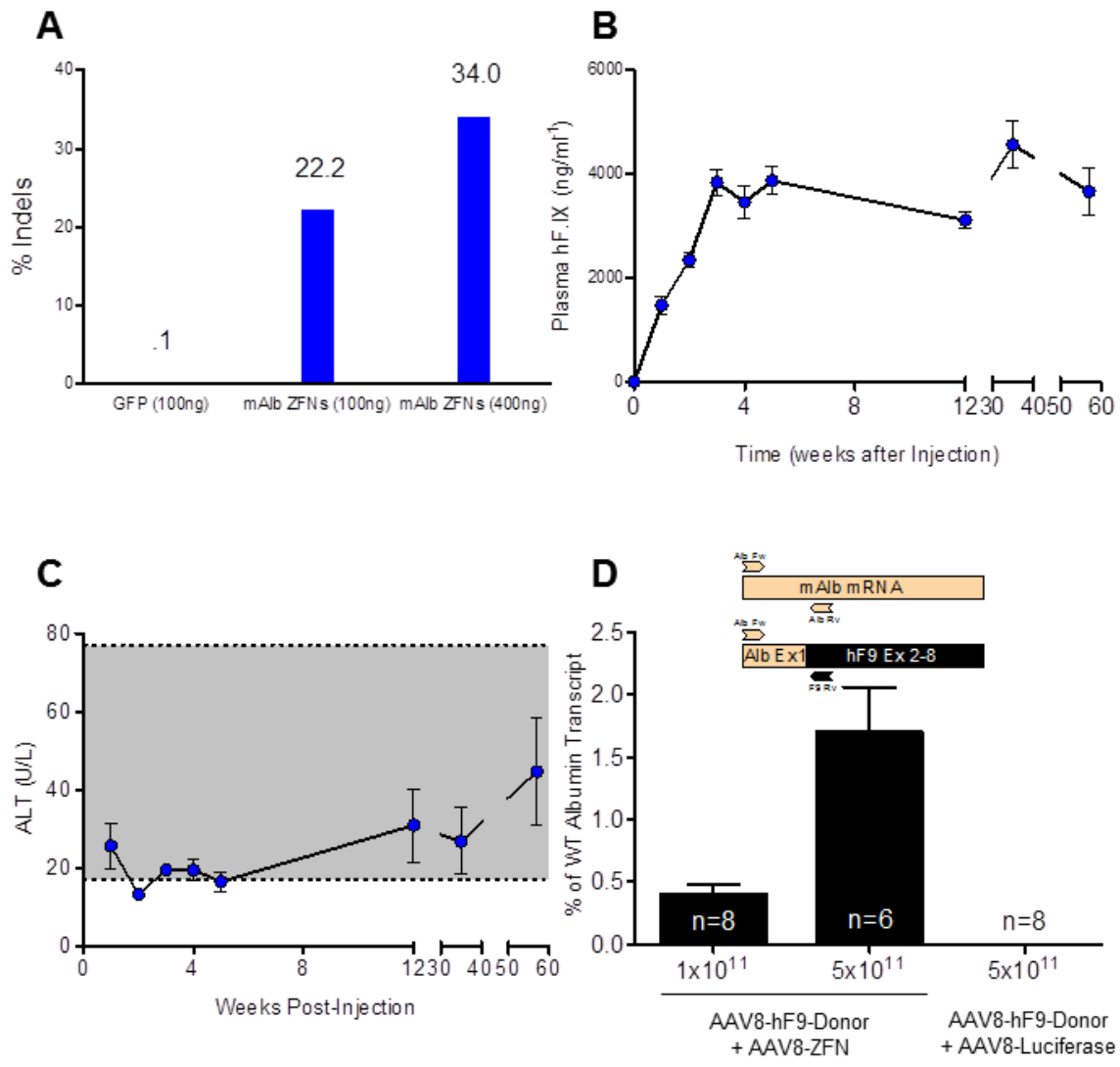

Figure 3.3 Characterization of mAlb-targeted ZFNs *in vitro* and *in vivo.*

(A) ZFN activity measured by indels in Hepa 1-6 cells transfected with indicated amount of ZFN or GFP mRNA. Genomic DNA was isolated and the target sequence was PCR amplified for Illumina MiSeq sequencing. Percentages indicate reads containing indels consistent with cleavage and NHEJ repair. (see *Methods*) **(B)** Levels of hF.IX in treated

mice remained stable for more than a year following IV injection with $5x10^{11}$ vg AAV8-hF9-Donor and $1x10^{11}$ vg AAV8-ZFN. **(C)** Plasma ALT values following treatment did not deviate from normal range (shaded area). **(D)** Quantitative PCR was used to determine the relative abundance of hybrid mAlb-hF9 mRNA vs. wild type mAlb mRNA (transcripts and priming scheme indicated schematically at top). Mice were injected with 1:1 ratio of ZFN:Donor at indicated doses. Total RNA was isolated from livers of mice 2 weeks post injection. As a negative control, Luciferase (Mock) + Donor was given at the higher dose of $5x10^{11}$ vg each. A 2-tailed Mann-Whitney test was used to compare 2 groups. n=6-8 mice/group. Error bars = s.e.m.

Figure 3.4

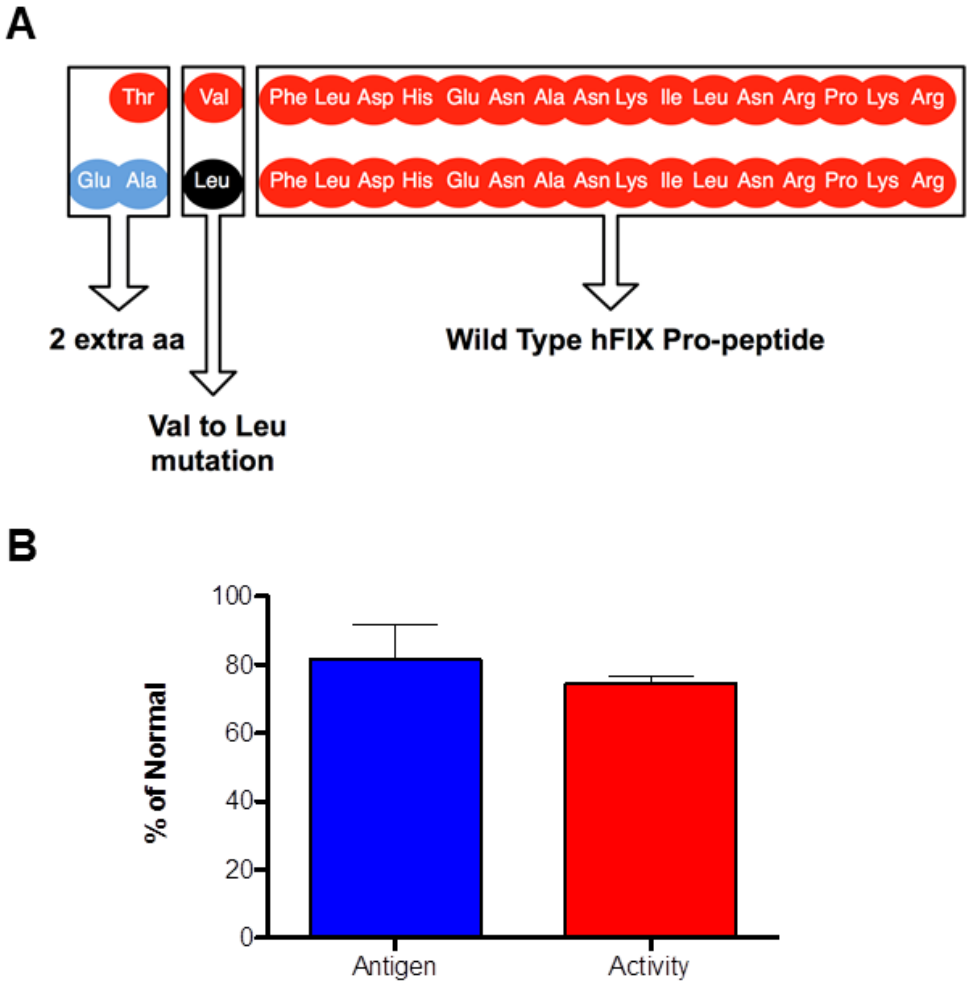

Figure 3.4 hF.IX activity is not affected by the N-terminal modification resulting from donor splicing with albumin exon 1.

(A) Schematic showing the wild type propeptide of hF.IX (top) and the expected propeptide resulting from the splicing event between mouse albumin exon 1 and the hF9 donor (below). **(B)** Hemophilia B mice were injected with $1x10^{11}$ vg of AAV8-ZFN and $5x10^{11}$ vg of AAV8-hF9-Donor. Twenty weeks post-injection, the biological activity of hF.IX was measured using a chromogenic assay and antigen levels were determined by ELISA. A 2-tailed Mann-Whitney test was used to compare 2 groups. There was no

significant difference in the hF.IX levels measured by these two assays. n=3 mice. Error bars=s.e.m. No activity or antigen were detected in uninjected mice.

Figure 3.5

Donor	Modifications to CDS of hF.VIII	Other features	Total length (bp)
hF8 Donor 1	B-domain deletion (SQ)	bGH polyA	4912
hF8 Donor 2	V3 Peptide (Glycosylation signal) B-domain deletion	Short polyA Codon optimization (McIntosh et al.)	4726

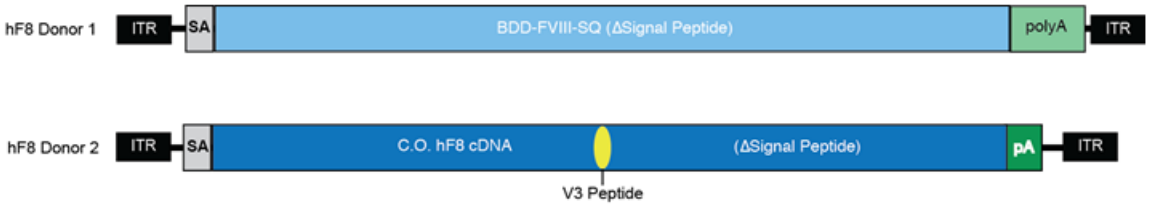

Figure 3.5 Donors used for hF.VIII studies.

Upper: Table summarizing donor features. Lower: Donor sketches highlighting key regions.

Figure 3.6

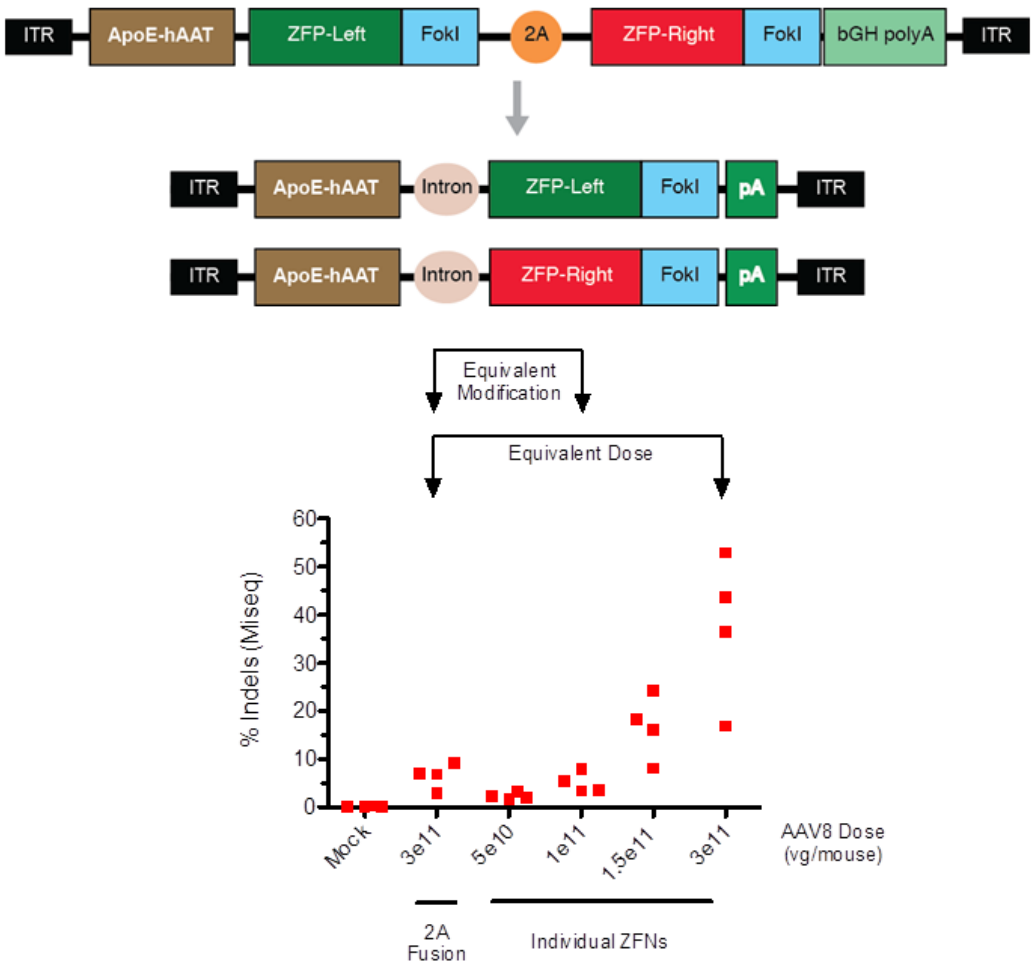

Figure 3.6 Individual ZFNs

Top**:** Bicistronic vector utilizing ribosomal skipping "2A" peptide for ZFN-Left and ZFN-Right expression. Middle: Individual ZFN vectors each encoding a single ZFN. Bottom graph: Indels at ZFN target site measured by Illumina MiSeq from livers of mice injected with indicated AAV dose at week 2 post treatment. Each point represents an individual mouse. Note that this study used the "hF8 Donor 1" from Figure 3.5.

Figure 3.7

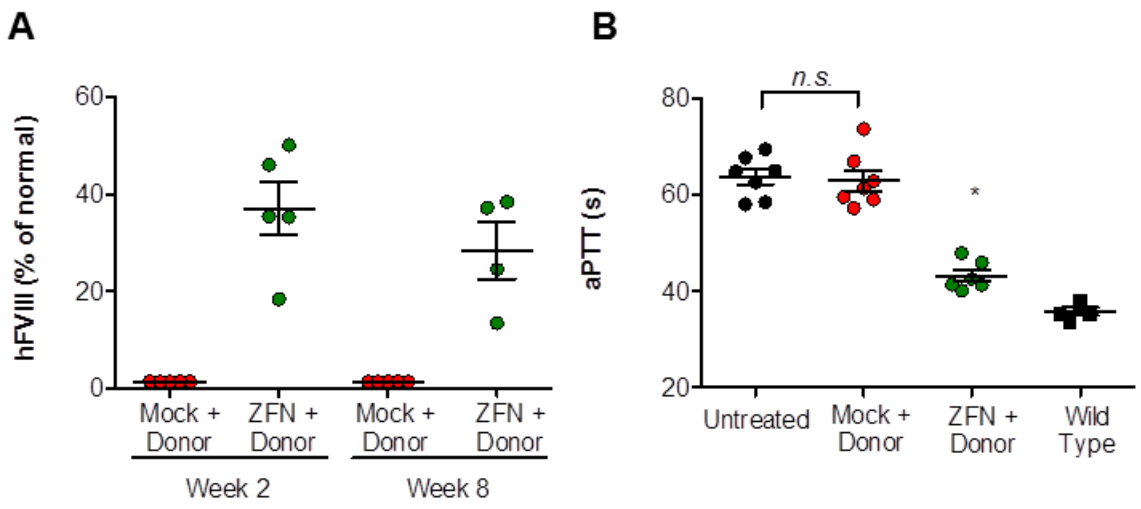

Figure 3.7 Targeting of albumin supports production of therapeutic levels of Factor VIII and functional correction of hemophilia A phenotype.

(**A**) F.VIII activity as determined by chromogenic assay in hemophilia A/CD4 deficient mice 2 and 8 weeks after treatment with $1x10^{11}$ vg of AAV8-Mock (●) $5x10^{10}$ vg of each individual AAV8-mAlb-ZFN (●) and $1x10^{11}$ vg of Donor 2 (see Methods for details). *p=0.08, Fisher's exact test. (**B**) Measurement of clot formation by activated partial thromboplastin time (aPTT) prior to, and 11 weeks after AAV administration. The aPTT of WT (■) and Untreated (●) mice are shown for comparison. A 2-tailed Mann-Whitney test was used to compare the 2 groups.

Figure 3.8

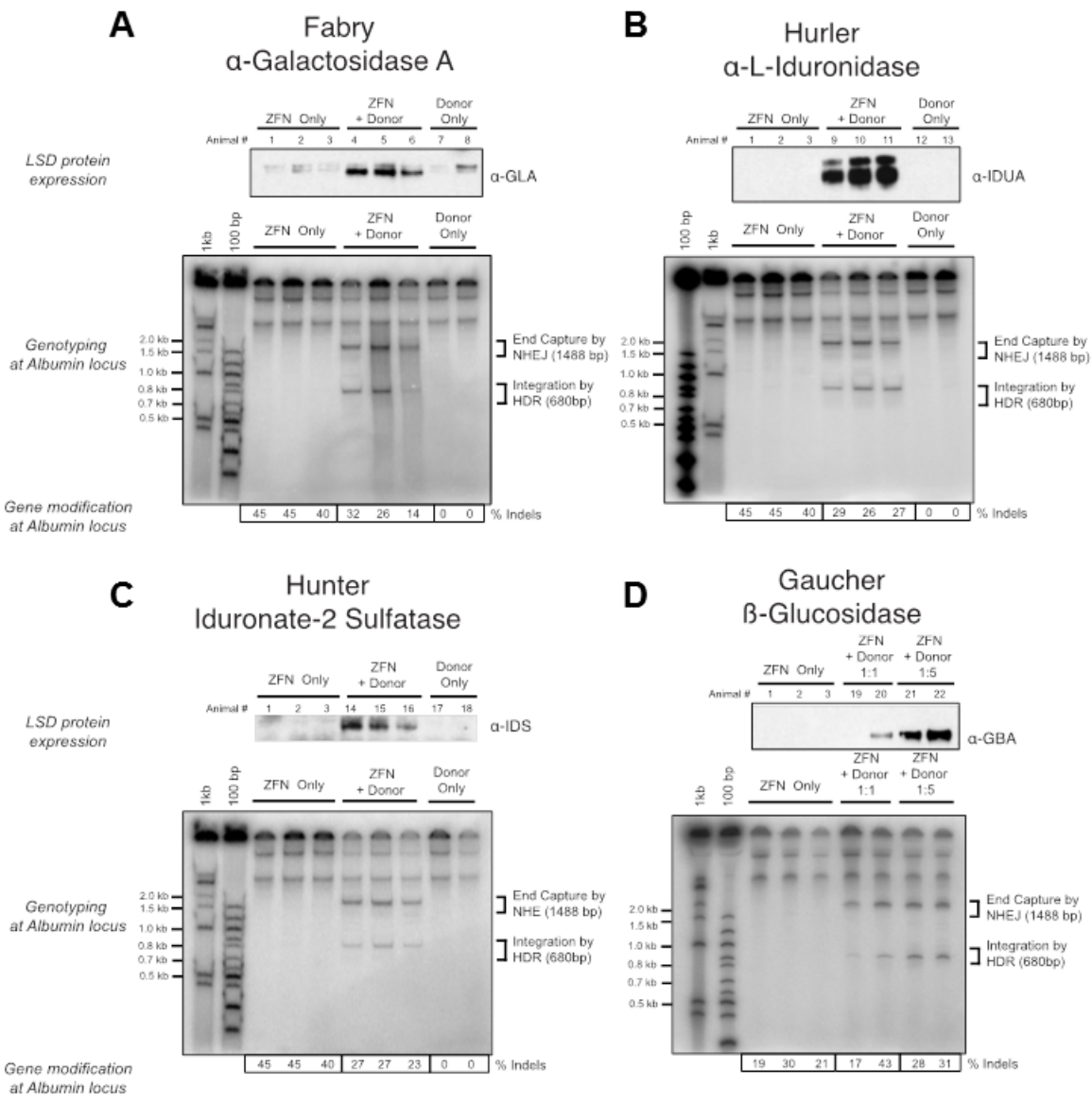

Figure 3.8 Expression of lysosomal enzymes deficient in Fabry and Gaucher diseases, as well as in Hurler and Hunter syndromes.

Upper panels: Western blot detection of α-Galactosidase A, ß-Glucosidase, Iduronate-2 Sulfatase and α-L-Iduronidase in liver lysates of mice 30 days following treatment with $1x10^{11}$ vg of AAV8-mAlb-ZFN and $1x10^{11}$ vg of AAV8-of the appropriate donor (see

Methods for details). Middle panels: PCR detection of bands consistent with homology directed (HDR) and homology independent (NHEJ) integration of donor at the albumin locus. Lower panel: Indel formation as measured by MiSeq sequencing. n=3 mice per group. Each lane represents an individual mouse.

Figure 3.9

Selex-based Off-target analysis study Day 30		*In vivo* / Mouse
Rank	Gene	% Indels
On target		31.4
1	Nfia	1.92
2	Stk40	0.85
3	Rab9	0.70
4	Ccdc101	0.62
5	Vstm4	0.53
6	Intergenic region, chr1	0.27
7	Il17rd	0.26
8	Intergenic region, chr14	0.25
9	Ppp1r12b	0.24
10	Tirap	0.23
11	Intergenic region, chr1	0.12
12	Tiam1	N.S.
13	Lrp2	N.S.
14	Spata16	N.S.
15	Intergenic region, chr8	N.S.
16	Intergenic region, chr3	N.S.
17	Nfib	N.S.
18	Intergenic region, chr1	N.S.
19	Hs3st3b1	N.S.
20	Intergenic region, chr7	N.S.
21	Gabrb2	N.S.
22	B4galt1	N.S.
23	Arhgef16	N.S.
24	Intergenic region, chr9	N.S.
25	Parva	N.S.
26	Pigu	N.S.
27	Intergenic region, chr8	N.S.
28	1810013L24Rik	N.S.
29	Intergenic region, chr2	N.S.
30	Arl8b	N.S.
31	Rptor	N.S.
32	Cd96	N.S.
33	Barx2	N.S.
34	Kcnj6	N.S.
35	Dpp10	N.S.
36	Fam49b	N.S.
37	Rbms3	N.S.
38	Intergenic region, chr9	N.S.
39	Sin3a	N.S.
40	Exoc4	N.S.

N.S. = not significant

Figure 3.9. mALB ZFN off-target activity.

Figure 3.10

A

MDYKDHDGDYKDHDIDYKDDDDKMAPKKKRKVGIHGVPAAMAERPFQCRI
CMRKFATSGSLTRHTKIHTGEKPFQCRICMRNFSRSDALSTHIRTHTGEK
PFACDICGRKFAQSATRTKHTKIHTHPRAPIPKPFQCRICMRNFSTSGHL
SRHIRTHTGEKPFACDICGRKFAQSGNLARHTKIHLRGSQLVKSELEEKK
SELRHKLKYVPHEYIELIEIARNSTQDRILEMKVMEFFMKVYGYRGKHLG
GSRKPDGAIYTVGSPIDYGVIVDTKAYSGGYNLPIGQADEMERYVEENQT
RDKHLNPNEWWKVYPSSVTEFKFLFVSGHFKGNYKAQLTRLNHITNCNGA
VLSVEELLIGGEMIKAGTLTLEEVRRKFNNGEINF

B

MDYKDHDGDYKDHDIDYKDDDDKMAPKKKRKVGIHGVPAAMAERPFQCRI
CMRNFSRSDHLSAHIRTHTGEKPFACDICGRKFATKSNRTKHTKIHTGSQ
KPFQCRICMRNFSDRSNLSRHIRTHTGEKPFACDICGRKFAWRSSLRAHT
KIHTGEKPFQCRICMRKFADSSDRKKHTKIHLRGSQLVKSELEEKKSELR
HKLKYVPHEYIELIEIARNSTQDRILEMKVMEFFMKVYGYRGKHLGGSRK
PDGAIYTVGSPIDYGVIVDTKAYSGGYNLPIGQADEMQRYVKENQTRNKH
INPNEWWKVYPSSVTEFKFLFVSGHFKGNYKAQLTRLNRKTNCNGAVLSV
EELLIGGEMIKAGTLTLEEVRRKFNNGEINF

Figure 3.10 Amino acid sequences of ZFNs used to target intron 1 of mAlb

(A) ZFN^{Left} and **(B)** ZFN^{Right} amino acid sequences used in the study. 3xFLAG tag is annotated in blue. The SV40 large T antigen nuclear localization sequence is annotated in green. FokI domain is annotated in red.

CHAPTER 4: MECHANISMS OF GENOME EDITING OF THE MURINE LIVER

The data in chapter 4 are preliminary and unpublished

Figures 4.1/4.2 were partially represented in chapter 2 (Figure 2.2F and 2.7A)

Summary

Genome editing has the potential to provide long-term therapeutic gene expression *in vivo*. We have previously demonstrated efficient editing in a mouse model of hemophilia B through liver-directed adeno-associated viral vector (AAV) delivery of a zinc finger nuclease (ZFN) pair and a corrective donor. As a consequence of a splice acceptor contained in the donor, both HDR and homology independent vector integration are capable of driving human factor 9 (hF.IX) expression, however, the relative contributions of each pathway is not known. In the work outlined in this chapter we sought to better understand the molecular requirements of *in vivo* genome editing in both adult and neonatal mice. Insights from these investigations allowed us to demonstrate two possible strategies to bias repair choice in the direction of HDR, with the potential to improve both the efficacy and safety of therapeutic gene targeting.

To address this question we designed a novel donor designed to report NHEJ and HDR repair by expressing one of two differentiable surface markers depending on the molecular outcome of the integration event. In neonatal mice, we observed predominantly expression consistent with HDR repair. Importantly, we were able to enrich for these cells in order to perform a southern blot, observing a band consistent with HDR in the enriched hepatocytes. In adult mice, reporter expression consistent with HDR appeared to be lower than in neonates, however the results were inconclusive, apparently due to high background expression from the excess of non-integrated episomal vectors.

Returning to hF.IX as our primary readout of genome editing, we compared expression levels in mice treated as neonates and as adults with equivalent AAV doses

and routes of administration using vectors with and without arms of homology. In mice treated as neonates, we observed significantly higher hF.IX expression 10 weeks post injection when using homologous donors. In contrast, mice treated as adults with the same vectors did not exhibit differences in expression with respect to donor homology. We repeated these experiments in mice with impaired NHEJ function ($Prkdc^{scid/scid}$), and observed a 95% reduction in homology independent targeting with no reduction in HDR. Finally, we asked whether HDR could be stimulated more specifically through the induction of DNA single strand breaks ("nicks") at the target site. We treated neonatal mice with homologous or non-homologous donors, as well as ZFNs or ZFNickases (which create DNA nicks rather than double strand breaks). ZFNickases induce robust genome editing with a far greater bias towards HDR than ZFNs. These data suggest ZFNickase treatment of neonatal mice could achieve therapeutic protein production with minimal integration at unintended sites.

Introduction

DNA double-strand breaks (DSBs), left unrepaired, are among the most catastrophic threats to a cell's viability, likely resulting in the loss of genetic information once the cell divides. Over the last few decades, research has revealed a great deal about the many cellular responses that have evolved to deal with DNA damage. In eukaryotes, two general pathways are capable of repairing DSBs: NHEJ and HDR (introduced in chapter 1). In higher eukaryotes, NHEJ is the more common mechanism, active throughout the cell cycle, while HDR is thought to be restricted to dividing cells particularly in the late S and G2 phases of the cell cycle. Both can be sub-divided due to the existence of multiple pathways leading to similar resolutions of a DNA break. Proteins involved in both pathways have been genetically knocked out in mice and often result in genome instability, sensitivity to radiation, and in many cases embryonic lethality.

The mechanism historically called NHEJ is often referred to as C-NHEJ (classical/canonical nonhomologous end joining (Alt, Zhang, Meng, Guo, & Schwer, 2013; H. Wang et al., 2003)). Ku70 and Ku80 are C-NHEJ factors that recognize DSBs as a heterodimer. These two proteins, together with DNA-PKcs (catalytic subunit of the DNA protein kinase complex) are able to activate Artemis, an endonuclease involved in end processing. Finally, the XRCC4-Lig4 complex mediates the actual joining of the broken DNA ends. C-NHEJ is best characterized in primary tissue in its critical function in the development of B and T cell antigen receptors. From a relatively small amount of genetic information encoded in the germline, millions of cells are able to generate

remarkable diversity by independently recombining coding regions of their B-cell receptor (immunoglobulin) or T-cell receptor genes. During this process, known as V(D)J recombination, coding regions from different locations of a linear chromosome are cut and ligated together (excising the intervening segment). DNA cleavage created during V(D)J recombination results in asymmetric products: (i) covalently sealed DNA ends (hairpins) that eventually form the immune receptor coding sequences and (ii) double stranded ends of the fragment excised from the genome, more similar to those made by restriction enzymes.

One of the most common immunodeficient mouse models, SCID, is the result of a mutation in the gene encoding DNA-PKcs (Prkdc). Interestingly, $Prkdc^{scid/scid}$ mice exhibit dysfunctional repair of hairpin ends (which results in the characteristic V(D)J deficiency) but are not deficient in the repair of ends which do not require processing (Alt et al., 2013). Although the relationship between the $Prkdc^{scid/scid}$ genotype and the fate of AAV vector genomes may depend on many factors, it is possible the hairpins in the ITRs require similar processing for NHEJ mediated integration.

Homology Directed Repair (HDR) is a key pathway by which many organisms protect their genomic integrity. In the somatic cells of higher eukaryotes (e.g. mammals), this pathway is less active than in other well characterized eukaryotic systems, such as yeast. Nonetheless, mutations in many proteins involved in HDR repair result in severe genetic diseases, highlighting the importance of this pathway in maintenance of genetic information. Like NHEJ, many details of the HDR pathway in mammalian cells are unknown, particularly with regard to the numerous levels of control that modulate the various proteins and thus the final outcomes of repair.

One of the major requirements for HDR repair of DSBs is the processing of the broken ends to generate single stranded DNA (ssDNA). In human cells, this involves the MRN complex of MRE11-RAD50-NBS, exonucleases EXO1 and CtIP, and the BLM helicase (Heyer, Ehmsen, & Liu, 2010). Exposed ssDNA is quickly bound by replication protein A, or RPA. Mediator proteins, like BRCA2 are able to substantially increase the rate that RPA is replaced with filaments of RAD51 protein monomers, which are involved in homology search and DNA-strand invasion, in a process called synapsis (San Filippo, Sung, & Klein, 2008). By bringing together the damaged locus, which now has a 3' overhang, and the template sequences for repair, a displacement loop (D-loop) can form to allow the overhang to "invade" the template DNA and act as a primer for DNA polymerization. This can be resolved in at least 3 different processes for which we have direct evidence in human cells: dHJ (double Holliday junction, rare in non meitic cells), SDSA (synthesis-dependent strand annealing, likely the most common in somatic cells), and BIR (break-induced replication, which may result in a loss of genetic information). Critical proteins in this process are regulated in terms of expression and post-translational modifications in a manner that is linked to the cell cycle. These multilayered mechanisms of control remain to be fully characterized, but in general there is strong interaction between cell cycle and phosphorylation, ubiquitylation, and other modifications to RPA (Fanning, Klimovich, & Nager, 2006), RAD51 (Sørensen et al., 2005), BRCA2 (Esashi et al., 2005), and CtIP (Yu, Fu, Lai, Baer, & Chen, 2006), which maximize activity during the S phase. This behavior is compatible with the teleological argument that the ideal template for repair is the sister chromatid after DNA replication, where no genetic information would be lost.

DNA “nicks,” or single strand breaks (SSBs) are also thought to be capable of stimulating HDR. Some of the most appropriate evidence of this for the work described in this chapter comes from the observation that wild-type AAV integrates preferentially at a specific site (AAVS1). Recombinant AAV integration does not display this preference, and the Rep protein is known to induce nicks (but not DSBs) at the AAVS1 locus. Expression of AAV Rep is able was shown to stimulate HDR using a plasmid donor at the AAVS1 site (van Nierop, de Vries, Holkers, Vrijsen, & Gonçalves, 2009). Since then, several groups have demonstrated the ability of nicks to stimulate HDR with potentially less NHEJ (Davis & Maizels, 2014; Metzger, McConnell-Smith, Stoddard, & Miller, 2011; Ramirez et al., 2012). This observation could be related to the fact that nicks are much more common than DSBs and are typically repaired by mismatch repair mechanisms, except during DNA replication, where an unrepaired nick could lead to replication fork collapse. Intriguingly, this is also the ideal cell cycle state for the promotion of HDR repair.

Materials and Methods

Animal experiments

Animal experiments were approved by the Institutional Animal Care and Use Committee at the Children's Hospital of Philadelphia. Previously described heterozygous male h*F9*mut (F9 ZFN, (Li et al., 2011)), wild type C57Bl/6 (Jackson laboratory), or B6.CB17-*Prkdc*^{scid}/SzJ (Jackson laboratory) mice were used. h*F9*mut mice were obtained by crossing male homozygote h*F9*mut mice with previously described HB females. For IV injections in adult mice, AAV vector was diluted to 200µl with PBS + 0.001% Pluronics before tail-vein injection. IP injections in neonatal mice were performed as previously described (Li et al., 2011). For retro-orbital injections in neonatal mice, vectors were administered according to an established protocol (Yardeni, Eckhaus, Morris, Huizing, & Hoogstraten-Miller, 2011). Plasma for human factor IX ELISA was obtained by retro-orbital bleeding into heparinized capillary tubes. Tissue for nucleic acid analysis was immediately frozen on dry ice after necropsy.

ZFN reagents and targeting vectors

ZFNs targeting the h*F9*mut locus and F9 targeting vectors have been previously described (Anguela et al., 2012), as well as the ELD:KKR mutations to the FokI domain to construct the obligate heterodimeric ZFNs (Doyon et al., 2011). Experiments shown in figures 4.10, 4.11, and 4.12 used individual ZFN vectors at the indicated total dose (1:1) ratio as decribed in chapter 2. AAV8 vectors were produced and titered as previously described (Ayuso et al., 2009),(Wright & Zelenaia, 2011).

Factor IX levels and activity

Human factor IX ELISA kit (Affinity Biologicals; Ancaster, ON, Canada) was used to quantify plasma hF.IX. All readings below the last value of the standard curve (15 ng/ml) were arbitrarily given the value of 15 ng/ml except where otherwise indicated.

Hepatocyte Isolation

Hepatocytes were isolated using a modified 2-step collagenase in situ perfusion (Duncan et al., 2010). Briefly, anesthetized mice were immobilized on a warmed dissecting board by rubber-bands. A ventral midline excision was made to expose the liver and lungs, and the ribs were cut on both sides to expose the heart. A 23-gauge butterfly needle (connected to a peristaltic pump) was inserted into the inferior cava via the right atrium, and the portal vein was cut to allow solution to exit. The mouse was perfused until completely blanched using warm EGTA containing solution 1, followed by collagenase IV containing solution 2 (recipes described below). When cells were sufficiently dissociated (roughly 5 minutes, depending on collagenase activity, liver size, and quality of cannulation, livers were removed from mice and placed into petri dishes. After removing the gallbladder, liver cells were mixed with 20mL solution 3 and filtered through a 70-micron filter into a 50mL conical tube. Cells were washed twice at 30x g for 5' to remove a majority of non-parenchymal cells, and finally subjected to an iso-density percoll gradient as described to further separate live hepatocytes (Kreamer et al., 1986).

Flow cytometry

All antibodies were obtained from BD. CD8-APC (BD 561421) and CD4-PE (BD 561843) staining was performed on freshly isolated 293T cells or hepatocytes by incubating in 200uL FACS buffer for 30' at 4C. Cells were washed twice at 1500rpm/5' (293T cells) or

30x g/5' (hepatocytes) before resuspension in FACS buffer for flow cytometric analysis. Fluorescence was read using a BD FACS Canto II in the Children's Hospital of Philadelphia (Colket Translational Research Building, Suite 5400).

MACS Based Enrichment of CD4+ Cells

Primary hepatocytes from hF9mut mice treated with ZFN and Dual Reporter were pooled and subjected to a second round of iso-density percoll enrichment to minimize the numbers of dead cells present (which were found to bind magnetic beads nonspecifically, and clogging Miltenyi LS columns used for enrichment). Staining was performed according to manufacturers instructions using CD4-PE primary antibody and magnetic bead conjugated anti-PE antibody (Miltenyi 130-048-801).

In Vitro Transfections

HEK 293T Cells were transfected according to manufacturers instructions with Lipofectamine LTX. Briefly, 1µg DNA (in TE) was diluted to 100µL in OptiMEM, and complexed with Lipofectamine LTX reagent (1µL in 100uL). Expression plasmids were derived from PiggyBac transposon system which constitutively express GFP under control of the PGK promoter and contain a CMV promoter driving each indicated expression cassette. All expression cassettes contained hF9 exon 1 and a truncated 3' coding sequence separated by hF9 intron 1. SA—2A—CD8, SA—2A—CD4, SA—2A—CD8—(Homology)—SA—2A—CD4 were inserted within intron 1 to generate the final expression cassettes.

Hydrodynamic Tail Vein Injections

Wild type C57Bl/6 male mice were injected with 2µg/mg plasmid DNA in Saline with injection volume of 10% (volume/mass) body weight. Non-signaling hCD8 and hCD4 constructs based on (Gadue, Huber, Paddison, & Keller, 2006) were synthesized by Integrated DNA Technologies (Coralville, Iowa) and GenScript (Piscataway, NJ), respectively. The ORFs were cloned into plasmids under control of the human alpha-1-antitrypsin promoter (Manno et al., 2006).

PCR-based genotyping

Primers binding to a sequence upstream of exon 1 unique to the h*F9*mut mini-gene and within a sequence unique to the donor were used to amplify targeting events from genomic DNA. Genomic DNA from mouse liver was isolated using the MasterPure complete DNA purification kit (Epicentre Biotechnologies; Madison, WI, USA). To detect the targeting of the donor cassette via NHEJ or HDR, gDNA was amplified using the P1 (5'ACGGTATCGATAAGCTTGATATCGAATTCTAG3') and P5 (5'GCCCTTCTGGAACTGGACGAACC3') primers binding respectively to a sequence upstream of exon 1 unique to the h*F9*mut mini-gene and within a sequence unique to the donor found in exon 8 of hF9. The PCR reactions were performed using Phusion High-fidelity DNA polymerase (New England BioLabs; Ipswich, MA, USA) in conjunction with GC Buffer and 3% dimethylsulphoxide for 25 cycles (10" denaturation at 98°C, followed by 1'50" of extension at 65°C). The PCR products were then purified with G50 columns, resolved by 5% PAGE and autoradiographed.

DNA analysis by Southern Blot

Genomic DNA was digested overnight at 37ºC with the restriction enzyme *Stu I*. The next day, 6x loading dye was added to the digested genomic DNA prior to loading on a 1% agarose/TAE gel with DNA Molecular weight Marker X (Roche) as a marker. Samples were run for 4-5 hours at 50-60 volts. Gel treatment was carried out prior to the transfer of the DNA to the blot, consisting of 0.25N HCl (1.5 M NaCl; 0.5M NaOH) for 15 minutes to allow depurinization of DNA and mitigate the bias towards higher transfer efficiencies of smaller fragments. The gel was next treated for 30 minutes in neutralizing solution (1M Tris; 3 M NaCl). Blotting was carried out using positively charged nylon membranes (Roche) and the Turboblotter system (Schleicher & Schuell, USA). This system allows the transfer of DNA to membranes by capillary action in high ionic strength buffer (10x SSC) through absorbent papers (GB002 and GB004, Schleicher & Schuell, Keene, New Hampshire) for 2 hours. The blot was then irradiated with 120,000 µJ of ultraviolet light for 25-50 seconds in a UV-Stratalinker 1800 (Stratagene; La Jolla, CA). Next, the blot was pre-hybridized for 2 hours at 65ºC in a solution containing proteins, SDS and ssDNA to block free binding sites and reduce subsequent non-specific binding. Hybridization was carried out overnight at 65ºC with a specific probe (synthesized as a gBlock by IDT (Coralville, Iowa) corresponding to intron 1 within the hF9mut construct but not the donor vector. The probe was radiolabeled using random primers and [α-^{32}P]-dCTP. The non-incorporated radioactive nucleotides were separated with Sephadex G-50 gel filtration columns (Probe Quant G-50 Micro Columns, Amersham). The hybridization was carried out overnight at 65ºC with rotational agitation. The following morning several washes were performed, consisting of consisted of 3 consecutive washes with progressively higher stringency: two 10-minute washes at room temperature with a low-stringency buffer solution and a final 15-minute wash at 65ºC

with a high-stringency buffer solution. Finally, the blots were exposed to a photographic film (Eastman KODAK Company, New York). The untargeted (unmodified) locus is expected to yield a 5530bp band, while the on target HDR-mediated integration of CD4 is expected to yield a 1772bp band.

Hybridization solution: 0.25 mM Na2HPO4 pH 7.2; 10% W/V SDS; 1 mM EDTA; 0.5% W/V Blocking Reagent (Roche Diagnostics).

Low astringency solution: 2x SSC; 0.1% W/V SDS

High astringency solution: 0.1x SSC; 0.1% W/V SDS

Statistics

Graphpad Prism was used to perform all the statistical tests. If data passed the D'Agostino & Pearson normality test, then a two-sided t-test was used. Otherwise, the nonparametric Mann-Whitney test (two-tailed) was used. In all tests, $p<0.05$ was considered significant.

Results

Based on data outlined in Chapters 2 and 3, we were aware that *in vivo* editing of the liver required nuclease activity as well as the appropriate target site to be present in the genome for production of secreted protein. Further, two experimental controls provided strong evidence that expression was derived from integrated donor rather than through recombination between extra-chromosomal vectors or through trans-splicing from an endogenous transcript to the episomal donor: (i) protein was not observed in mice treated with Mock (expressing luciferase) and Donor and (ii) expression was not diluted as one would expect from episomes following 2/3 partial hepatectomy (as one would expect from episomal expression).

Evidence for both NHEJ and HDR involvement in AAV donor integration

To investigate the contributions of NHEJ and HDR pathways to the observed editing phenotype (the expected outcomes are depicted in **Figure 4.1**), we amplified the targeted locus from liver genomic DNA of mice treated as adults. By designing primer pairs to flank the integration junction (one annealing to the mouse chromosome upstream of the ZFN target site, and the other annealing to the donor cassette), we observed bands consistent with both repair mechanisms (**Figure 4.2**). Band identities were Topo-cloned and sequence verified, suggesting both processes contribute to functional correction in our model in adult mice. Through a similar PCR-based assay our lab previously published evidence of both HDR and NHEJ in mice treated as neonates ((Li et al., 2011)). However, the AAV inverted terminal repeats (ITRs) possess strong secondary structure (80% G/C content, Tm >95C), making quantitative PCR analysis difficult due to the very low amplification efficiency of ITR-containing sequences. In

addition, the “gold standard” method to characterize the state of DNA, Southern blot, is not sensitive enough to detect modifications that are expected to be several orders of magnitude less abundant than a single copy allele.

Development and evaluation of a “Dual Reporter” to distinguish between NHEJ and HDR

In order to perform a more quantitative analysis of the relative contribution of HDR and NHEJ, we developed a novel reporter (conceptually similar to the positive/negative selection used in ES cells to generate knock-in and knockout mice). As outlined in **Figure 4.3**, the reporter (“Dual Reporter”) is intended to generate distinct outcomes depending on whether sequences that are outside of the arms of homology are excluded during genome editing. The human CD4 marker (in red) is flanked by arms of homology, and thus should be expressed on the cell surface of hepatocytes that undergo HDR mediated editing using the dual reporter. Alternatively, we would expect the human CD8 marker (in blue) to be expressed on hepatocytes in the case of homology independent insertion of the reporter. Extracellular surface markers were chosen due to the availability of high quality detection reagents and their suitability for use in downstream manipulations such as magnetic bead enrichment.

Our previous results using an hF9 donor relied on splicing of endogenous exon 1 with exons 2-8 of F9 from the donor. Since we were unsure if fusion of the hF.IX signal peptide encoded in exon 1 would adversely affect the reporter (conformation, stability, localization, etc…), we inserted a picornavirus “2A” sequence between the splice acceptor (SA) and the CD8/CD4 open reading frames. Ribosome skipping caused by the “2A” peptide should allow translation of CD8 or CD4 with only 2 additional amino acids

rather than an extraneous F9 signal peptide. Finally, to avoid the possibility of confounding effects due to the reporter genes themselves causing a phenotype in the mouse liver, we employed non-signaling variants of CD8 and CD4.

We first tested the SA—2A—CD8, SA—2A—CD4, and SA—2A—CD8—Homology—CD4 constructs by generating expression plasmids driven by the CMV promoter and transiently transfecting HEK 293T cells. GFP was expressed constitutively as a transfection control. By flow cytometry, we were able to detect surface expression of both CD8 and CD4 on transfected cells (**Figure 4.4A-E**). Interestingly, when both CD8 and CD4 were inserted in tandem (as we would expect in the case of the entire reporter vector integrating at the target locus), we were unable to detect CD4 expression derived from skipping of the CD8 splice acceptor, despite the fact that expression/detection of CD4 was more robust than CD8 (**Figure 4.4F**). This may reflect the strong transcription termination activity of the bovine growth hormone poly-adenylation signal. Most importantly, this finding simplifies the interpretation of the dual reporter, with CD8 and CD4 expression representing NHEJ and HDR, respectively.

After determining that the SA and “2A” peptide did not interfere with expression or detection of either surface antigen, we next asked whether these would be expressed and detected in hepatocytes *in vivo*. We generated plasmids containing expression cassettes similar to those in Figure 4.3, driven by the strong liver specific hAAT promoter, and treated mice via hydrodynamic tail vein injection. Surface staining was performed two days after delivery by isolating single hepatocytes via 2-step collagenase perfusion. We observed detectable shifts in fluorescence for both reporters, confirming

expression by hepatocytes *in vivo* and compatibility of CD4 and CD8 with hepatocyte isolation procedures (**Figure 4.5**).

The Dual Reporter supports the notion that HDR is the predominant mechanism of integration in neonatal mice

We treated hF9mut neonates with IP administration of $5x10^{10}$ vg AAV8-ZFN/Mock and $2.5x10^{11}$ vg AAV8-Dual-Reporter (identical to the original doses described in our earlier neonatal study(Li et al., 2011)). When sacrificed as adults, hepatocytes isolated from the livers of mice treated with ZFN and Dual Reporter exhibited surface staining of CD4 (consistent with HDR mediated targeting) on roughly 1.5% of hepatocytes (**Figure 4.6**). Mice that did not harbor the hF9mut cassette and those that received Mock + Dual Reporter did not express measurable levels of CD4, consistent with our observations using hF9 donors. CD8 expression appeared similar between all groups, suggesting a less substantial contribution from NHEJ mediated vector integration.

Magnetic bead enrichment of CD4 expressing hepatocytes yielded approximately 13-fold enrichment in CD4+ cells, from which genomic DNA was isolated. CD4 enriched genomic DNA was pooled from two experiments, representing 10 mice in total, and analyzed by southern blot using a radiolabeled probe which hybridized to the intronic region within the hF9mut locus. We detected a ~1.8kb band in the CD4 enriched but not unenriched (Neg) cells, consistent with HDR in mice treated as neonates (**Figure 4.7**).

Ambiguous results in adult mice treated with Dual Reporter

In adult mice, results from the Dual Reporter were less conclusive. Mice were treated with doses $1x10^{11}$ vg ZFN and $5x10^{11}$ vg Dual Reporter via tail vein injection, identical to the majority of the experiments conducted with hF9 donors in order to make the best comparisons to previous results in adult animals. The most interesting finding was that the predominant reporter gene expressed in all groups was the opposite of what was seen in mice treated as neonates (**Figure 4.8**), suggesting a greater contribution of NHEJ in adults. There was no statistically significant difference seen in CD8 expression between mice that harbored the ZFN target site and those that did not (hF9mut vs. WT, **Figure 4.8**). As these results were not consistent with hF.IX expression data, we hypothesize that either the signal (on target vector integration) was insufficiently low for a meaningful measurement, or that the noise was insufficiently high (e.g. expression of CD8 derived from ITR promoter activity, as suggested by CD8 expression in Mock + Dual Reporter treated mice). In either case, the rate of NHEJ mediated vector integration could not be appropriately with these tools. We did note low levels of CD4 expression in adult mice treated with ZFN + Dual Reporter, suggesting some HDR contribution to the total hF.IX expression. Although we cannot directly compare these results with the outcomes in neonatal mice (due to the differences in dose and route of delivery), the relative ratios of NHEJ and HDR appear to be reversed in adult mice, suggesting a predominant role for NHEJ in mediating targeted integration in mice treated as adults.

Evaluation of donor vectors with and without arms of homology in adult and neonatal mice

An alternative approach to characterize the contributions of HDR and NHEJ is to compare expression of hF.IX derived from donors with and without arms of homology to the target site. Expression resulting from non-homologous donors is by definition the result of homology independent repair, whereas expression derived from donors with flanking arms of homology can reflect both repair mechanisms. In order to make the most direct comparisons, we performed experiments using the same route of administration (IV) via tail vein or retro-orbital injection for adults and neonates, respectively. In addition, all donor hF9 cassettes contained the same codon optimized sequences (< 85% similarity to wild-type) to avoid homology between this portion of the cassette and the hF9mut target locus (that contains a truncated wild-type hF9 Exons 1-6). Mice treated as adults, with ZFNs targeting either the hF9mut knock-in locus or the wild-type albumin locus, did not display a difference in hF.IX expression whether the donors did or did not contain arms of homology (**Figure 4.9**, reproduced from chapters 2 and 3). On the other hand, mice treated as neonates, with the same AAV doses and route of administration (IV via retro-orbital injection), exhibited substantially (6-10 fold) more hF.IX expression when treated with donors containing arms of homology to the target site (**Figure 4.10**). This difference was evident in both hF9mut mice treated with human hF9 ZFNs and WT mice treated with mAlb ZFNs, suggesting the observation was not a unique characteristic of the highly recombinogenic Rosa26 locus in which the hF9mut cassette is inserted. These results demonstrate that gene targeting with ZFNs does not require homology in adult mice, but is largely homology-dependent in neonates. These findings are consistent with the presence of ongoing cell division in the developing neonatal liver, during which HDR factors are expressed and activated.

Evaluation of gene targeting in adult mice deficient in NHEJ (SCID)

We repeated these experiments in Prkdc$^{scid/scid}$ mice to determine if a deficiency in NHEJ but not HDR repair would skew the observed hF.IX expression in mice treated with homologous and non-homologous donors. Neonatal SCID mice treated with $1x10^{11}$ AAV8-mAlb-ZFN and $5x10^{11}$ AAV8-Homology-Donor exhibited high levels of hF.IX expression, comparable to the levels observed in WT (Prkdc$^{wt/wt}$) mice (**Figure 4.11**, blue). In contrast, when treated with donors without homology to the albumin locus, mice expressed substantially less hF.IX, with a mean expression of 46.5 ± 7.7 ng/mL 4 weeks post treatment. This value is nearly 15-fold less than what was measured in Prkdc$^{wt/wt}$ mice at similar timepoints. This finding supports the conclusion that DNA-PKcs promotes AAV integration.

Gene targeting with ZFNickases to promote HDR in neonatal mice

We next asked whether HDR could be stimulated even more specifically through the induction of DNA single strand breaks (DNA "nicks") at the target site instead of DSBs ((Kim et al., n.d.; Ramirez et al., 2012). As before, we treated neonatal mice with ZFNs and homologous or non-homologous donors. In addition, we replaced the ZFNs with ZFNickases, in which one FokI nuclease domain's catalytic activity was inactivated with the D450A mutation ((Sanders, Catto, Bellamy, & Halford, 2009; Waugh & Sauer, 1993)). ZFNickases were indeed active, resulting in ~250 ng/mL hF.IX 4 weeks post injection with homologous donor (**Figure 4.12A**). Interestingly, we could not detect hF.IX in mice treated with ZFNickase and non-homologous donor (LOD: 15ng/mL). To rule out the possibility that our inability to detect hF.IX expression in neonatal mice treated

without homologous donors was simply due to the lower efficacy of ZFNickases compared to ZFNs, we attempted to normalize HDR efficiency by increasing the ZFNickase dose 4 fold. Four weeks post treatment, we observed much higher levels of hF.IX in mice treated with 4X ZFNickase and homologous donor (2041 ± 269 ng/mL, **Figure 4.12B**), but were again unable to detect hF.IX in mice treated with the non homologous donor. Together, these data suggest neonatal hepatocytes favor HDR pathways for genome editing, and that manipulation of the DNA damage response is capable of further enhancing this preference. Refinements based on improved molecular understandings of genome editing will continue to increase both the efficiency and safety profiles of *in vivo* targeting strategies.

Discussion

We have now utilized several independent methods to investigate the mechanisms of DNA repair choice during *in vivo* genome editing in both neonatal and adult mice. While PCR analysis showed that both NHEJ and HDR contribute to the observed phenotype, these results were largely non-quantifiable.

Our results with a novel Dual Reporter to assess HDR and NHEJ revealed a preference for HDR in neonatal mice. Unfortunately, the Dual Reporter did not yield as interpretable results in adult mice. A notable difference between the hF9 and Dual Reporter is the requirements for expression are more restrictive for hF9 donors, since they lack the first exon of F9 (which provides the signal peptide). Secretion of hF.IX protein cannot result from basal expression from the ITR's (weak) promoter activity. Off target integration could lead to hF.IX production if the donor integrates in the forward orientation of an expressed gene, as long as the mature mRNA transcript is in the correct reading frame. Indeed, we observed evidence of expression deriving from mice treated with ZFN + hF9-Donor in mice lacking the hF9mut target site, associated with off target cleavage within another gene expressed in liver (see chapter 2, Figure 2.9). In contrast, the Dual Reporter design is expected to share the requirement for in frame splicing, but since it contains a 2A sequence and the full CD8 open reading frame, expression derived from ITR promoter activity can not be ruled out, and was observed in adult mice treated with Mock + Dual Reporter. In a small pilot experiment (data not shown), we observed a reduction in CD8 expression after performing partial hepatectomy on mice treated with Dual Reporters, consistent with this hypothesis. CD8 expression was higher in mice treated with ZFN, however the values were not

consistently statistically significant between WT mice and hF9mut mice harboring the ZFN target site, suggesting off target expression made a substantial contribution to this expression. Alternatively, other changes to a cell undergoing sustained DNA damage (both on and off target) could have driven increased expression relative to the Mock control).

Experiments comparing expression derived from homologous and non-homologous donors corroborated the results of the Dual Reporter experiments. Armed with a reproducible system to easily read out indicators of NHEJ and HDR mediated repair, we were able to further investigate the molecular requirements of *in vivo* genome editing of the liver. In addition, with the knowledge that HDR is playing a substantial role in targeting in neonatal livers, we were able to employ strategies to push the DNA repair choice balance heavily in the direction of HDR using ZFNickases.

As off target DNA damage and unintended integrations are the primary concern for in vivo genome editing, these experiments provide a useful tool to quantify the specificity of targeted gene addition. Using the readout of hF.IX expression from non-homologous donor as a “worst case” scenario with respect to untemplated integration, we estimate that the HDR/NHEJ ratio is improved by at minimum 17 fold using ZFNickases than with ZFNs. Additional qPCR analysis could be helpful in determining the full extent of this difference, as we were bound by the lower limit of detection of hF.IX in plasma. In settings where it is possible to use HDR therapeutically (e.g. when the donor cassette can be comfortably packaged with homology arms within an AAV vector, and when the target tissues are dividing), arms of homology would provide a second constraint (in addition to the specificity of the nuclease) limiting off-target integration.

The Prkdc$^{scid/scid}$ mutation did not appear to reduce HDR in mice treated as neonates, however homology-independent vector integration was largely diminished (~20 fold). These data are consistent with the known role of DNA-PKcs in processing DNA hairpins, like those present in the AAV ITRs, which could limit the extent of NHEJ mediated integration at the target site (and presumably off-target sites as well). Further studies are warranted to determine whether transient inhibition of NHEJ factors would provide an overall reduction in random integration, since the current body of literature describes mixed effects of NHEJ inhibition in mouse liver (no effect, (Paulk, Marquez Loza, Finegold, & Grompe, 2012); increased integration, (Song et al., 2004)). Specifically inhibiting the processing of ITR hairpins could have important advantages over obstructing NHEJ globally. This would be ideal for maximizing the specificity and safety of in vivo gene correction: limiting homology-independent AAV integration without preventing NHEJ repair of other (spontaneous or nuclease-induced) double strand breaks.

These data point to homology directed recombination as the primary mechanism of protein production from genome editing in neonatal mouse liver, and suggest large gains can be made in both efficacy and specificity through deeper understanding of the molecular determinants of this therapeutic approach.

Figure 4.1

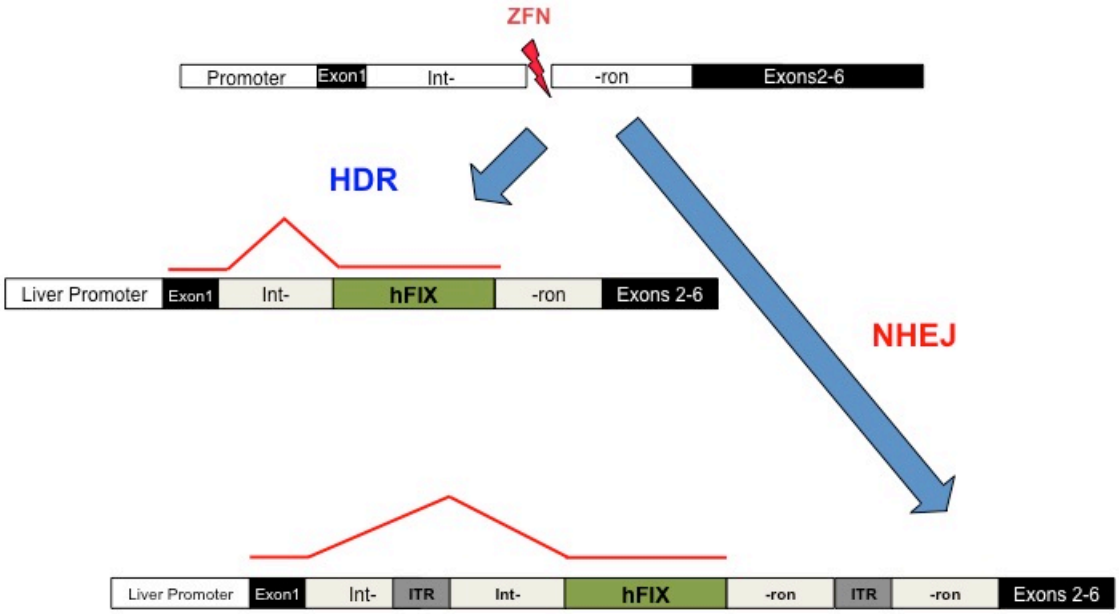

Figure 4.1 Schematic of NHEJ and HR-mediated Integration at the hF9mut target locus.
Expected outcome of HDR mediated genome engineering (middle) and NHEJ mediated vector integration in the forward orientation (bottom). Red lines above illustrations represent splicing to generate wild-type h*F9* transcript.

Figure 4.2

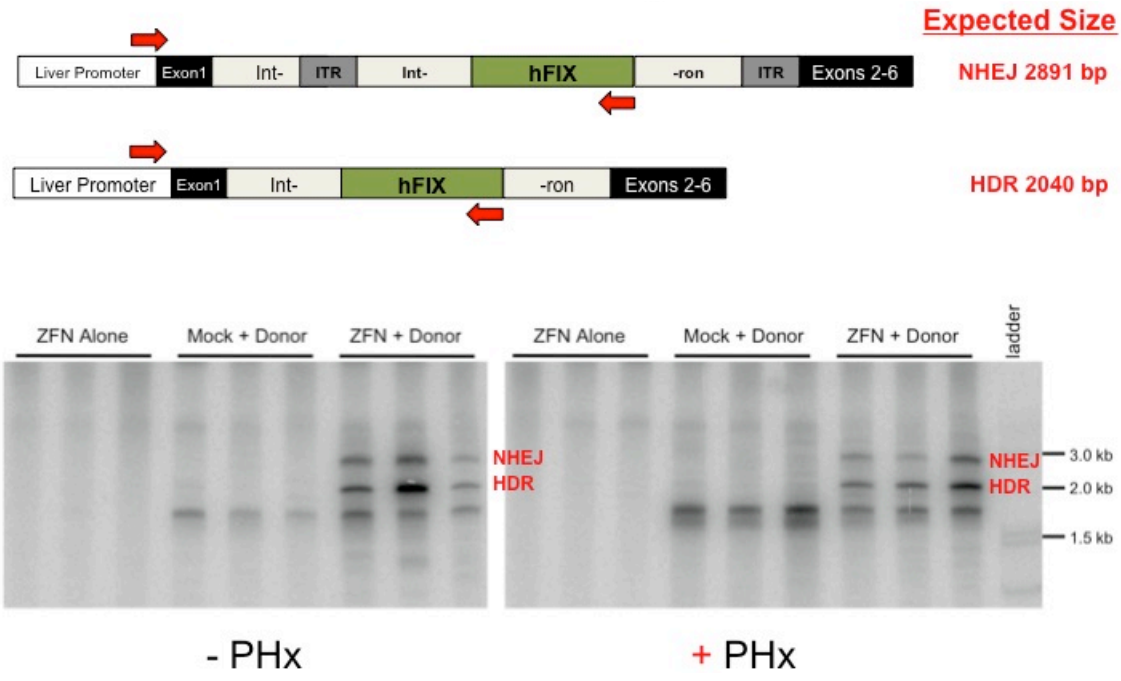

Figure 4.2 PCR Detection of Bands Consistent with NHEJ and HR Mediated Repair of h*F9*mut locus.

PCR detection of ~2.8kb and ~2.0kb bands consistent with NHEJ and HDR, respectively, using primers annealing within the genome and the donor (as illustrated in upper panel). Lower band appears in the presence of donor, and appears to be due to amplification with one primer.

Figure 4.3

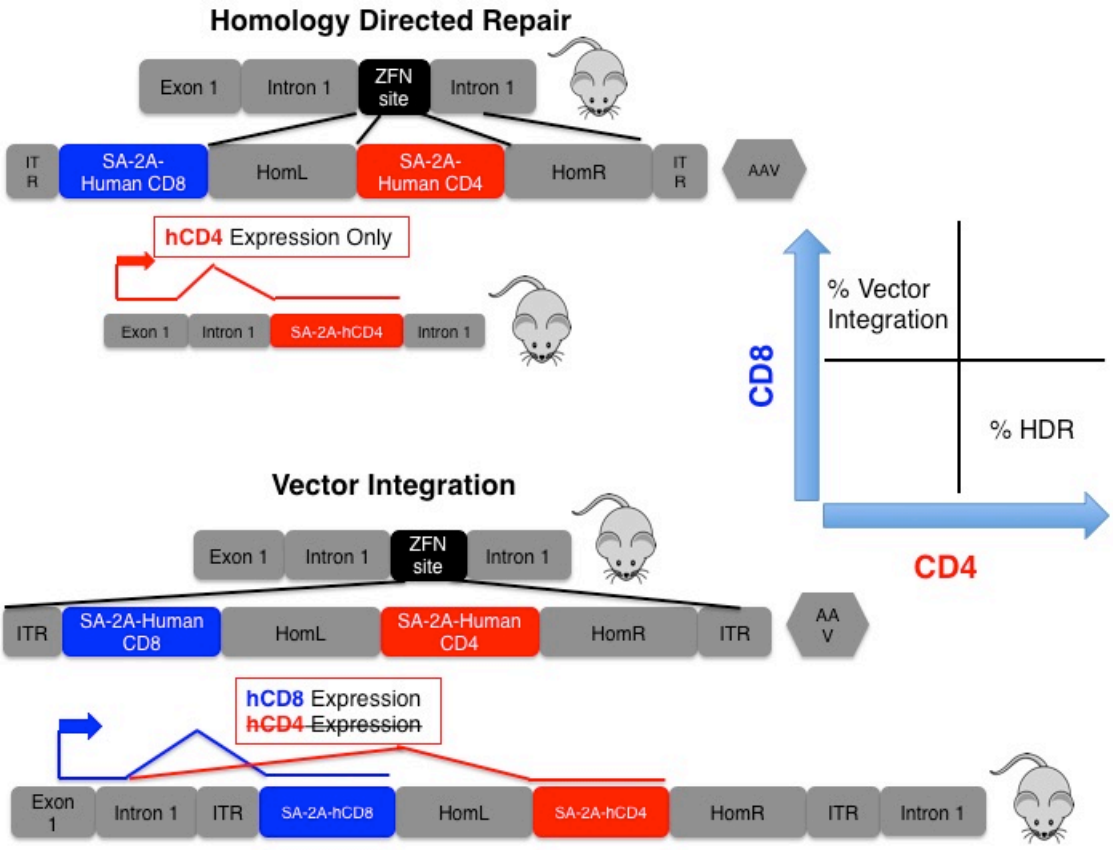

Figure 4.3 Dual Reporter Schematic.
Layout of CD8/CD4 Dual Reporter (designated with AAV) and expected outcomes of HDR (upper) and NHEJ (lower) mediated integration within the h*F9*mut locus. In the case of HDR, only the CD4 expression cassette flanked by arms of homology is expected to be inserted, resulting in expression of human CD4 on the surface of hepatocytes. Vector integration (in the forward orientation) is expected to integrate the entire AAV cassette, and lead to expression of hCD8. Skipping of the splice site, resulting in hCD4 expression from homology independent integration is a formal possibility, however does not appear to occur frequently based on transient transfection experiments presented in Figure 4.4.

Figure 4.4

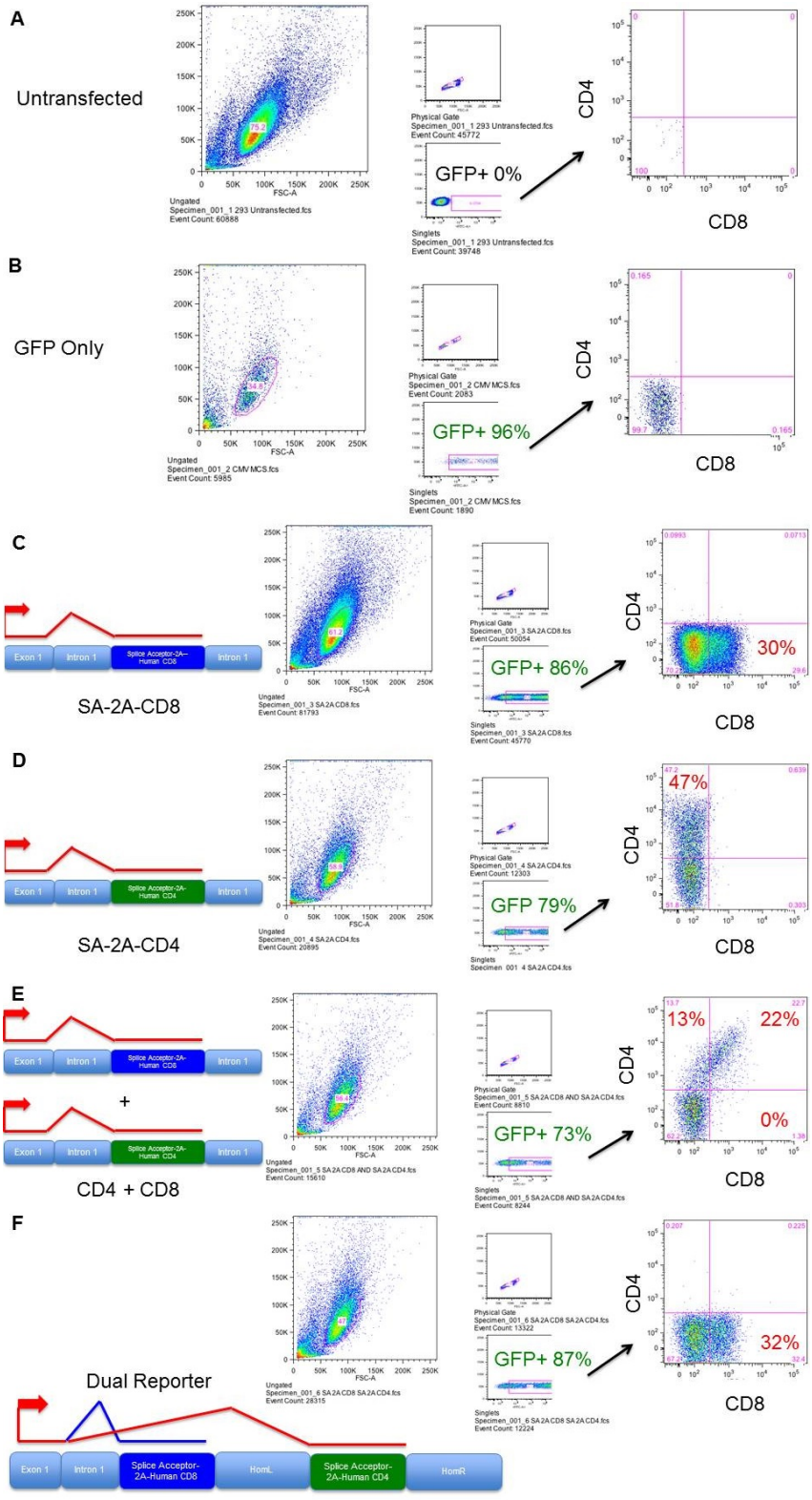
A
Untransfected
GFP+ 0%
CD4
CD8
B
GFP Only
GFP+ 96%
CD4
CD8
C
Exon 1
Intron 1
Splice Acceptor-2A-Human CD8
Intron 1
SA-2A-CD8
GFP+ 86%
30%
CD4
CD8
D
Exon 1
Intron 1
Splice Acceptor-2A-Human CD4
Intron 1
SA-2A-CD4
GFP 79%
47%
CD4
CD8
E
Exon 1
Intron 1
Splice Acceptor-2A-Human CD8
Intron 1
+
Exon 1
Intron 1
Splice Acceptor-2A-Human CD4
Intron 1
CD4 + CD8
GFP+ 73%
13%
22%
0%
CD4
CD8
F
Dual Reporter
Exon 1
Intron 1
Splice Acceptor-2A-Human CD8
HomL
Splice Acceptor-2A-Human CD4
HomR
GFP+ 87%
32%
CD4
CD8

Figure 4.4 *In Vitro* Validation of Dual Reporter Expression Cassettes. Transient transfection of HEK293T cells with plasmids approximating various outcomes that could potentially arise from Dual Reporter integration. Fluorescence measured by flow cytometry using CD4-PE and CD8-APC conjugated antibodies. Cells gated on FSC/SSC (size/granularity) (left), single cells, GFP expression (FITC channel) (middle), and finally by CD4-PE/CD8-APC fluorescence intensity (right). (**A**) Untransfected. (**B**) PGK-GFP only (transfection control). (**C**) SA—2A—CD8 expression driven by CMV promoter used in all expression cassettes. (**D**) SA—2A—CD4 expression. (**E**) Double transfection with plasmids represented in panels C and D, demonstrating the ability to identify double positive populations. (**F**) Measurable expression of only hCD8 in cells transfected with SA—2A—CD8—(Homology Arm)—SA—2A—CD4 cassette, suggesting splice skipping is suppressed due to the strong polyadenylation sequence of the hCD8 expression cassette.

Figure 4.5

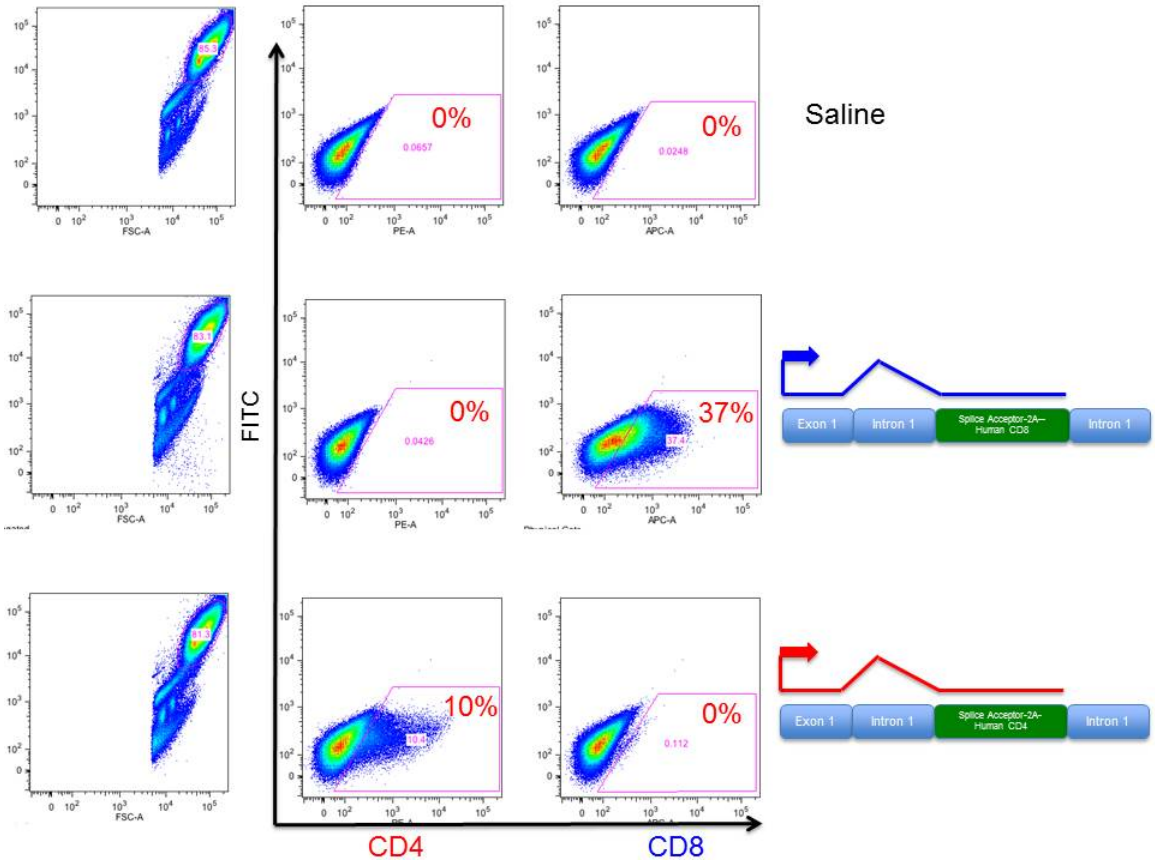

Figure 4.5 *In Vivo* Validation of Dual Reporter Expression Cassettes. Representative flow cytometry plots demonstrating CD4 and CD8 expression in mice treated with hydrodynamic tail vein injection of saline (top panel), SA—2A—CD8 expression cassette (middle panel), or SA—2A—CD4 cassette (bottom panel). Cells were isolated from mice by 2-step collagenase perfusion and stained for analysis using flow cytometry. Gated on hepatocytes SSC/FSC (left panels). PE-hCD4 (center panels) and APC-hCD8 (right panels) markers are relative to FITC (y axis), which represents the strong autofluorescence observed in primary hepatocytes.

Figure 4.6

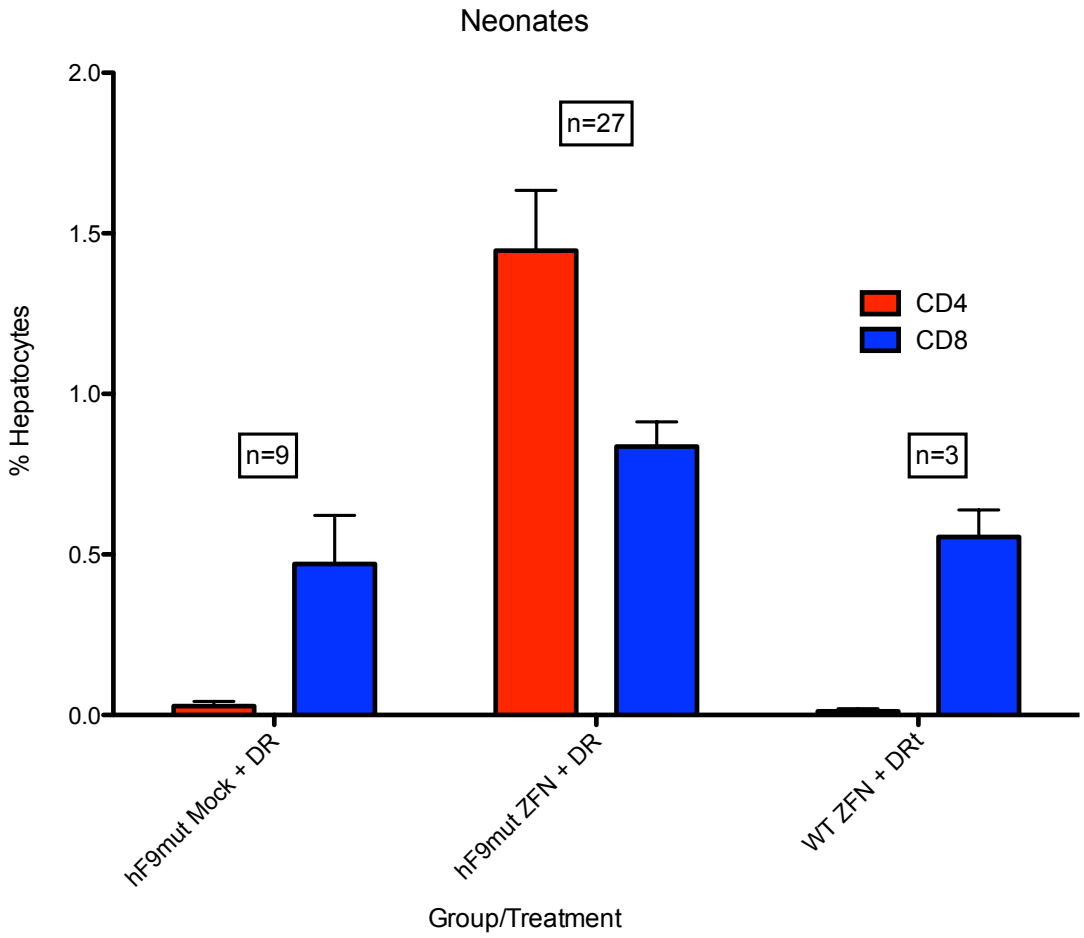

Figure 4.6 CD8/CD4 Expression in Mice Treated as Neonates with ZFN and Dual Reporter

h*F9*mut neonates were treated with $5x10^{10}$ vg AAV8-ZFN/Mock and $2.5x10^{11}$ vg AAV8-Dual-Reporter, doses identical to previously described experiments in neonatal mice (Li et al., 2011). Robust CD4 expression (indicative of HDR) was detected only in mice treated with ZFN and Dual Reporter and also harbored the h*F9*mut target site (center). CD8 expression (indicative of NHEJ mediated vector integration) was measurable but did not appear to differ substantially between groups.

Figure 4.7

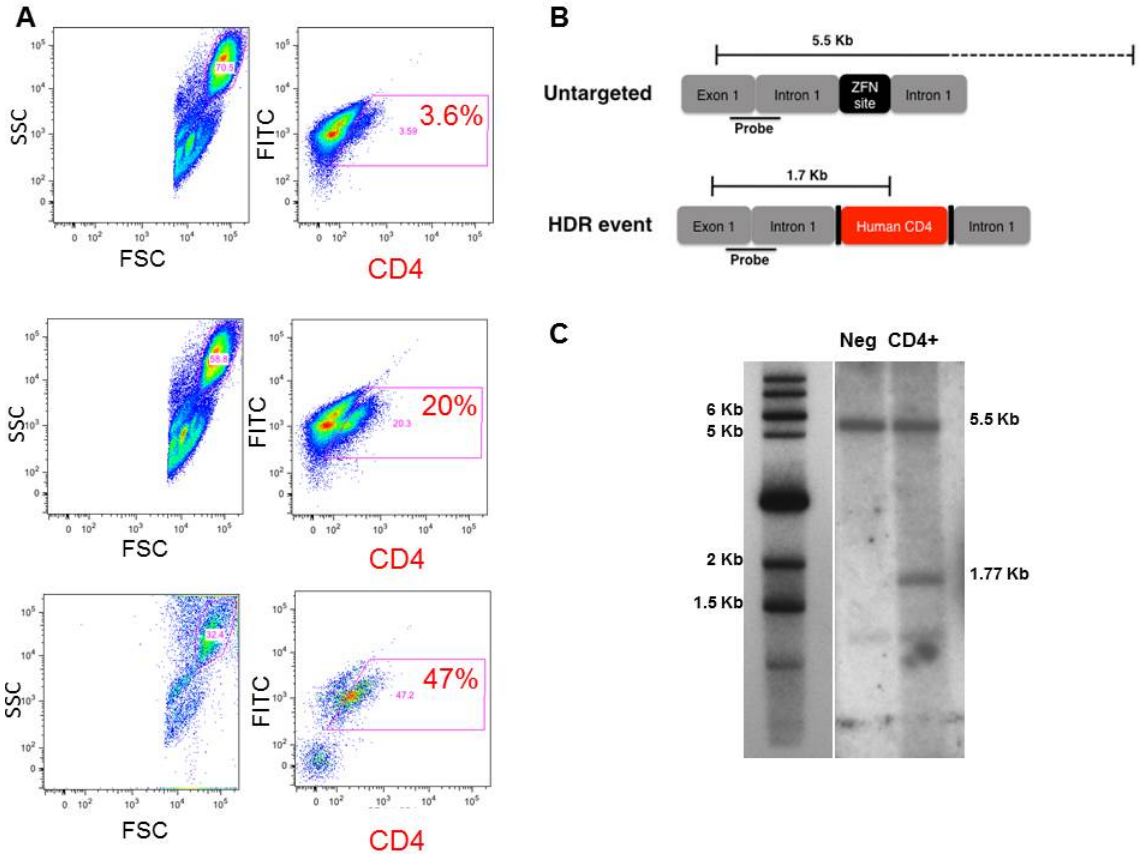

Figure 4.7 Magnetic Bead Enrichment of CD4 Expressing Hepatocytes
(A) Flow cytometric plots of primary hepatocytes pooled from mice treated with ZFN and Dual Reporter. Upper: Unenriched. Middle: First column. Lower: Second column, resulting in almost 50% CD4+ hepatocytes. (B) Schematic representing probe and expected bands indicative of untargeted allele and HDR-mediated integration of Dual Reporter. (C) Southern blot demonstrating band consistent with HDR in the enriched (CD4+ column) but not unenriched (Neg) column.

Figure 4.8

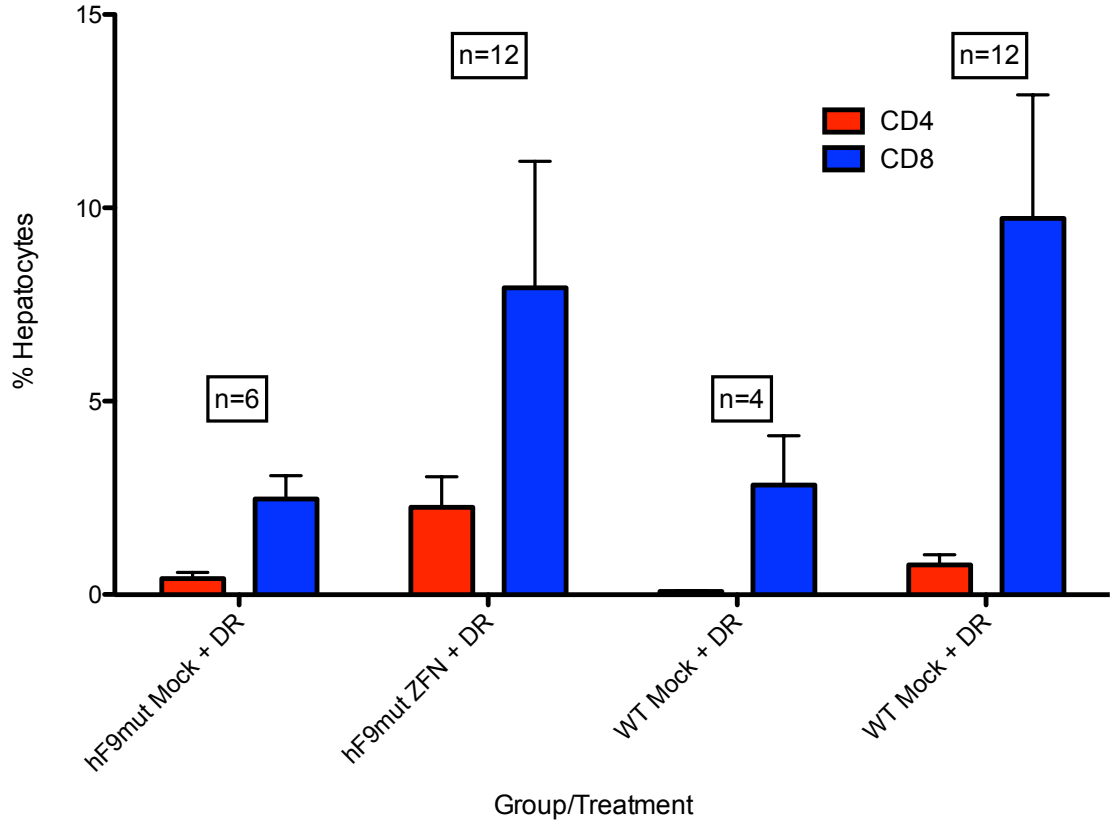

Figure 4.8 CD8/CD4 Expression in Mice Treated as Neonates with ZFN and Dual Reporter

Mice were treated with $1x10^{11}$ vg ZFN and $5x10^{11}$ vg Dual Reporter via tail vein injection, identical to the majority of the experiments conducted with hF9 donors. In all groups, CD8 expression was greater than that observed in mice treated as neonates. CD4 Expression appeared to be greater in mice harboring the hF9mut cassette and receiving ZFN.

Figure 4.9

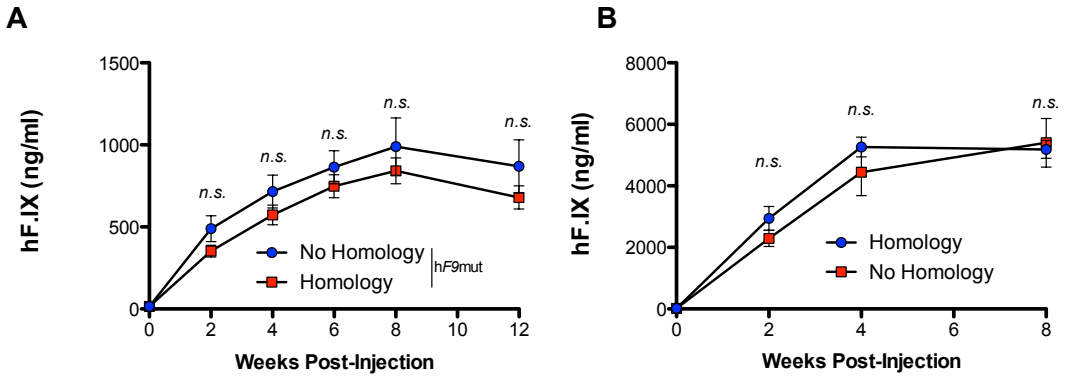

Figure 4.9 Adult Mice Treated With ZFN and Donors With and Without Homology

Adult mice treated with $1x10^{11}$ vg ZFN and $5x10^{11}$ vg Donor with and without arms of homology. (A) hF9mut mice treated with N2 ZFNs (targeting human F9), reproduced from figure 2.7A: No statistically significant difference in expression between mice treated with homologous donor (blue, human F9 arms of homology) and non-homologous donor (red, mAlb arms of homology). (B) WT mice treated with mAlb ZFNs: No statistically significant difference in expression between mice treated with homologous donor (blue, mAlb arms of homology) and non-homologous donor (red, human F9 arms of homology).

Figure 4.10

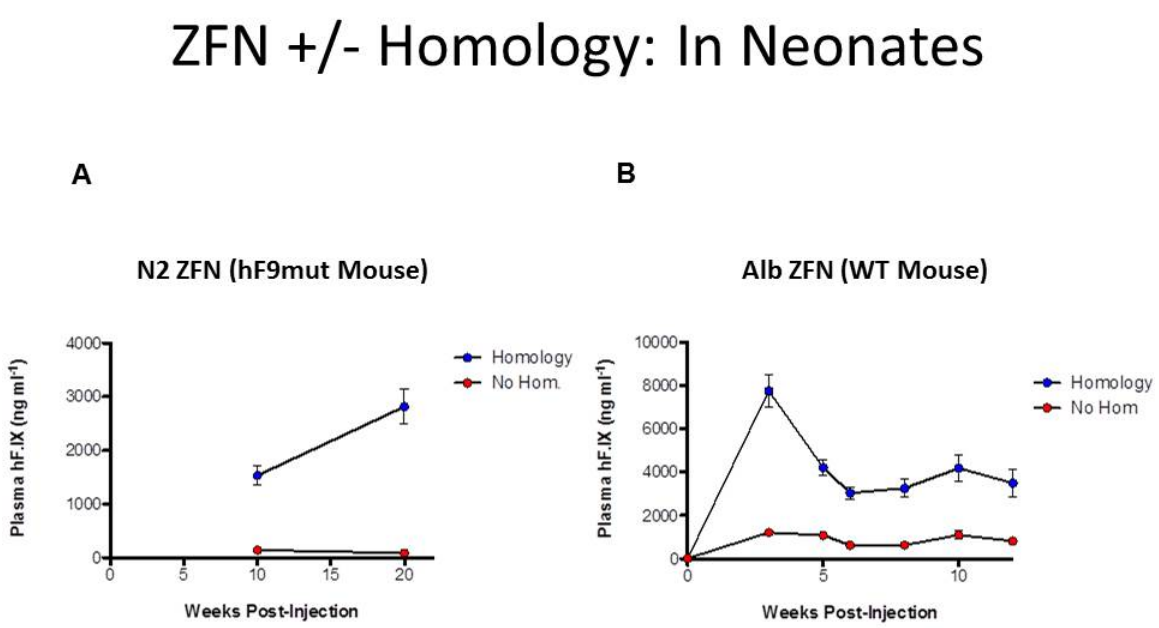

Figure 4.10 Mice Treated as Neonates With ZFN and Donors With and Without Homology

Mice treated as neonates via retro-orbital injection with $1x10^{11}$ vg ZFN and $5x10^{11}$ vg Donor with and without arms of homology. (A) hF9mut mice treated with N2 ZFNs: 10 fold greater expression in mice treated with homologous donor (blue, human F9 arms of homology) vs those treated with non-homologous donor (red, mAlb arms of homology). (B) WT mice treated with mAlb ZFNs: 6-10 fold difference in expression between mice treated with homologous donor (blue, mAlb arms of homology) and non-homologous donor (red, human F9 arms of homology).

Figure 4.11

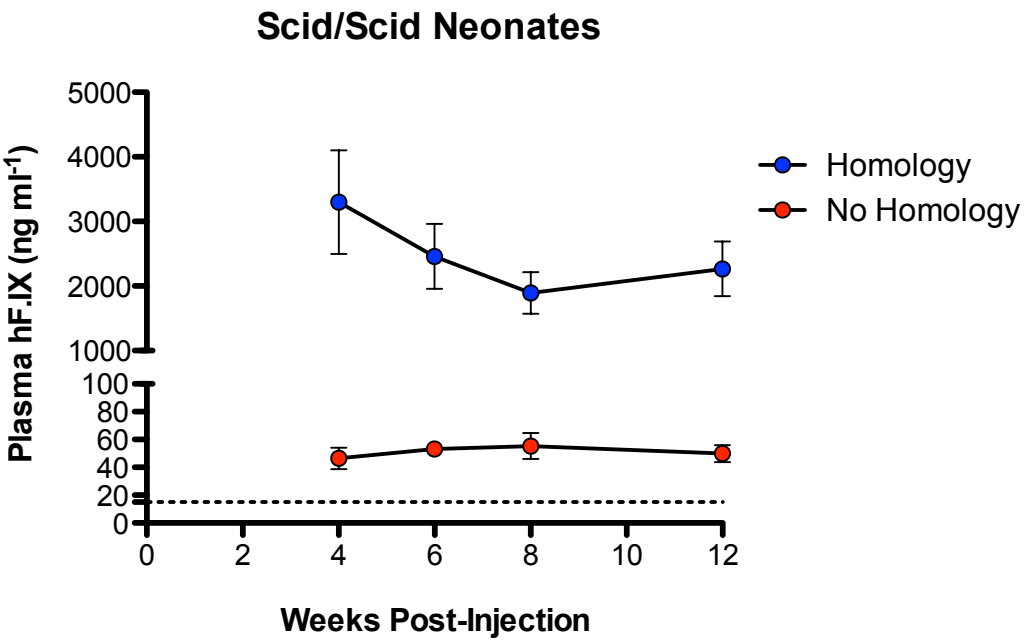

Figure 4.11 Prkdc$^{scid/scid}$ Mice Treated as Neonates With Homologous and non-Homologous donors

Mice treated as neonates via retro-orbital injection with 1x10^{11} vg ZFN and 5x10^{11} vg Donor with and without arms of homology. Blue: Similar levels of expression to WT mice treated with similar doses (see Figure 4.10). Red: Substantially reduced expression in mice treated with non-homologous donors.

Figure 4.12

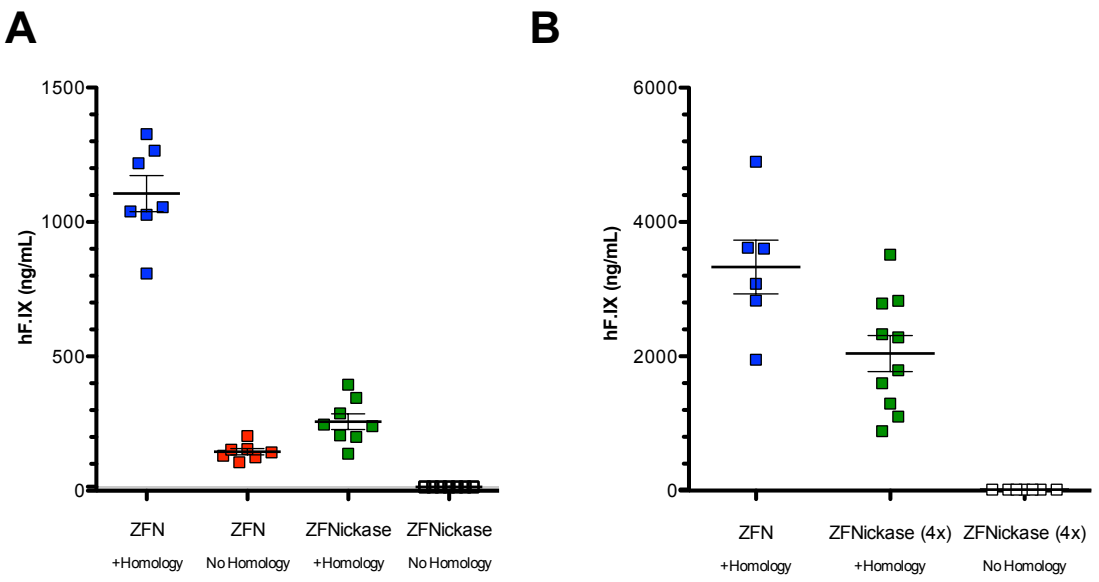

Figure 4.12 hF9mut Mice Treated With ZFN or ZFNickase and Homologous or Non-homologous Donors

(A) Mice treated as neonates via retro-orbital injection with $1x10^{11}$ vg ZFN/ZFNickase and $5x10^{11}$ vg Donor with and without arms of homology. Plasma hF.IX concentrations shown 4 weeks post treatment. As observed previously, ZFNs elicit robust levels of expression with homologous donor (blue), and ~10-fold less with non-homologous donor (red). ZFNickases induced roughly 4-fold less expression with homologous donor (green), with levels that were undetectable with non-homologous donor (clear). (B) Mice treated as neonates via retro-orbital injection with $1x10^{11}$ vg ZFN and $5x10^{11}$ vg homologous donor or $4x10^{11}$ vg ZFN and $5x10^{11}$ vg Donor with and without arms of homology. ZFN treated animals with homologous donor exhibited the highest levels of expression (blue), however at an increased dose ZFNickase + homologous donor treated animals demonstrated robust levels of hF.IX expression approaching 40% of normal (green). hF.IX was not detected in the plasma of mice treated with ZFNickase + non-homologous donor (clear).

CHAPTER 5: CONCLUSIONS AND FUTURE DIRECTIONS

The results described in the preceding chapters indicate that multiple DNA repair mechanisms are capable of mediating efficient site-directed integration of a therapeutic transgene in the liver. Further, a broader understanding of the molecular underpinnings of this process is likely to reveal new approaches to increase the efficacy and specificity of *in vivo* genome editing. Historically, the term gene targeting has been used synonymously with HDR mediated insertion of a desired transgene, the less common DSB repair pathway in mammals. Although HDR is capable of error-free repair using an appropriate template, there are circumstances when it may be either inactive (quiescent cells) or incapable (large transgenes that cannot be packaged with homology arms) of promoting therapeutic levels of therapeutic donor integration. The more active pathway, NHEJ, is often defined as the "error prone" repair choice, useful only for gene disruption. It is worth noting that nucleases are very processive, and will continue to cleave their recognition site until it is destroyed by small insertions and deletions. Since these "indels" are the most common method to quantify NHEJ, it is hard to determine the number of times a break is repaired perfectly in living cells (Bétermier, Bertrand, & Lopez, 2014).

In our studies, we find NHEJ is capable of efficient integration of a therapeutic transgene, and may contribute to nearly all of the observed protein expression in mice treated as adults. This would be an intriguing approach to treat diseases caused by deficiencies in genes much larger than the AAV packaging capacity. Instead of replacing an entire gene, a large exon corresponding to the disease mutation could be inserted into an intron to generate wild type mRNA through splicing.

HDR appears to be responsible for the majority of expression in mice treated as neonates, opening many avenues to further improve this preference in order to maximize the safety profile of liver genome editing. By the same logic of substituting nickases for nucleases, it may be possible to stimulate HDR repair using enzymes with even less genotoxic potential, for example through chromatin remodeling. The next generation of HDR promoting reagents will benefit from unraveling of the still incompletely characterized mechanisms of DSB repair in mammalian cells.

Off target cleavage and the potential for off target integration are the most important safety concerns for genome editing using DNA modifying enzymes, and future directions will include development of strategies to reduce these unwanted events. This is true for ZFNs, as well as other reagents that have been described since these studies were initiated, including clustered regulatory interspaced short palindromic repeat-based CRISPR/Cas9 nucleases. While it is encouraging that phenotypic correction of diseases is possible without observing overt toxicity, the studies presented were not powered to demonstrate smaller differences in health outcomes. As the technology and technical knowledge required to perform high throughput sequencing of viral integrations (or even entire genomes) continues to improve, we will have the ability to detect increasingly rare off target events(Gabriel et al., 2011; Li et al., 2010).

One improvement that could be made is a technique to regulate expression of the nuclease, since there is no benefit to continuous expression subsequent to its role in editing of the genome. One solution would be to include the ZFN target site within the expression cassette that would be translated as an N-terminal fusion to the ZFN monomers, such that indels due to cleavage would likely disrupt the open reading frame.

The advantage of this solution is that it would act as a feedback loop, allowing ZFNs to inactivate themselves only when the levels of expression are sufficient for their activity (and thus would still function at their target site). In addition, this would not unnecessarily complicate the approach, as opposed to methods that require expression of transactivators or repressors, each with their own potential safety implications. The main disadvantages are: (i) Inclusion of the target sequence would need to be within the open reading frame, and thus must be compatible with functional nuclease activity. Since ZFNs are often fused with an N-terminal 3xFLAG tag, and the target sequence could be inserted in multiple ways (two orientations, each with 3 reading frames), it is likely this limitation would be overcome in most cases. (ii) Inactivation through indel formation may efficiently eliminate ZFN expression, although it would not necessarily stop the translation of a novel polypeptide (due to frame shift). In this case, the strategy may mitigate the safety concerns of off-target nuclease activity, but not the potential for neo-antigen expression to trigger an immune response against transduced cells. Ideally, advances in delivery technologies like mRNA conjugates could address both issues by allowing transient delivery of nucleases without AAV. Together with AAV-based delivery of the donor, which does not contain an enhancer or promoter, this approach would substantially reduce the possibility of integration mediated oncogene activation.

An important consideration is that unlike simpler drugs such as small molecule inhibitors, where it is more likely the drug interacts similarly with the human target and its homologue in an animal model, the nature of DNA modifying reagents means the exact sequence of the target genome will be very important in determining off target activity. Even with sensitive assays capable of detecting miniscule levels of unintended cleavage,

the specific off targets will likely be the most important factors in determining the oncogenic risks of these approaches. Although it is of great scientific interest to draw conclusions about differences in specificity of different classes of nucleases, it is clear that our current understanding is insufficient to fully predict genotoxic risks. For example, mouse studies of HSC transplantation following retroviral transduction, even with human cells, do not always predict specific risks of clonal outgrowth seen in human trials (Cavazzana-Calvo et al., 2010). On the other hand, in one of the largest natural experiments of the molecular biology era, millions of humans infected with HIV possess trillions of lentiviral integrations in their CD4 T-cells. Given the clinical experience in HSC gene therapies, we might have expected a substantial number of HIV infected patients to develop viral integration mediated leukemias, yet this does not appear to be the case. There is great therapeutic potential for genome editing to correct many debilitating illnesses, especially in dividing tissues, where episomal AAV expression is unlikely to persist. The therapeutic potential of DNA modifying reagents must be optimized and evaluated empirically, weighing the potential risks as well as the costs of inaction in the face of devastating diseases.

Alt, F. W., Zhang, Y., Meng, F.-L., Guo, C., & Schwer, B. (2013). Mechanisms of Programmed DNA Lesions and Genomic Instability in the Immune System. *Cell*, *152*(3), 417–429. doi:10.1016/j.cell.2013.01.007

Anguela, X. M., Sharma, R., Doyon, Y., Miller, J. C., Li, H., Haurigot, V., et al. (2013). Robust ZFN-mediated genome editing in adult hemophilic mice. *Blood*, *122*(19), 3283–3287. doi:10.1182/blood-2013-04-497354

Anguela, X. M., Sharma, R., Doyon, Y., Wong, S. Y., Paschon, D. E., Li, H., et al. (2012). In Vivo Genome Editing of Liver Albumin for Therapeutic Gene Expression: Rescue of Hemophilic Mice Via Integration of Factor 9. *ASH Annual Meeting Abstracts*, *120*(21), 751 EP –.

Aposhian, H. V., Qasba, P. K., Osterman, J. V., & Waddell, A. (1972). Polyoma pseudovirions: an experimental model for the development of DNA for gene therapy. *Federation Proceedings*, *31*(4), 1310–1314.

Ayuso, E., Mingozzi, F., Montane, J., Leon, X., Anguela, X. M., Haurigot, V., et al. (2009). High AAV vector purity results in serotype- and tissue-independent enhancement of transduction efficiency. *Gene Therapy*, *17*(4), 503–510. doi:10.1038/gt.2009.157

Barzel, A., Paulk, N. K., Shi, Y., Huang, Y., Chu, K., Zhang, F., et al. (2014). Promoterless gene targeting without nucleases ameliorates haemophilia B in mice. *Nature*. doi:10.1038/nature13864

Bennett, J., Ashtari, M., Wellman, J., Marshall, K. A., Cyckowski, L. L., Chung, D. C., et al. (2012). AAV2 gene therapy readministration in three adults with congenital blindness. *Science Translational Medicine*, *4*(120), 120ra15. doi:10.1126/scitranslmed.3002865

Bétermier, M., Bertrand, P., & Lopez, B. S. (2014). Is non-homologous end-joining really an inherently error-prone process? *PLoS Genetics*, *10*(1), e1004086. doi:10.1371/journal.pgen.1004086

Bibikova, M., Carroll, D., Segal, D. J., Trautman, J. K., Smith, J., Kim, Y. G., & Chandrasegaran, S. (2001). Stimulation of homologous recombination through targeted cleavage by chimeric nucleases. *Molecular and Cellular Biology*, *21*(1), 289–297. doi:10.1128/MCB.21.1.289-297.2001

Branzei, D., & Foiani, M. (2008). Regulation of DNA repair throughout the cell cycle. *Nature Reviews. Molecular Cell Biology*, *9*(4), 297–308. doi:doi:10.1038/nrm2351

Bushman, F. D. (2014). Engineering the human genome: reflections on the beginning. *Human Gene Therapy*, *25*(5), 395–400. doi:10.1089/hum.2014.2524

Carroll, D. (2011). Genome Engineering With Zinc-Finger Nucleases. *Genetics*, *188*(4), 773–782. doi:10.1534/genetics.111.131433

Cavazzana-Calvo, M., Hacein-Bey, S., de Saint Basile, G., Gross, F., Yvon, E., Nusbaum, P., et al. (2000). Gene therapy of human severe combined immunodeficiency (SCID)-X1 disease. *Science (New York, N.Y.)*, *288*(5466), 669–672.

Cavazzana-Calvo, M., Payen, E., Negre, O., Wang, G., Hehir, K., Fusil, F., et al. (2010). Transfusion independence and HMGA2 activation after gene therapy of human β-thalassaemia. *Nature*, *467*(7313), 318–322. doi:10.1038/nature09328

Davis, L., & Maizels, N. (2014). Homology-directed repair of DNA nicks via pathways distinct from canonical double-strand break repair. *Proceedings of the National Academy of Sciences*, *111*(10), E924–32. doi:10.1073/pnas.1400236111

Doyon, Y., Vo, T. D., Mendel, M. C., Greenberg, S. G., Wang, J., Xia, D. F., et al. (2011). Enhancing zinc-finger-nuclease activity with improved obligate heterodimeric architectures. *Nature Methods*, *8*(1), 74–79. doi:10.1038/nmeth.1539

Duan, D., Yue, Y., & Engelhardt, J. F. (2003). Consequences of DNA-dependent protein kinase catalytic subunit deficiency on recombinant adeno-associated virus genome circularization and heterodimerization in muscle tissue. *Journal of Virology*, *77*(8), 4751–4759.

Duncan, A. W., Taylor, M. H., Hickey, R. D., Hanlon Newell, A. E., Lenzi, M. L., Olson, S. B., et al. (2010). The ploidy conveyor of mature hepatocytes as a source of genetic variation. *Nature*, *467*(7316), 707–710. doi:10.1038/nature09414

Esashi, F., Christ, N., Gannon, J., Liu, Y., Hunt, T., Jasin, M., & West, S. C. (2005). CDK-dependent phosphorylation of BRCA2 as a regulatory mechanism for recombinational repair. *Nature*, *434*(7033), 598–604. doi:10.1038/nature03404

Fanning, E., Klimovich, V., & Nager, A. R. (2006). A dynamic model for replication protein A (RPA) function in DNA processing pathways. *Nucleic Acids Research*, *34*(15), 4126–4137. doi:10.1093/nar/gkl550

Fratantoni, J. C., Hall, C. W., & Neufeld, E. F. (1968). Hurler and Hunter syndromes: mutual correction of the defect in cultured fibroblasts. *Science (New York, N.Y.)*, *162*(3853), 570–572.

Gabriel, R., Lombardo, A., Arens, A., Miller, J. C., Genovese, P., Kaeppel, C., et al. (2011). An unbiased genome-wide analysis of zinc-finger nuclease specificity. *Nature Biotechnology*. doi:10.1038/nbt.1948

Gadue, P., Huber, T. L., Paddison, P. J., & Keller, G. M. (2006). Wnt and TGF-beta signaling are required for the induction of an in vitro model of primitive streak formation using embryonic stem cells. *Proceedings of the National Academy of Sciences of the United States of America*, *103*(45), 16806–16811. doi:10.1073/pnas.0603916103

Genovese, P., Schiroli, G., Escobar, G., Di Tomaso, T., Firrito, C., Calabria, A., et al. (2014). Targeted genome editing in human repopulating haematopoietic stem cells. *Nature*, *510*(7504), 235–240. doi:10.1038/nature13420

Gierasch, L. M. (1989). Signal sequences. *Biochemistry*, *28*(3), 923–930. doi:10.1021/bi00429a001

Hendrie, P. C., Hirata, R. K., & Russell, D. W. (2003). Chromosomal integration and homologous gene targeting by replication-incompetent vectors based on the autonomous parvovirus minute virus of mice. *Journal of Virology*, *77*(24), 13136–13145.

Heyer, W.-D., Ehmsen, K. T., & Liu, J. (2010). Regulation of homologous recombination in eukaryotes. *Annual Review of Genetics*, *44*, 113–139. doi:10.1146/annurev-genet-051710-150955

Hirata, R. K., & Russell, D. W. (2000). Design and packaging of adeno-associated virus gene targeting vectors. *Journal of Virology*, *74*(10), 4612–4620.

Howe, S. J., Mansour, M. R., Schwarzwaelder, K., Bartholomae, C., Hubank, M., Kempski, H., et al. (2008). Insertional mutagenesis combined with acquired somatic mutations causes leukemogenesis following gene therapy of SCID-X1 patients. *The*

Journal of Clinical Investigation, *118*(9), 3143–3150. doi:10.1172/JCI35798
Kim, E., Kim, S., Kim, D. H., Choi, B.-S., Choi, I.-Y., & Kim, J. S. (n.d.). Precision genome engineering with programmable DNA-nicking enzymes.
Kreamer, B. L., Staecker, J. L., Sawada, N., Sattler, G. L., Hsia, M. T., & Pitot, H. C. (1986). Use of a low-speed, iso-density percoll centrifugation method to increase the viability of isolated rat hepatocyte preparations. *In Vitro Cellular & Developmental Biology : Journal of the Tissue Culture Association*, *22*(4), 201–211.
Li, H., Haurigot, V., Doyon, Y., Li, T., Wong, S. Y., Bhagwat, A. S., et al. (2011). In vivo genome editing restores haemostasis in a mouse model of haemophilia. *Nature*, *475*(7355), 217–221. doi:10.1038/nature10177
Li, H., Malani, N., Hamilton, S. R., Schlachterman, A., Bussadori, G., Edmonson, S. E., et al. (2010). Assessing the potential for AAV vector genotoxicity in a murine model. *Blood*. doi:10.1182/blood-2010-08-302729
Lind, P., Larsson, K., Spira, J., Sydow Bäckman, M., Almstedt, A., Gray, E., & Sandberg, H. (1995). Novel Forms of B-Domain-Deleted Recombinant Factor VIII Molecules. *European Journal of Biochemistry*, *232*(1), 19–27. doi:10.1111/j.1432-1033.1995.tb20776.x
Liu, Q., Segal, D. J., Ghiara, J. B., Barbas, C. F., III. (1997). Design of polydactyl zinc-finger proteins for unique addressing within complex genomes. *Proceedings of the National Academy of Sciences of the United States of America*, *94*(11), 5525–1260. doi:10.1016/j.cell.2015.02.038
Livak, K. J., & Schmittgen, T. D. (2001). Analysis of relative gene expression data using real-time quantitative PCR and the 2(-Delta Delta C(T)) Method. *Methods (San Diego, Calif.)*, *25*(4), 402–408. doi:10.1006/meth.2001.1262
Lombardo, A., Genovese, P., Beausejour, C. M., Colleoni, S., Lee, Y.-L., Kim, K. A., et al. (2007). Gene editing in human stem cells using zinc finger nucleases and integrase-defective lentiviral vector delivery. *Nature Biotechnology*, *25*(11), 1298–1306. doi:10.1038/nbt1353
Magami, Y., Azuma, T., Inokuchi, H., Kokuno, S., Moriyasu, F., Kawai, K., & Hattori, T. (2002). Cell proliferation and renewal of normal hepatocytes and bile duct cells in adult mouse liver. *Liver International*, *22*(5), 419–425. doi:10.1034/j.1600-0676.2002.01702.x
Mann, R., Mulligan, R. C., & Baltimore, D. (1983). Construction of a retrovirus packaging mutant and its use to produce helper-free defective retrovirus. *Cell*, *33*(1), 153–159.
Manno, C. S., Arruda, V. R., Pierce, G. F., Glader, B., Ragni, M., Rasko, J., et al. (2006). Successful transduction of liver in hemophilia by AAV-Factor IX and limitations imposed by the host immune response. *Nature Medicine*, *12*(3), 342–347. doi:10.1038/nm1358
Markowitz, D., Goff, S., & Bank, A. (1988). A safe packaging line for gene transfer: separating viral genes on two different plasmids. *Journal of Virology*, *62*(4), 1120–1124.
McIntosh, J., Lenting, P. J., Rosales, C., Lee, D., Rabbanian, S., Raj, D., et al. (2013). Therapeutic levels of FVIII following a single peripheral vein administration of rAAV vector encoding a novel human factor VIII variant. *Blood*. doi:10.1182/blood-2012-10-462200
Metzger, M. J., McConnell-Smith, A., Stoddard, B. L., & Miller, A. D. (2011). Single-strand nicks induce homologous recombination with less toxicity than double-strand

breaks using an AAV vector template. *Nucleic Acids Research*, *39*(3), 926–935. doi:10.1093/nar/gkq826
Miller, A. D., & Buttimore, C. (1986). Redesign of retrovirus packaging cell lines to avoid recombination leading to helper virus production. *Molecular and Cellular Biology*, *6*(8), 2895–2902.
Mitchell, C., & Willenbring, H. (2008). A reproducible and well-tolerated method for 2/3 partial hepatectomy in mice. *Nature Protocols*, *3*(7), 1167–1170. doi:10.1038/nprot.2008.80
Moynahan, M. E., & Jasin, M. (2010). Mitotic homologous recombination maintains genomic stability and suppresses tumorigenesis. *Nature Reviews. Molecular Cell Biology*, *11*(3), 196–207. doi:10.1038/nrm2851
Nathwani, A. C., Reiss, U. M., Tuddenham, E. G. D., Rosales, C., Chowdary, P., McIntosh, J., et al. (2014). Long-term safety and efficacy of factor IX gene therapy in hemophilia B. *New England Journal of Medicine*, *371*(21), 1994–2004. doi:10.1056/NEJMoa1407309
Nathwani, A. C., Tuddenham, E. G. D., Rangarajan, S., Rosales, C., McIntosh, J., Linch, D. C., et al. (2011). Adenovirus-Associated Virus Vector–Mediated Gene Transfer in Hemophilia B. *New England Journal of Medicine*, *365*(25), 2357–2365. doi:10.1056/NEJMoa1108046
Noguchi, M., Yi, H., Rosenblatt, H. M., Filipovich, A. H., Adelstein, S., Modi, W. S., et al. (1993). Interleukin-2 receptor gamma chain mutation results in X-linked severe combined immunodeficiency in humans. *Cell*, *73*(1), 147–157.
Pattanayak, V., Ramirez, C. L., Joung, J. K., & Liu, D. R. (2011). Revealing off-target cleavage specificities of zinc-finger nucleases by in vitro selection. *Nature Methods*. doi:10.1038/nmeth.1670
Paulk, N. K., Marquez Loza, L., Finegold, M., & Grompe, M. (2012). AAV-mediated gene targeting is significantly enhance by transient inhibition of NHEJ or the proteasome *in vivo*. *Human Gene Therapy*. doi:10.1089/hum.2012.038
Perez, E. E., Wang, J., Miller, J. C., Jouvenot, Y., Kim, K. A., Liu, O., et al. (2008). Establishment of HIV-1 resistance in CD4+ T cells by genome editing using zinc-finger nucleases. *Nature Biotechnology*, *26*(7), 808–816. doi:10.1038/nbt1410
Porteus, M. H., Cathomen, T., Weitzman, M. D., & Baltimore, D. (2003). Efficient gene targeting mediated by adeno-associated virus and DNA double-strand breaks. *Molecular and Cellular Biology*, *23*(10), 3558–3565.
Rabbitts, T. H., Bucher, K., Chung, G., Grutz, G., Warren, A., & Yamada, Y. (1999). The effect of chromosomal translocations in acute leukemias: the LMO2 paradigm in transcription and development. *Cancer Research*, *59*(7 Suppl), 1794s–1798s.
Ramirez, C. L., Certo, M. T., Mussolino, C., Goodwin, M. J., Cradick, T. J., McCaffrey, A. P., et al. (2012). Engineered zinc finger nickases induce homology-directed repair with reduced mutagenic effects. *Nucleic Acids Research*. doi:10.1093/nar/gks179
Rouet, P., Smih, F., & Jasin, M. (1994a). Expression of a site-specific endonuclease stimulates homologous recombination in mammalian cells. *Proceedings of the National Academy of Sciences of the United States of America*, *91*(13), 6064–6068.
Rouet, P., Smih, F., & Jasin, M. (1994b). Introduction of double-strand breaks into the genome of mouse cells by expression of a rare-cutting endonuclease. *Molecular and Cellular Biology*, *14*(12), 8096–8106. doi:10.1128/MCB.14.12.8096
San Filippo, J., Sung, P., & Klein, H. (2008). Mechanism of eukaryotic homologous

recombination. *Annual Review of Biochemistry*, *77*, 229–257. doi:10.1146/annurev.biochem.77.061306.125255
Sanders, K. L., Catto, L. E., Bellamy, S. R. W., & Halford, S. E. (2009). Targeting individual subunits of the FokI restriction endonuclease to specific DNA strands. *Nucleic Acids Research*, *37*(7), 2105–2115. doi:10.1093/nar/gkp046
Shimotohno, K., & Temin, H. M. (1981). Formation of infectious progeny virus after insertion of herpes simplex thymidine kinase gene into DNA of an avian retrovirus. *Cell*, *26*(1 Pt 1), 67–77.
Siner, J. I., Iacobelli, N. P., Sabatino, D. E., Ivanciu, L., Zhou, S., Poncz, M., et al. (2013). Minimal modification in the factor VIII B-domain sequence ameliorates the murine hemophilia A phenotype. *Blood*, *121*(21), 4396–4403. doi:10.1182/blood-2012-10-464164
Song, S., Lu, Y., Choi, Y.-K., Han, Y., Tang, Q., Zhao, G., et al. (2004). DNA-dependent PK inhibits adeno-associated virus DNA integration. *Proceedings of the National Academy of Sciences of the United States of America*, *101*(7), 2112–2116. doi:10.1073/pnas.0307833100
Stocker, J. T., Dehner, L. P., & Husain, A. N. (2012). *Stocker and Dehner's Pediatric Pathology* (3rd ed.). Lippincott Williams & Wilkins.
Sørensen, C. S., Hansen, L. T., Dziegielewski, J., Syljuåsen, R. G., Lundin, C., Bartek, J., & Helleday, T. (2005). The cell-cycle checkpoint kinase Chk1 is required for mammalian homologous recombination repair. *Nature Cell Biology*, *7*(2), 195–201. doi:10.1038/ncb1212
Tabin, C. J., Hoffmann, J. W., Goff, S. P., & Weinberg, R. A. (1982). Adaptation of a retrovirus as a eucaryotic vector transmitting the herpes simplex virus thymidine kinase gene. *Molecular and Cellular Biology*, *2*(4), 426–436.
Tan, N. S., Ho, B., & Ding, J. L. (2002). Engineering a novel secretion signal for cross-host recombinant protein expression. *Protein Engineering*, *15*(4), 337–345.
Thomas, K. R., & Capecchi, M. R. (1987). Site-directed mutagenesis by gene targeting in mouse embryo-derived stem cells. *Cell*, *51*(3), 503–512.
Urnov, F. D., Miller, J. C., Lee, Y.-L., Beausejour, C. M., Rock, J. M., Augustus, S., et al. (2005). Highly efficient endogenous human gene correction using designed zinc-finger nucleases. *Nature*, *435*(7042), 646–651. doi:10.1038/nature03556
van Nierop, G. P., de Vries, A. A. F., Holkers, M., Vrijsen, K. R., & Gonçalves, M. A. F. V. (2009). Stimulation of homology-directed gene targeting at an endogenous human locus by a nicking endonuclease. *Nucleic Acids Research*, *37*(17), 5725–5736. doi:10.1093/nar/gkp643
Wang, H., Perrault, A. R., Takeda, Y., Qin, W., Wang, H., & Iliakis, G. (2003). Biochemical evidence for Ku-independent backup pathways of NHEJ. *Nucleic Acids Research*, *31*(18), 5377–5388.
Wang, L., Wang, H., Bell, P., McMenamin, D., & Wilson, J. M. (2012). Hepatic gene transfer in neonatal mice by adeno-associated virus serotype 8 vector. *Human Gene Therapy*, *23*(5), 533–539. doi:10.1089/hum.2011.183
Waugh, D. S., & Sauer, R. T. (1993). Single amino acid substitutions uncouple the DNA binding and strand scission activities of Fok I endonuclease. *Proceedings of the National Academy of Sciences of the United States of America*, *90*(20), 9596–9600.
Wei, C. M., Gibson, M., Spear, P. G., & Scolnick, E. M. (1981). Construction and isolation of a transmissible retrovirus containing the src gene of Harvey murine

sarcoma virus and the thymidine kinase gene of herpes simplex virus type 1. *Journal of Virology*, *39*(3), 935–944.

Wright, J. F., & Zelenaia, O. (2011). Vector Characterization Methods for Quality Control Testing of Recombinant Adeno-Associated Viruses. In *Methods in Molecular Biology* (Vol. 737, pp. 247–278). Totowa, NJ: Humana Press. doi:10.1007/978-1-61779-095-9_11

Yang, J., Zhou, W., Zhang, Y., Zidon, T., Ritchie, T., & Engelhardt, J. F. (1999). Concatamerization of adeno-associated virus circular genomes occurs through intermolecular recombination. *Journal of Virology*, *73*(11), 9468–9477.

Yardeni, T., Eckhaus, M., Morris, H. D., Huizing, M., & Hoogstraten-Miller, S. (2011). Retro-orbital injections in mice. *Lab Animal*, *40*(5), 155–160. doi:10.1038/laban0511-155

Yin, H., Xue, W., Chen, S., Bogorad, R. L., Benedetti, E., Grompe, M., et al. (2014). Genome editing with Cas9 in adult mice corrects a disease mutation and phenotype. *Nature Biotechnology*. doi:10.1038/nbt.2884

Yu, X., Fu, S., Lai, M., Baer, R., & Chen, J. (2006). BRCA1 ubiquitinates its phosphorylation-dependent binding partner CtIP. *Genes & Development*, *20*(13), 1721–1726. doi:10.1101/gad.1431006